INVESTIGATING SILICA NANOPARTICLES/POLYMER COMPOSITES

A coarse-grained molecular dynamics study

vorgelegt von
Diplom-Chemiker
Elsa Perrin
ORCID: 0000-0001-5728-8277

von der Fakultät II - Mathematik und Naturwissenschaften
der Technischen Universität Berlin
und der
PSL Universität Paris, Frankreich
im Rahmen des Doppel-Promotionsabkommens
zur Erlangung des akademischen Grades

Doktor der Naturwissenschaften
- Dr. rer. nat. -

genehmigte Dissertation

Promotionsausschuss:

Vorsitzender: Dr. François-Xavier Coudert (PSL University)
Gutachter: Prof. Dr. Benoit Coasne (Grenoble Alpes University)
Gutachter: Prof. Dr. Joachim Dzubiella (Freiburg University)

Tag der wissenschaftlichen Aussprache: 02. Juli 2018
an der Ecole normale supérieure, Paris

Berlin 2019

THÈSE DE DOCTORAT

de l'Université Paris Sciences et Lettres
PSL University

Préparée dans le cadre d'une cotutelle entre l'Ecole Normale Supérieure et Technische Universität Berlin

Investigating silica nanoparticles / polymer composites: A coarse-grained molecular dynamics study

Caractérisation de composites polymères / nanoparticules de silice : une étude de dynamique moléculaire gros-grains

Ecole doctorale n°388

CHIMIE PHYSIQUE ET CHIMIE ANALYTIQUE DE PARIS CENTRE

Spécialité CHIMIE PHYSIQUE

COMPOSITION DU JURY :

M. COASNE Benoît
Université Grenoble Alpes, Rapporteur

M. DZUBIELLA Joachim
Humboldt Universität zu Berlin, Rapporteur

Mme. KLAPP Sabine
Technische Universität Berlin, Examinatrice

Mme. MARCELLAN Alba
Sorbonne Universités, Examinatrice

M. COUDERT François-Xavier
Chimie ParisTech, Président du jury

Mme. BOUTIN Anne
Ecole Normale Supérieure, Directrice de thèse

M. SCHOEN Martin
Technische Universität Berlin, Directeur de thèse

Soutenue par Elsa PERRIN
le 2 juillet 2018

Dirigée par **Anne BOUTIN**
Martin SCHOEN

Multi-language Acknowledgement

I acknowledge Joachim Dzubiella and Benoit Coasne who have accepted to review this manuscript and for the interest they showed toward my work. I am grateful to Sabine Klapp, Alba Marcellan and François-Xavier Coudert who agreed to be part of my jury members. I thank all the jury members for the interesting discussion during the PhD defense.

I am grateful to Ludovic Jullien, director of the P.A.S.T.E.U.R. laboratory at École normale supérieure Paris, and to Ame Thomas, director of the chemistry department of the Technische Universität Berlin, for receiving me as a PhD student in their laboratory and for giving me the opportunity to bring to fruition this work.

I thank my PhD advisors, Anne Boutin and Martin Schoen for supervising this thesis, for their understanding, their availability and their guidance. Beside them, I could discuss my results, present them at numerous conferences and gain more independence and perspective regarding the work I was doing.

Ich danke Martin Schoen für seine Aufnahme an der TU Berlin und für seine Hilfe am Anfang meiner Doktorarbeit. Vielen Dank für dein Interesse an einem von dir ungewöhnlichen Thema. Deine Kentnisse in mehreren Bereichen der physischen Chimie und Molekulardynamik-Simulation haben mir erlauben, die Perspektiven meiner Arbeit zu erweitern.

Je tiens aussi à remercier Anne Boutin pour m'avoir donné envie de m'engager dans une thèse et pour m'avoir accompagnée pendant ces trois années. Grâce à la confiance que tu m'as accordée, ces trois années ont été très enrichissantes pour moi, tant sur le plan scientifique que personnel. Ce fut un immense plaisir de travailler avec toi.

I also would like to thank all the researchers I had the chance to collaborate with. In particular, François-Xavier Coudert for its involvement in this project, for the interesting discussions we had, for its supervision and, of course, for our Tuesday climbing sessions ! I am grateful to Marie-Laure Bocquet who supervised my master internship on quantum DFT. Thank you for your availability and for showing me your enthusiasm toward research and science. I also thank Alba Marcellan for sharing with us her interesting research on silica nanoparticles, PAAm, PDMA and more. In particular I have really appreciated discussions on the "macroscopic" behavior of polymers and the interest to build a bridge

in between experiments and simulations. Alba gave me the opportunity to perform experiments, or let's say to work with "real" polymers, more than working with them on a computer. I am also grateful to Anne-Charlotte Le Gulluche for guiding me across the laboratory and explaining me everything I wanted to know about experiments.

Many thanks to all the permanent members of my group at ENS, for showing me their passion for science, for very interesting discussions with them and for helping me in hard times: Damien Laage, Daniel Borgis, Marie-Laure Bocquet, Maximilien Levesque, Nicolas Chéron, Nicolas Lévy and Rodolphe Vuilleumier. I am also grateful to Nadine Rechenberg from TU Berlin and to Stéphanie Benabria, Anne Halloppé, Marie Chayla and Nathalie Etienne for their great support, for their kindness and for their cheerfulness.

I thank the members from the theoretical chemistry group at TU Berlin: Sergej Schlotthauer, Stefi Wandrei, Robert Skutnik and Till Stieger. You have been such great coworkers ! Je remercie aussi tous les membres, anciens, nouveaux, en master, en thèse ou en post-doc du groupe de Chimie Paris : Fabien Trousselet, Guillaume Fraux, Jack Evans, Jean-Mathieu Vanson, Laura Scalfi et Romain Gaillac et du groupe de théorie à l'ENS : Antoine Carof, Benoit Grosjean, Cédric Gageat, Clarisse Péan, Elsa Desmaele, Hugo Bessone, Irene Maffuci, Sohvi Luukkonen, Stéphanie Essafi. Toute ma gratitude va bien évidement aux nombreux relecteurs de ce manuscrit: Benoit Grosjean, Caroline Rossi-Gendron, Elsa Desmaele, Léon Grappe, Sebastian, Sohvi Luukkonen, Alison Tebo et Wilbert Smit. Merci pour votre temps et votre vigilance !

Je souhaite également remercier mes amis sans qui ces trois années auraient été moins drôles, moins sportives, moins intéressantes, et surtout plus difficiles à passer. J'ai eu un plaisir immense à retrouver la plupart d'entre vous pendant ma soutenance de thèse, et je vous suis reconnaissante de m'avoir soutenue jusqu'au bout. Merci à tous mes amis, de Paris ou de Berlin, pour votre présence avant, pendant, et après ces annés de doctorat : Charlotte, Geneviève, Jürgen, Pauline, Cécile, Julie, Lorien, Faris, Guillaume, Oriane, Benoit, Sophie, Antonin, Gaelle, Caroline, Olivier, Félix, Thomas, Audrey, Andrea, Manon, les copains de la zumba : Julie (again!), Mélanie, Marion, Philippine, Mattildi/a, Wilbert, et évidemment Irene.

Je terminerai par remercier ma famille, mes parents et mes sœurs, pour leur soutien et leur présence à mes côtés tout au long de cette aventure. Mon cheminement aurait sûrement été différent sans leur confiance lors des étapes qui m'ont menée jusqu'ici. Enfin, merci Léon pour pas mal de choses. Merci pour ta présence à mes côtés, merci pour ton soutien, ton aide, tes encouragements, pour avoir été si compréhensif et pour le rester.

Abbreviations

BD: Brownian Dynamics

CG: Coarse-Grained

CGMD: Coarse-Grained Molecular Dynamics

COM: Center Of Mass

DFT: Density Functional Theory

DPD: Dissipative Particle Dynamics

FENE: Finite Extensibility Nonlinear Elastic

GGA: Generalized Gradient Approximation

LB: Lattice-Boltzmann

LAMMPS: Large-scale Atomic Molecular Massively Parallel Simulator

LDA: Local Density Approximation

LJ: Lennard-Jones

MC: Monte Carlo

MD: Molecular Dynamics

NP: Nanoparticle

PAAm: polyacrylamide

PBC: Periodic Boundary Conditions

PBE functional: Perdew-Burke-Ernzehof functional

PDMA: poly(N,N-dimethylacrylamide)

PMF: Potential of Mean Force

SCF: Self-Consistent Field

STM: Scanning Tunneling Microscopy

TOC: Total Organic Carbon

VASP: Vienna Ab initio Simulation Package

Symbols

$\beta = 1/k_B T$

ΔF: free energy difference

ΔF_B: free energy barrier

d: distance between beads and surface

D: distance between the center of mass of the polymer chain and the surface

D_{diff}: diffusion coefficient

D_S: distance between two silica surfaces

η_s: solvent viscosity

h: Planck constant

K: strength constant

k_B: Boltzmann constant = $1.38 \cdot 10^{-23}\ J \cdot K^{-1}$

l_x, l_y, l_z: simulation cell dimensions

m: particle mass

M_w: molecular weight

N: number of particles

P: pressure

P(d): normalized histogram probability distribution of d

Q: partition function

Q_{NVT}: canonical partition function

T: temperature

$\mathbf{r}$: position vector of a particle

r_0: equilibrium position of the center of mass of the polymer

r_{COM}: position of the center of mass of the polymer

U(r_1, r_2, ..., r_N): energy of a system containing N particles at positions $\mathbf{r}_1$, $\mathbf{r}_2$, ..., $\mathbf{r}_N$

V: volume

V_{US}: umbrella sampling bias potential

Beads name:

S: surface bead

C: polymer's backbone chain bead

A_{PDMA}: PDMA's A bead

A_{PAAm}: PAAm's A bead

Contents

General Introduction

General Introduction

What is the similarity between contact lenses, wound dressing, artificial snow, sanitary napkins and diapers? They all contain hydrogels. A hydrogel is a water-swollen cross-linked polymeric network. It is widely used for daily objects such as contact lenses, super-absorbant hygiene products, wound dressing, and also in the medical field in targeted drug delivery systems, scaffold for tissue engineering or even in food additives. Furthermore, hydrogels have large similarities with biological soft tissues such as skin, muscles, liver or lungs. The structure, biochemistry and osmotic properties of these organs are obviously more complicated than hydrogels. Nevertheless, the latter turns out to be a reasonable model of extracellular matrices for biological studies. Therefore, due to their high water content (up to 90 %), to their soft mechanical properties and to their ability to reply to external stimuli, hydrogels are promising materials for biocompatible applications. Polymer properties can usually be tuned with external parameters such as pH, temperature, electric or magnetic field, ionic strength and solvent composition. However, their high water content leads to weak mechanical properties in terms of elastic modulus and deformability. Their brittleness therefore restricts the range of applications of hydrogels.

It is of most importance to benefit from a method that enables to reinforce the polymer network. Solutions that exist use a second interpenetrating polymer matrix such as nanofibers or nanoparticles. It is now well known that introducing nanoparticles within the polymer network leads to an enhancement of the mechanical properties if interactions between polymer chains, water and nanoparticles are favorable. Inclusion of inorganic nanoparticles in swollen hydrogels was first realized by the group of Haraguchi in 2002 who introduced clay nanoparticles inside a poly(N-alkylacrylamide) network. The resulting material underwent large modifications in terms of swelling behavior, transparency

and mechanical properties that were significantly improved. Later on, scientists from the ESPCI (École Supérieure de Physique et de Chimie Industrielles de la ville de Paris) have demonstrated that introducing silica nanoparticles in a poly(N,N-dimethylacrylamide) hydrogel leads to a strong reinforcement of the hydrogel mechanical properties. Such hybrid material is also designated as "nanocomposite gel" or "hybrid hydrogels" or even "nanohybrid hydrogel".

Adhesion of hydrogels on surfaces is a crucial issue because it has applications in many different fields and on different surfaces. For instance, adhesion of hydrogels on solid surfaces such as glasses or ceramics and on wet surfaces such as biological tissues is still a challenging task nowadays. This problem is therefore of first relevance. However, hydrogels are known to be difficult to work with. Because of their high water content, they are soft, slippery and brittle. Some methods have been proposed in the literature such as the use of cross-linkers or electrolyte polymers. However, such methods can be difficult to implement and require pH changes or the application of an electric field.

Following previous work on the enhancement of the hydrogel mechanical properties by the addition of silica nanoparticles at the ESPCI, Alba Marcellan and Ludwik Leibler proposed a novel method to enhance adhesion between two hydrogels. They use inorganic particles as cross-linkers to glue together two hydrogel networks. This method relies on the ability of silica nanoparticles to adsorb on polymer chains and to behave as connectors in between polymer chains. Furthermore, in such material, polymer chains have the ability to reorganize on the nanoparticles surface and dissipate energy when undergoing external stress. The bridge introduced between the two hydrogels by the nanoparticles leads to a material that can undergo and resist to large deformations. In their work, Marcellan, Leibler and co-workers have even extended their method to the repair of a soft tissue. They therefore propose a new surgical adhesive able to repair skin wounds and soft tissues such as liver or lungs. The latter being very difficult to suture because they would tear when being stitched, having a surgical adhesive is of uttermost importance.

Nevertheless, in a broader view, understanding the behavior of such system is a challenging task which is relevant to many families of materials in a wide range of domains. Progress in fundamental understanding of both the chemical and physical properties is currently limited by a lack of a robust model. More precisely, the coupling between the chemistry of adsorption and the resulting mechanical properties is poorly understood. The aim of this work is to employ a multiscale approach that is able to give insight into the multiple phenomena occurring within the system. This is a broad task. In order to tackle this goal, several specific questions will be answered all along this manuscript. This work aims at finding a molecular path that allows to understand macroscopic mechanical properties, at probing the dynamic of polymer chains in the vicinity of the interface and at investigating the role played by water by using simulations. More specially, the first step is to choose, to design and to build a model that will allow for a better understanding of the system behavior. Afterwards, certain features of the model are tested, such as the reliability of an implicit or an explicit water model and its ability to reproduce experimental behaviors. Different quantities such as the local dynamic of polymer chains in the vicinity of the silica surface, their solvation and the manner polymer chains desorb from the silica surface are probed in order to understand the behavior of the system. This study relies on few hypotheses that needs mentioning. First, a flat surface is considered: a possible effect of the nanoparticles curvature is therefore neglected. Second, polymers that are considered are not cross-linked. To that extend, we do not strictly model a hydrogel.

The manuscript is organized as follows. The first chapter consists of a broad introduction of surgical adhesives and nanocomposite materials, and a review of what is being done in those broad fields, experimentally and theoretically. The second chapter is devoted to simulation methods. We present density functional theory and molecular dynamics. Computer simulation methods that are being widely used within the polymer material field are also reviewed and discussed. The third chapter consists of a presentation of the model we built, its verification and its limitations. The comparison of two solvent models,

implicit and explicit, is reported in the fourth chapter. In this chapter, we probe the local dynamics of polymer chains on the surface of silica, as well as the strength of interaction between polymer chains and the silica surface, and the solvation of polymer chains far from the surface and in its vicinity. In the fifth chapter, we investigate the detachment of polymer chains from silica surfaces. The evolution of the polymer shape, along with the evolution of different interaction energies are studied. Moreover, interactions that are occurring within the system are examined in order to give insight into the precise role played by each component of the system, namely the polymer chain, water and the silica surface. We then constrain a polymer chain between two silica surfaces and explore the evolution of the polymer behavior when the chain is subject to a mechanical constraint in the sixth chapter. Finally, in the seventh chapter, we present results of experimental adsorption of polymer chains on silica nanoparticles that I had the opportunity to execute. The main results are then gathered and a model rationalizing different behaviors of poly(N-alkylacrylamide) and of poly(N,N-dimethylacrylamide) on silica is proposed. We finally suggest further theoretical investigations to improve our model and to bring it closer to experiments.

Part I

State of the art and methods

Chapter 1

Nanocomposites

Before going deeper into the technical description of the theoretical tools that have been used all along this work, this chapter presents an overview of the broad field of the topic of my thesis. The idea of this research is to give a theoretical insight into the hydrogel / silica nanoparticles system that have been developed by Alba Marcellan and co-workers in 2014 [1]. It is difficult to glue together hydrogels, even if they are good adhesives, because it requires pH change [2], chemical reactants [3], heating, *etc.* Rose et al. [1] have shown that it is possible to glue together two hydrogel strips by using an aqueous solution of silica nanoparticles (see figure 1.1). The resulting system is strongly bonded and is able to undergo large deformations without failure. This proof of concept was applied to the gluing of two pieces of calf liver with a silica nanoparticles solution.

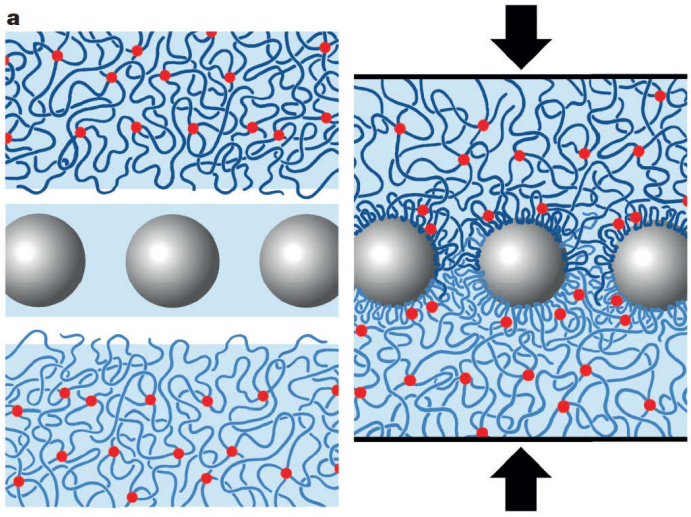

Figure 1.1 – Schematic illustration of the gluing of hydrogels using a droplet of silica nanoparticles. Picture from reference [1].

However, interactions between silica nanoparticles and hydrogel remain poorly understood as well as the ability of the resulting material to highly dissipate energy under pressure. The aim of the present work is to provide a robust yet simple model that allows us to address this question. This work is thus related to surgical adhesives. Nonetheless, in a broader view, it definitely stands in the nanocomposite field, which is a very rich, broad and varied one. This chapter therefore consists of a review of the surgical adhesive field (from a chemist's point of view) and of the nanocomposite material field. The aim of this chapter is not to give an exhaustive review, but instead to give insight into their most significant features.

1.1 Surgical adhesives

Several surgical adhesives have been developed for skin wound healing and for cardiac, liver and lung surgery. They are used for human surgery as well as for animal surgery. Surgical adhesives should fulfill two objectives: (i) keeping in contact the two sides of the biological tissue by *in vivo* mechanical adhesion of the adhesive and (ii) assist the local hemostasis[1] by enhancing the coagulation and healing process [4]. More generally, surgical adhesives should "cause adherence of tissue to tissue or tissue to non-tissue surfaces, as for prostheses, to control bleeding and to serve as a barrier to gas and liquids" [5]. There are already a large number of surgical adhesives on the market and commonly used by surgeons and veterinarians. They display an interesting range of properties: fast, convenient and less painful application, enhancement of local hemostasis, no suture removal and excellent cosmetic result [5]. Those surgical adhesives are made of polymers because the latter insure good contact between surfaces by covering asperities and retarding fracture by dissipating energy under stress [6, 7]. However, the currently available surgical adhesives still have significant limitations and drawbacks. The most important ones are the cytotoxicity (low biocompatibility), a slow degradation, a drying time that can be

1. Hemostasis is the first stage of wound healing and corresponds to the physiological process ensemble that contributes to stop bleeding.

long, a complicated application method when it requires *in situ* polymerization and a low adherence to wet surfaces [5, 8]. Most of the surgical adhesives that are already used are polymer-based. We will briefly review them and present a new type of surgical adhesive that relies on the adhesion of silica nanoparticles on the biological tissue [1]. This new method was develop by Alba Marcellan, Ludwik Leibler and co-workers at École Supérieure de Physique et de Chimie Industrielle de la ville de Paris (ESPCI).

1.1.1 Polymer-based surgical adhesives

Polymer-based surgical adhesives can be divided in three categories: natural adhesives, synthetic adhesives and semi-synthetic adhesives [4, 5].

Natural adhesives

Natural adhesives are usually composed of proteins that are present in the human or animal body. First natural adhesives that conquered the market are composed of fibrin[2]. Such natural adhesive consists of fibrinogen and of thrombin that are put in contact together. This leads to the polymerization of fibrinogen into fibrin that is insoluble in a few minutes. Fibrin adheres to the biological tissue and is released within a few days [4, 5]. It exists other natural adhesives based on gelatin (from bone collagen), bovine thrombin or polysaccharides. These adhesives have several advantages. Among them, their biocompatibility, the fact that they are completely resorbable and they enhance healing are worth noting. However, they suffer from an application procedure that is not easy to use, a polymerization that can be long (polymerization of fibrin is complete in two hours [4]) and weak mechanical properties.

Semi-synthetic adhesives

In order to improve the mechanical stability and the adhesion on biological tissues, semi-synthetic adhesives couple a natural compound (gelatin, polysaccharides, *etc.*) and a synthetic compound (for instance aldehyde) as polymerization reagent [8]. For instance,

2. Fibrin is a fibrous protein that is formed by the polymerization of fibrinogen by the action of thrombin. It is involved in the coagulation process.

BioGlue® is a mixture of gelatin and of glutaraldehyde [4, 8]. The compounds are stored in a two-compartment syringe in order to prevent direct contact between toxic glutaraldehyde and biological tissues. Polymerization occurs in two minutes and the adhesive glues well on dry or wet surfaces. However, it is difficult to release and it is so tough that it can prevent or slow down healing.

Synthetic adhesives

Synthetic adhesives are composed of elements that are unknown to the human body. Even though, with good mechanical properties and a simplified use, synthetic adhesives are gaining interest from surgeons. There exists a wide range of synthetic adhesives, based on different polymer types such as polyethylene glycol or cyanocrylate [5, 8]. Their polymerization is efficient, varying from 60 to 120 seconds. However, their degradation time ranges from 30 days to 2 years.

1.1.2 A novel class of surgical adhesives

In the course of the last decades, efforts of the scientific community led to important progress in the field of surgical adhesives. The latter are widely used in substitution or as support for staples and sutures. However, the currently available tissue adhesives still have significant limitations such as their low mechanical properties, toxicity, instructions for use and degradation time.

Experimentalists from ESPCI in Paris developed in 2014 a new surgical adhesive composed of nanoparticles (NP) and of water [1]. They were actually able to insure good adhesion between a silica NP solution of Ludox® TM-50 and a calf's liver. They spread the silica NP solution on two pieces of liver and, after pressing them with a finger for 30 seconds, an adhesion energy of 25 ± 5 J/m^2 was measured (figure 1.2). This is the first attempt to use silica NP as surgical adhesive.

This innovative method was then succesfully applied on living rats [9]. The proposed

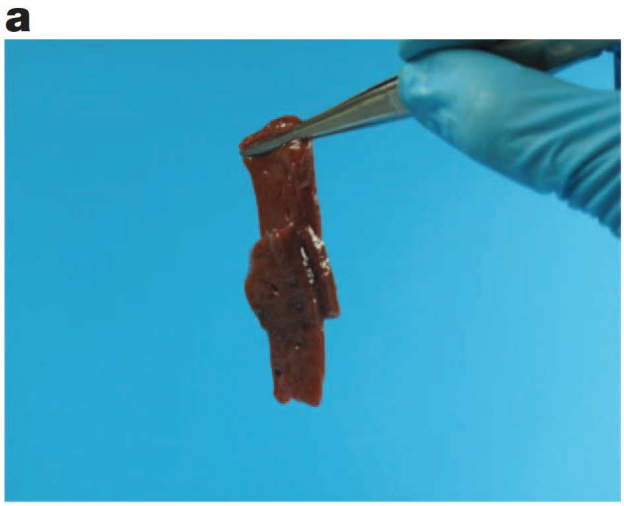

Figure 1.2 – Two pieces of calf liver were glued together by spreading silica NP solution between them. Picture from reference [1].

method is rather simple (see figure 1.3): an aqueous silica NP solution is spread with a micropipette or a brush at the wound surface of a tissue (left side of figure 1.3), and the wound edges are pressed together with fingers (blue arrows on the right side). As a result, nanoparticles form multiple connectors that maintain the wound close.

This method was compared with classical suture and with synthetic surgical adhesive

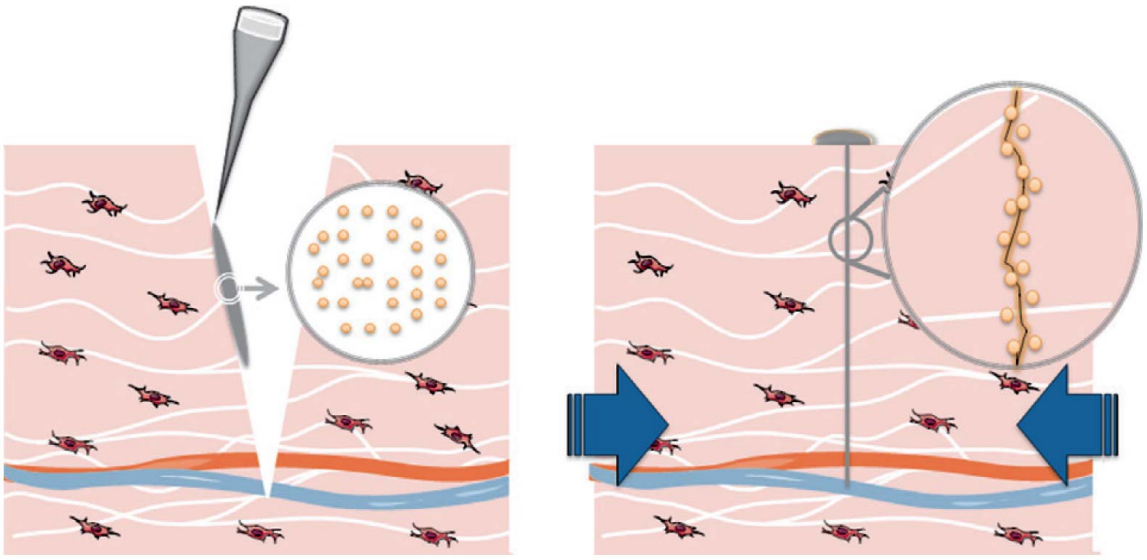

Figure 1.3 – The concept of using silica NP solution for wound closure. Picture from reference [9].

based on cyanoacrylate (Dermabond®) [9]. A dorsal wound of 1.5 cm in length and 3 mm

in depth was healed using the three mentioned methods (figure 1.4). In the three cases, the wound did not reopen. However, after three days, one can see that the healing is more efficient when a silica nanoparticles solution is used. The wound that is treated with the cyanoacrylate adhesive has the slowest healing. Dermabond® adhesive causes local inflammation of the skin and forms a tough layer that prevents good contact between the two edges of the wound and therefore slows down the healing process. Hence, the use of an aqueous silica nanoparticles solution turns out to be satisfactory in terms of biocompatibility (there is no wound inflammation), of good mechanical properties (the wound did not reopen) and of hemostasis (the healing was fast).

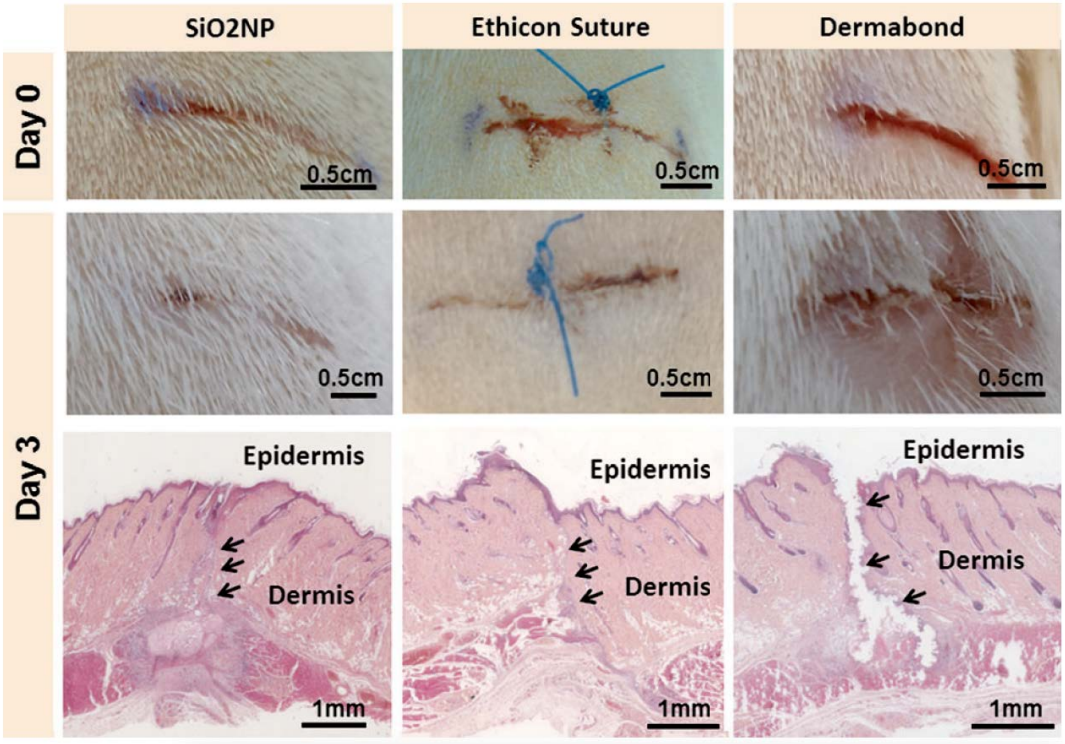

Figure 1.4 – *In vivo* comparison of wound healing with aqueous silica NP solution (left), with suture (middle) and with cyanoacrylate adhesive (Dermabond®) on rats. Picture from reference [9].

1.2 Hybrid hydrogels to reinforce hydrogels

Hydrogel is a model of choice to study extracellular matrices of biological tissues [10]. As mentioned in the introduction, a hydrogel is a reticulated polymer network, which is filled with water (see figure 1.5) [11]. There are many various applications of hydrogels,

ranging from vehicles for drug delivery [12], microlenses [13], to scaffolding for tissue engineering [14]. The authors of reference [1] use hydrogels as a model of biological tissue to study the adhesion of silica nanoparticles on wounds. Nevertheless, the scope of hydrogel applications is severely limited by their weak mechanical properties [15]. Hydrogels are actually brittle, with fracture energy around 10 J/m^2 [6, 12, 16–20], due to the small polymer chains density caused by the high water content and to the heterogeneity of the polymer network [21, 22]. Hydrogels energy fracture is well below the one of natural rubber ($\sim$ 10 000 J/m^2 [6]) or of cartilage ($\sim$ 1 000 J/m^2 [23]). Over the last decades, intense effort has been made to find means to reinforce hydrogels. Those means range from double-network hydrogels [24–26], which are composed of two polymer networks: one which has a high density of cross-links (the first or sacrificial network, that will break first and dissipate energy) and one which is poorly cross-linked (the second network, that maintains integrity of the gel) to hydrogels with hybrid chemical and physical cross-linkers [18, 27–30] (see figure 1.5).

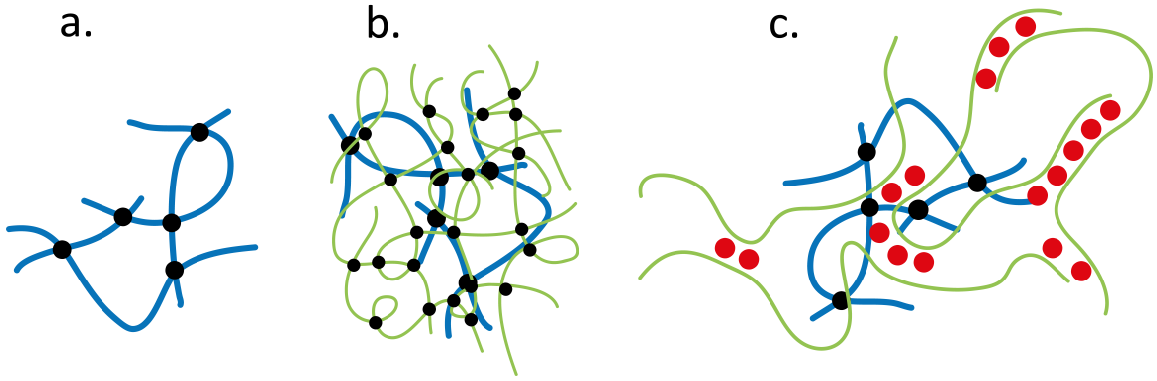

Figure 1.5 – a. Normal hydrogel: polymer chains are in blue and cross-links are back circles. b. Double-network hydrogel: the first polymer network is in green and the second in blue. c. Hydrogel with hybrid chemical and physical cross-linkers: blue chains are chemically cross-linked while green chains form ionic cross-links through Ca^{2+} ions (red circles). Inspired by figure 1 of reference [18].

1.2.1 Nanocomposites

Another solution to reinforce hydrogels is to use nanoparticles as connectors. The resulting system, containing NP and hydrogel, is a type of nanocomposite material [31–35]. Nanocomposites refer to multiphase solid materials whose one of the phases has at least

one dimension below 100 nm or whose properties are due to a nano-scale structure. This broad definition gathers various materials such as porous media, colloids, gels and copolymers, but usually corresponds to the combination of a bulk matrix and nano-dimensional phases of different chemistry and structure. The resulting properties of nanocomposites (whether mechanical, electrical, thermal, optical, electrochemical or catalytic) in general differ significantly from the bulk properties of its components. The design of nanocomposite materials is a fast-growing field, both for fundamental research and industrial applications. This rapidly expanding field generates many exciting new materials with novel properties, either by combining desirable properties of the parent phases into a single material, or new properties arising by virtue of the nano-scale microstructure or interactions between the parent phases. Composites consisting of nanoparticles embedded in a polymer matrix are a class of nanocomposite.

1.2.2 PAAm and PDMA

The nanocomposite material we are interested in corresponds to the one used by Rose et al. [1]. We consider silica NP, polyacrylamide (PAAm) on the one hand and poly(N,N-dimethylacrylamide) (PDMA) on the other hand (figure 1.6). PAAm is less sterically hindered than PDMA. The hydrogen, oxygen and nitrogen atoms of PAAm are more available to interact with the silica surface than PDMA. PAAm should therefore better adsorb on the silica surface than PDMA. However, PAAm hydrogels do not glue on silica NP [36, 37] whereas PDMA glues readily onto silica NP [38]. Gluing two PDMA strips with a silica nanoparticles solution leads to an adhesion energy equals to 6.6 ± 1.6 J/m^2 between the two PDMA strips (see figure 1.7) while it is really difficult to measure an adhesion energy between two PAAm strips glued with silica nanoparticles: adhesion between the two strips is poor and prevents any adhesion energy measurement [1]. One of the aim of the present work is to understand the source of those two drastically different behaviors.

It is necessary, in order to reinforce hydrogels by the introduction of NP, that the polymer chains adsorb readily onto the NP's surface. Adsorption is a surface phenomenon

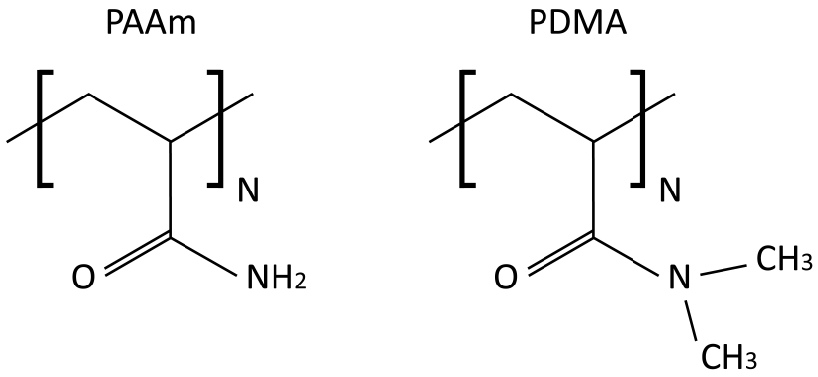

Figure 1.6 – Polyacrylamide (PAAm) and poly(N,N-dimethylacrylamide) (PDMA).

where the polymer chains attach with various strengths to the silica surface. In our case, adsorption brings into play weak interactions such as Van der Waals interactions or the formation of hydrogen bonds. There are typically three steps that lead to the adsorption of a polymer solution to a solid surface: (i) diffusion of polymer chains from bulk to interface, (ii) adsorption of the polymer chain on the solid surface and (iii) relaxation of the polymer chain and rearrangement of the adsorbed layer that occurs by means of dynamical desorption and adsorption. Although the two first steps, diffusion and adsorption, are relatively fast, the last step is the limiting one [39].

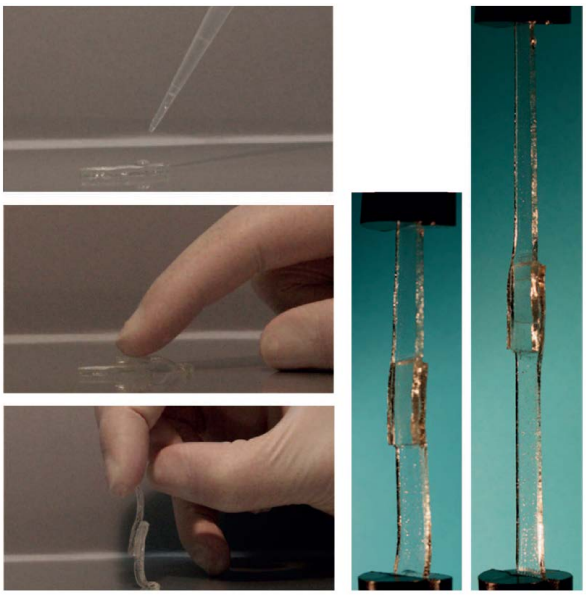

Figure 1.7 – Gluing two PDMA strips by spreading a droplet of silica nanoparticles solution in between them and simply bringing them into contact (left picture). The resulting junction is able to undergo large deformations (right picture). Pictures from reference [1].

Moreover, the resulting reinforcement of the hydrogel depends on the number of chains able to adsorb on the NP's surface and therefore on the polymer concentration [40, 41]. Pefferkorn and co-workers defined a critical concentration below which polymers adsorb on the surface by forming monolayers. Above this concentration, the adsorbed chains undergo rearrangements [40, 41]. In this high concentration regime, one can find polymer chains forming tails (chain ends that are not adsorbed on the surface), trains (consecutive adsorbed monomers), loops (consecutive non-adsorbed monomers, in between two trains) and entanglements (see figure 1.8). However, the precise adsorption mechanism of polymer chains on the NP's surface remains poorly understood. Particularly, when polymer chains are neutral, it is not clear whether the adsorption is due to the formation of hydrogen bonds between polymer chains and the NP's surface [36], or to hydrophobic interactions [42, 43], or both.

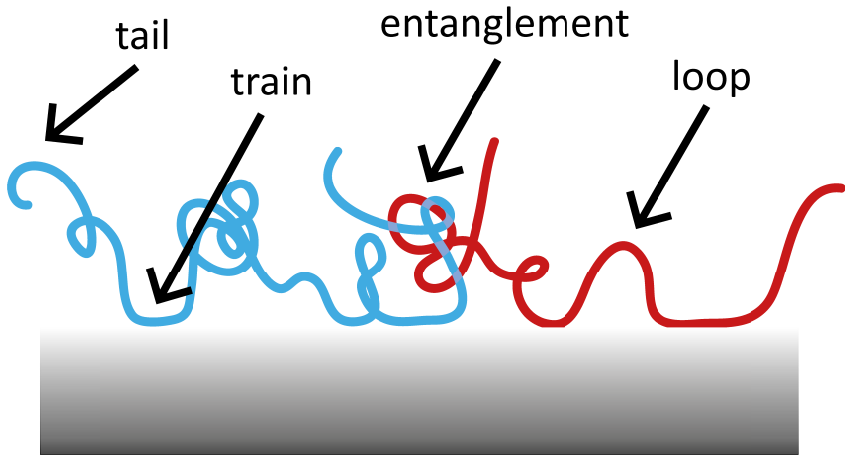

Figure 1.8 – Entangled adsorbed layer of polymer chains with trains, tails and loops.

According to several studies, PAAm is able to adsorb on silica surface when the latter is not hydrated and has free silanols on its surface [36, 44–46]. A free silanol is a hydroxyl group which is bound to a silicon atom and that does not form hydrogen bonds with its environment, meaning that there is neither water molecule nor other silanol in its vicinity [36, 40, 46]. The authors of reference [1] have used hydrated silica where silanols are able to interact with water molecules. According to the authors of reference [36, 37], water

molecules adsorb readily on the silica surface and prevent PAAm chains from adsorbing on silica. The non-adsorption of PAAm on silica is therefore due to a low probability of forming hydrogen bonds between PAAm monomers and silica than between water and silica.

Other authors say that hydrophobic interactions, dominating hydrogen bond formation, explain the different behaviors of PAAm and PDMA [42, 43]. Zhang *et al.* suggest to rationalize the efficient adsorption of PDMA on silica with the model reproduced in figure 1.9. This model assumes that PDMA adsorbs on silica surface by forming hydrogen bonds between the oxygen atom of the carbonyl group and the hydroxyl group of silica surface. Zhang and co-workers consider that efficient adsorption of PDMA on silica surface is due to the formation of hydrogen bonds, but also to the strength of hydrophobic interactions. The latter occurs through p, π conjugation between nitrogen atoms of the PDMA and hydroxy groups of silica, reinforced by the presence of two hydrophobic alkyl groups on the nitrogen, that increase the strength of the hydrogen bond. When polymer chains are adsorbed on silica, hydrophobic alkyl groups attempt to approach the surface, thereby hunting and releasing water molecules from the interface. Once hydrophobic groups are in the vicinity of the silica surface, they prevent water molecules from adsorbing on the surface and replacing polymer chains [42, 43, 47]. Within the framework of this model, the lack of hydrophobic groups on the nitrogen atom of PAAm explains why it does not adsorb on silica.

However, the model of Zhang and co-workers is questionable. It first assumes that the strength of hydrogen bonds is lower than hydrophobic forces due to the presence of alkyl groups that enhance conjugation between nitrogen atoms of the PDMA and hydroxy groups of silica. This needs to be confirmed with extra quantum calculations (see chapter 3). Then, the model considers that the entropic gain due to the release of water in the bulk and to the hydrophobic interaction is higher than interaction between water and silica. The model suffers from a lack of extensive calculations on the considered interface,

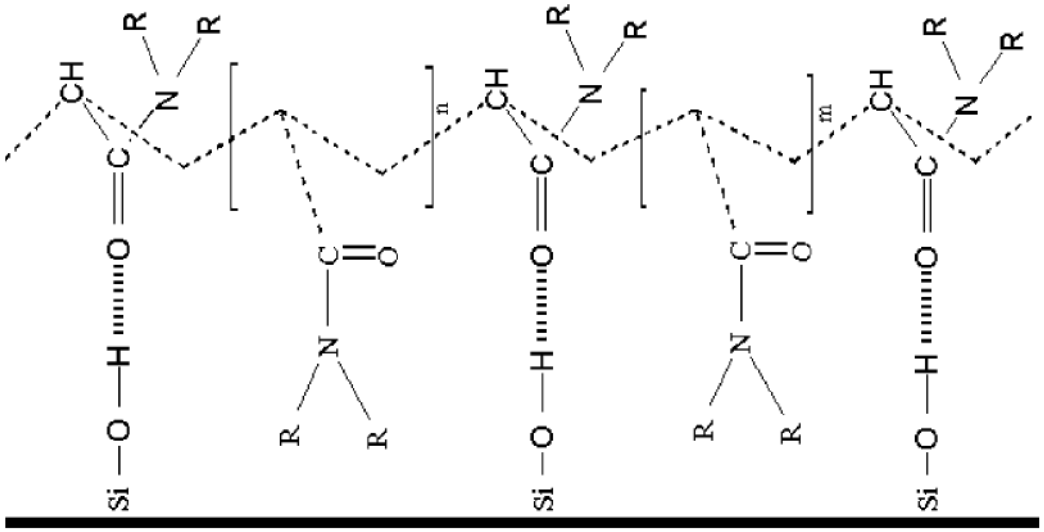

Figure 1.9 – Model of PDMA adsorption on a silica surface. Picture from reference [43].

which will be done in the following chapters: we will give more insight into the atomistic details of the adsorption of PAAm and PDMA in chapter 3. Therefore, this model does not allow to plainly understand different behaviors of PAAm and PDMA.

Another important feature of PAAm and PDMA gels is their swelling behavior. It is well known that swelling strongly depends on the cross-links density [48]. Nevertheless, for the same cross-linker density, the swelling ratio of PAAm is 1.4 times higher than the one of PDMA [49]. We will investigate this behavior in chapter 5.

1.2.3 Silica nanoparticles

It is also essential to take into account the ability of silica nanoparticles to aggregate within the nanocomposite material [50–53]. Silica has different behaviors as pH changes because pH governs surface charge density through the presence of groups -$SiOH_2^+$, -SiOH and -SiO^- (see figure 1.10). When pH equals 9-10, silica surface is negatively charged, leading to repulsion between silica nanoparticles and insuring that silica particles are

stable and well dispersed. This behavior is represented in figure 1.10 by the "no salt" curve, which has a vertical asymptote when pH equals 8, which indicates that silica suspension is stable. When pH is above 8, silica suspension remains stable. Stability then decreases with pH. When pH=3, the silica solution is in a metastable state. It is close to the zero point charge of silica where silica surface is neutral and covered with -SiOH. There are numerous collisions and contacts between silica nanoparticles. However, due to the formation of a hydration layer on the silica surface, particles do not aggregate [52]. As pH decreases below 3, silica surfaces are positively charged and covered with $-SiOH_2^+$, leading to repulsion between silica nanoparticles. With those considerations, the authors of reference [1] work at a pH between 8.5 and 9.5 where silica nanoparticles are negatively charged.

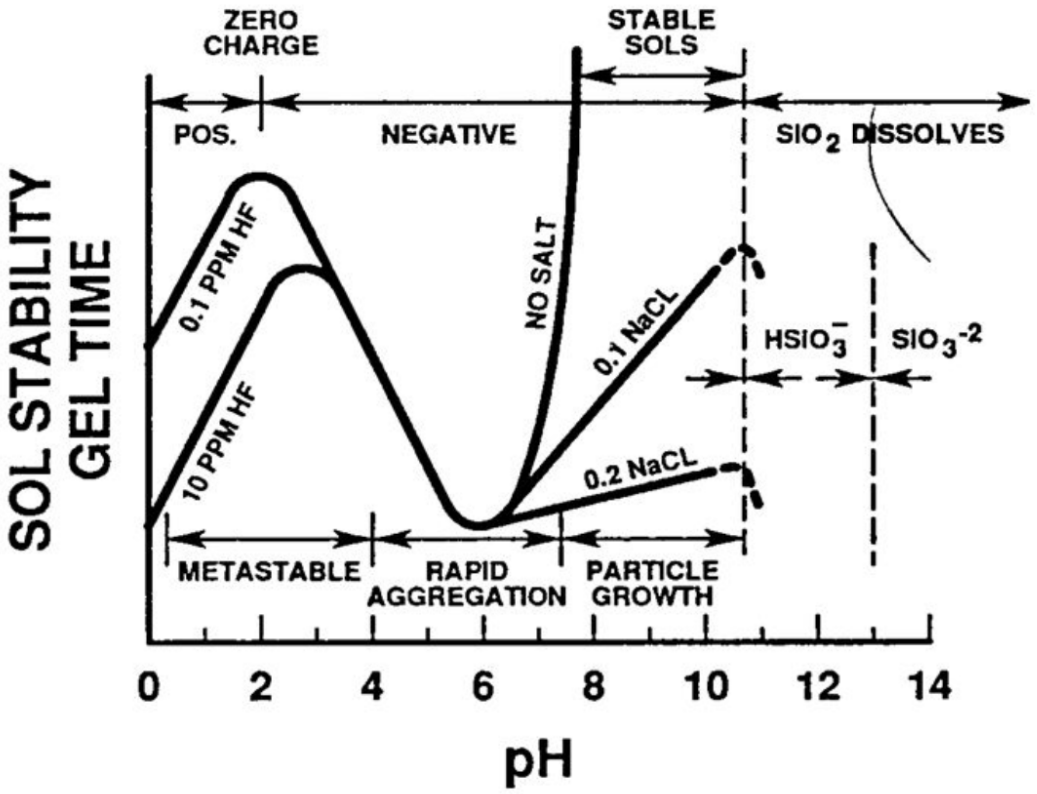

Figure 1.10 – Stability of colloidal silica and coagulation time, depending on pH and on NaCl concentration. Picture from reference [52].

1.2.4 Adhesion between polymers and nanoparticles

When NP are added to a polymer matrix, certain properties are unexpectedly improved, well above what would be predicted by classical mixture rules. In this section we will not consider complex systems containing block copolymers or polymer blends which have numerous interesting properties (electric, magnetic, optical, *etc.*) [54–58]. We restrain ourself to the study of nanocomposites containing NP and polymers. There is a large scientific community investigating nanocomposites, or more generally systems containing an interface between polymer chains and a solid surface. We review here some of the work, mostly theoretical, that has been done on the changes caused by the introduction of NP or of a solid surface in a polymer network [59]. Extensive studies have been done on the evolution of polymer chains dynamic when nanoparticles or a surface are inserted [60–64], on the effect of the nanoparticles size [65–69], on the understanding of the interaction between polymer chains and the surface [70–86], on the resulting mechanical properties of the nanoparticles-enriched polymer network [32, 81, 87–93] and on the thermal response of polymer-NP mixtures [94–100], to cite some of the investigative fields of polymer-NP systems. The study of polymer-nanoparticles systems is therefore a broad field with many interesting work that is being done even though several outstanding issues still need to be addressed [58].

The authors of reference [1], after gluing two PDMA strips with a droplet of a silica nanoparticles solution, have demonstrated that the resulting junction undergoes large deformations without failure. The silica particle diameter that they used is larger than the averaged size of the polymer network, leading to the adsorption of several monomer units on the silica surface [101, 102]. Therefore, when considering the scale of the polymer chain, its adsorption is irreversible due to the adsorption of numerous monomers anchored on the silica surface. It is not possible to completely detach a polymer chain. The junction between the two PDMA strips is then able to undergo large deformations. When the junction between the two PDMA strips is deformed, PDMA chains adsorbed on silica are under pressure. If one monomer desorbs from the silica surface (see the red chain from

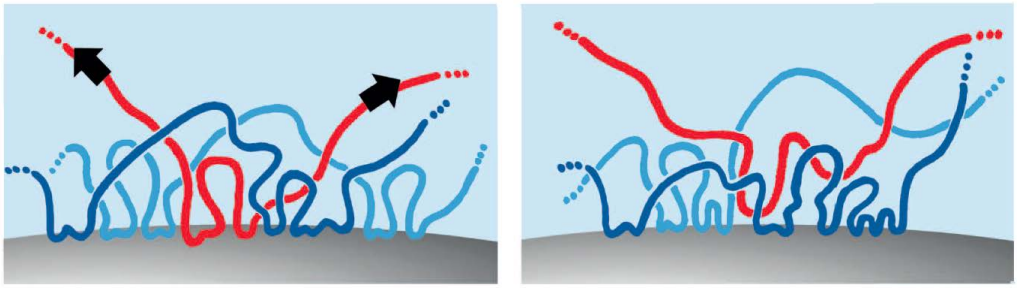

Figure 1.11 – Schematic representation of adsorption of polymer chains on the surface of silica nanoparticles. Picture from reference [1].

figure 1.11), it will instantaneously be replaced by a monomer of the dark blue chain. Black and red chains can belong to the same polymer molecule or to different chains. If we now zoom in and focus on monomers, they undergo rapid adsorption/desorption mechanisms [39]. These exchange process results in efficient dissipation of energy when the junction undergoes large deformations.

This is, to our knowledge, the main explanation that rationalizes the improvement of hydrogels mechanical properties by the addition of nanoparticles. However, this explanation suffers from a lack of a robust model, able to bind the atomistic details of the polymer/silica interface to the resulting enhancement of the material's mechanical properties.

1.3 Our system

To summed up the aim of this work: we want to understand why PDMA glues on silica nanoparticles while PAAm does not. We therefore work with two systems, one containing PAAm and the second containing PDMA. Both polymers are put in contact with a silica surface. The surface is flat, the effect of curvature is therefore neglected. This is quite an important hypothesis, considering the fact that it is well established that mechanical properties of nanocomposites vary with the nanoparticles size [68]. The effect of curvature will be considered in further studies. We also consider neutral polymers and a neutral surface. This is again an important assumption yet reasonable when focusing on chains

rearrangement of large systems. Another important hypothesis of our work is the following: we consider polymer chains that are not cross-linked. To that extend, our system does not model hydrogels. However, the interface between polymer chains and silica surface as well as the effect of water in the vicinity of the interface are extensively investigated and, as first assumption, might not much depend on the cross-link density.

Outcome of the chapter

This study belongs to the broad field of nanocomposites and more precisely on the understanding of the gluing of surgical adhesives composed of silica nanoparticles. The aim of the presented work is to investigate the behavior of PAAm and PDMA on a silica surface and more importantly the role played by water.

Chapter 2

Simulation methods

Computer simulation is a rather young field whose rise dates back from the 50's. The end of the war makes the computers that had been used to decrypt messages accessible to non-military applications. The modern version of the Markov Chain used in Monte Carlo (MC) simulations was developed by Stanislaw Ulam in the late 40's within the framework of a nuclear weapons project. Compared to MC, the beginnings of Molecular Dynamics (MD) were a bit late. One has to wait until 1957 with Alder and Wainwright to simulate elastic collisions between hard spheres [103]. A long path has been traveled since those first simulations. Nowadays it exists a wide range of computer simulation methods that allow one to investigate different properties of various systems at the desired time and length scale. Computer simulation covers a broad range of methods and developments.

Simulations are complementary to experiments as well as theoretical and analytical models, and can be used as a bridge between them. On the one hand, experiments provide macroscopic quantities that can be somewhat difficult to interpret in terms of microscopic quantities because of the interplay between parameters. Computer simulations allow to compute microscopic quantities that can be average into macroscopic ones, it is therefore an important and non-negligible tool that helps to understand experimental results. Moreover, computer simulations have the ability to uncouple the effect of several experimental parameters and to highlight the role played by each of them. Computer simulations are sometimes the tool to use when several experimental setups fail to understand an experimental system. On the other hand, theoretical models often rely on important hypotheses that draw the model away from the experimental reality and make theoretical results diffi-

cult to interpret. Computer simulations help refining or validating a theoretical model and allow to rationalize experimentally observed tendencies. Last but not least, thanks to the understanding that computer simulations provide on molecular systems, we are able to predict properties, behaviors and quantities of the considered system in the desired state. We can then use *in silico* simulations of systems that are not experimentally reachable: at high temperature or pressure for instance. Computer simulations are therefore considered as a mean to extrapolate from what is experimentally reachable.

A broad range of methods is covered by computer simulations. Different methods are adapted to different length, time scale and observable quantities. It is therefore possible to simulate a system at the micro scale, then reach the macro scale and deal with multi scale study of the system. Accessing macroscopic quantities from microscopic ones is done by the mean of statistical physics.

Alongside with this chapter we first present some features of computer simulations that are necessary to the comprehension of the simulation methods that I used during my thesis. We then introduce two methods: Density Functional Theory and Molecular Dynamics.

2.1 Modeling

Computer simulations refer to different simulation methods. Various methods depend on the amount of atoms, the system and the descriptive level of the system one wants to assess. All methods rely on a discrete description of the system as a particle ensemble where particles can be atoms, group of atoms, molecules or even macromolecules. Computer simulations are based on statistical physics whose laws and concepts allow one to establish a link between measured microscopic quantities, such as particles position and energies, to macroscopic observables. Therefore, the basic idea of computer simulation is to probe the *phase space* in order to extract the system properties.

2.1.1 From statistical physics to the modeling of molecular systems

Statistical physics is the bridge between microscopic quantities and macroscopic observables (and therefore comparison with experimental data). From a microscopic point of view, the system of interest can be considered as an ensemble of N point particles which are characterized, at a given time, by a position q_i and a momentum p_i. Each $\{q_i, p_i\}$ state corresponds to a microstate of the system which is, in other words, a microscopic state of the studied system. The microstates ensemble of the N particles of the system is a $6N$ dimension space and corresponds to the phase space. Therefore, a macroscopic quantity A is computed by averaging the corresponding microscopic quantity a over the microstates j weighted by their occupancy probability or *Boltzmann probability* P_j:

$$\langle A \rangle = \sum_j a_j P_j. \tag{2.1}$$

Macroscopic quantities are thus computed by summing over a probability distribution of the microstates. However, when the system is at its equilibrium, its microscopic state fluctuates in the course of time. Due to the high number of microscopic degrees of freedom of the system, it is impossible to directly compute the time evolution of those fluctuations. Instead of considering one unique microstate, Gibbs proposed to consider a large number of microstate replicas in a different microscopic state [104]. The ensemble of microstate replicas has to obey certain external constraints like temperature, volume, pressure, density, ... This ensemble corresponds to a *statistic ensemble*. The statistic ensemble is therefore a bridge between microstates of a system and the related macroscopic observables. Each statistic ensemble is characterized by different thermodynamic conditions that correspond to different experimental conditions. There exist several statistic ensembles and the most notably used ones include:

- the canonical ensemble, defined by a constant number of particles N, a constant volume V and a constant temperature T. It corresponds to a close system of a

constant volume, in equilibrium with a thermostat;

- the microcanical ensemble defined by constant N, V and total energy E;
- the grand canonical ensemble defined by constant chemical potential μ, V and T;
- the isenthalpic-isobaric ensemble defined by constant N, pressure P and enthalpy H;
- the isothermal-isobaric ensemble defined by constant N, P and T.

In this work the canonical and the isobaric-isothermal ensembles have exclusively been used. This choice will be justified later on. The probability of a given microstate depends on the considered statistical ensemble. It is noteworthy that all the statistical ensembles are equivalent, meaning that at the thermodynamic limit, the computed macroscopic quantity does not depend on the considered statistical ensemble. In the canonical ensemble, the probability to find the system in the state j, P_j, is given by:

$$P_j = \frac{\exp(-\beta E_j)}{\sum_j \exp(-\beta E_j)}, \tag{2.2}$$

where $\beta = \frac{1}{k_B T}$ with k_B the Boltzmann constant, E_j is the energy associated to state j and $\sum_j \exp(-\beta E_j) = \mathcal{Z}$ the partition function of the system. The partition function encompasses, based on microstates individual energy, the way probabilities are partitioned among the different microstates. The partition function is a key quantity in statistical physics in the sense that it is necessary for computing all the thermodynamic properties of a system. For non simple systems, it is however impossible to explicitly compute the partition function $\mathcal{Z}$. One can instead numerically compute direct averages of microscopic quantities in the statistical ensemble. If we consider a system with M different configurations C_k, one can average over the different configurations C_k of the microscopic quantity $a(C_k)$:

$$\langle A \rangle = \frac{1}{M} \sum_{k=1}^{k=M} a(C_k), \tag{2.3}$$

where the different configurations C_k are generated by sampling the phase space. In order to obtain a realistic value of $\langle A \rangle$, a good sampling of the phase space is of first importance.

However, due to the complexity of the studied systems and the related phase space, it is sometimes impossible to sample the whole phase space and therefore to consider all the accessible configurations C_k of the system for computational resources reasons. One has to replace an exclusive sampling of the different possible configurations of the system by a representative sampling of the statistical ensemble that guarantees that equations 2.1 and 2.3 are equal.

2.1.2 Sampling the phase space

Computer simulations combined with statistical physics allow one to compute macroscopic quantities of a given system from microscopic information of the system. The macroscopic observable corresponds to the average of the corresponding microscopic quantity over a large number of microstates, where each microstate corresponds to a given point of the phase space. In order to insure a representative sampling of the phase space, the Boltzmann probability, which corresponds to an occurrence probability, is associated to each point of the phase space. In other words, a so-called "rare event" will have associated a small Boltzmann weight, or occurrence probability, while a state which is easy to reach by the system will have an important Boltzmann weight.

Therefore, molecular simulation is all about generating a reasonable phase space sampling in an affordable computation time. There are two main methods to achieve this goal: Molecular Dynamics (MD) and Monte-Carlo (MC) simulations. While MD samples the phase space by following the system evolution over the course of time and generates time averages, MC is a stochastic method that generates ensemble averages. According to the ergodic hypothesis which claims that time and ensemble averages are equivalent, MC and MD sample the phase space in different ways and lead to the same macroscopic computed observable. In this work we consider only MD simulations that have the advantage to follow the time evolution of the system and give access to dynamical quantities.

2.1.3 Periodic boundary conditions

Systems are investigated in computer simulations by considering a simulation cell with a finite volume V and a finite number of particles N. Due to limited computational resources, it is not possible to simulate simulation cells with large N and V that would mimic macroscopic experimental systems. Simulated systems have therefore a large portion of particles that are found to be on the surface of the simulation cell. This feature leads to strong boundary effects that cannot be neglected and that modify the system behavior. The *periodic boundary conditions* (PBC) are used to avoid this computational artifact. PBCs consist of duplicating the simulation cell in one, two or the three space dimensions. Large systems approximated by PBCs therefore consist of a pseudo infinite number of unit cells where one of these is the original simulation cell, and others are copies called *images*. A particle from the original simulation cell will interact with the other particles in the same cell, but also with particles from the images. The pseudo infinite system that is obtained with this method limits boundary effects. PBCs do not impact the computation of short range Van der Waals interactions.

Figure 2.1 is a representation of the use of PBCs when the simulation cell contains one yellow glue stick, one red polymer chain, one spaghetti plate and one black nanoparticle. The simulation cell (in red) is infinitely reproduced in the two directions. Therefore, the yellow glue stick of the original simulation cell interacts with the red polymer chain on its right in the same simulation cell and also with the polymer chain that is on his left in the neighboring simulation cell. Practically, only the red simulation cell is simulated. If the yellow glue stick leaves the red simulation cell through its left side, it will reappear on the right of the red simulation cell.

Computer simulations can be performed at different time and length scales. Different scales imply different methods, models and hypotheses. The range of lengths that are covered by molecular simulations goes from the electronic scale where simulated systems are several Å wide to the macroscale were the characteristic length of the considered sys-

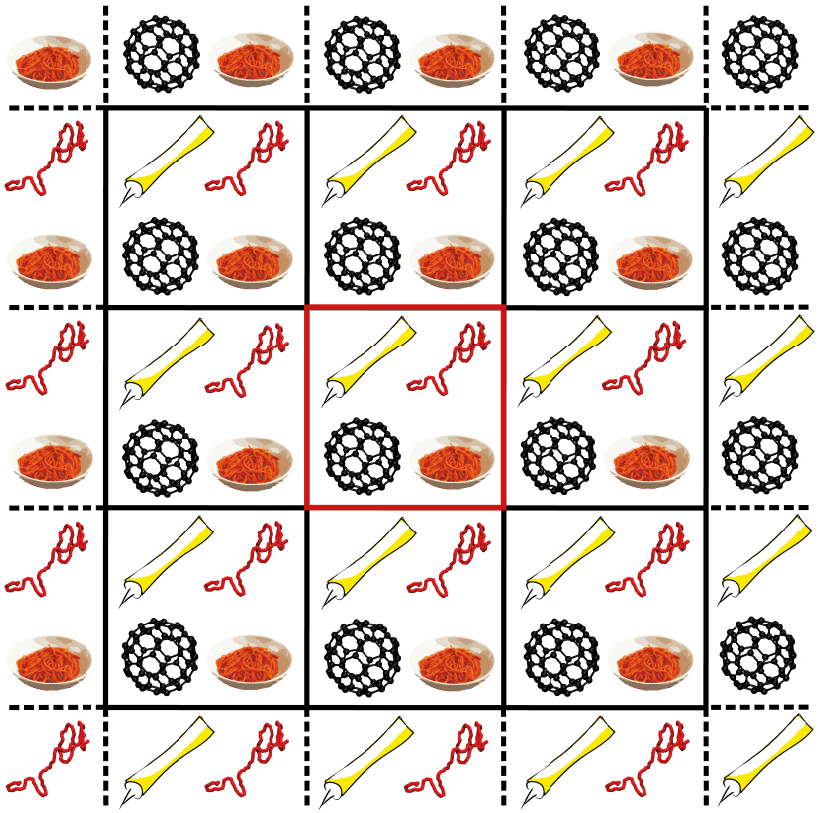

Figure 2.1 – Representation of PBC in two dimensions. The simulation cell, in red, is infinitely reproduced in the two directions.

tem is μm or even mm. In this project I used a quantum method: the Density Functional Theory (DFT) and a molecular method, the MD. We now present in more details this two methods.

2.2 Density functional theory

2.2.1 Schrödinger equation and density functional theory

The electronic scale, through quantum mechanics methods, gives insights into the chemical interactions of the polymer/NP interface, that is to say into the adsorption of polymers on the silica NP surface (adsorption type, through covalent or non-covalent binding, hydrogen-bonds formation, van der Waals interaction, *etc.*). Due to the high computational cost of the electronic methods, one has to consider small systems. In our case, a flat, well organized silica surface and small polymer fragments will be considered.

We now consider a system containing n electrons and N nuclei. We use the Born-Oppenheimer approximation for this system [105], in which the nuclei are considered as immobile compared to the move of electrons, the mass of nuclei being larger than the mass of electrons. This approximation encompasses the fact that electrons move fast and they instantaneously adapt to the move of nuclei. Within this approximation, the system is described by a polyelectronic wave function $\Psi(\mathbf{r})$ and the Schrödinger equation:

$$\mathcal{H}\Psi(\mathbf{r}) = \left(-\sum_i \frac{1}{2}\nabla^2_{r_i} - \sum_{k,i} \frac{Z_k}{|\mathbf{R}_k - \mathbf{r}_i|} + \sum_{i<j} \frac{1}{|\mathbf{r}_i - \mathbf{r}_j|} \right) \Psi(\mathbf{r}), \tag{2.4}$$

where $-\sum_i \frac{1}{2}\nabla^2_{r_i}$ is the kinetic energy of the electron i, $\frac{Z_k}{|\mathbf{R}_k - \mathbf{r}_i|}$ the interaction energy between nucleus k and electron i, $|\mathbf{R}_k - \mathbf{r}_i|$ the distance between nucleus k standing in $\mathbf{R}_k$ and electron i in $\mathbf{r}_i$, $\frac{1}{|\mathbf{r}_i - \mathbf{r}_j|}$ the coulombic interaction energy between electrons i and j and $|\mathbf{r}_i - \mathbf{r}_j|$ the distance between the two electrons. When a system is in a state $|\Psi\rangle$, its energy is $E[\Psi] = \frac{\langle\Psi|\mathcal{H}|\Psi\rangle}{\langle\Psi|\Psi\rangle}$. The variational principle states that the minimization of the functional $E[\Psi]$ with respect to all n-electrons wave functions give the ground state $|\Psi_0\rangle$

and the corresponding energy $E_0 = E[\Psi_0]$.

Electrons being fermions, they respect the Pauli's exclusion principle, hence the wave function has to be antisymmetric. The Slater formalism allows one to express the antisymmetric wave function $\Psi(\mathbf{r})$ as the determinant of monoelectronic wave functions φ_i that are orthogonal to each other:

$$\Psi(\mathbf{r}) = \frac{1}{\sqrt{N}} \begin{vmatrix} \varphi_1(\mathbf{r}_1) & \cdots & \varphi_N(\mathbf{r}_1) \\ \vdots & \ddots & \vdots \\ \varphi_1(\mathbf{r}_N) & \cdots & \varphi_N(\mathbf{r}_N) \end{vmatrix} \tag{2.5}$$

However, it is impossible to solve this system, containing n particles, analytically. There are methods such as Hartree-Fock and post-Hartree-Fock that approach a solution of the electronic wave function by the mean of the variational principle and the mean-field approach.

Another approach is to use the Density Functional Theory (DFT). It is an *ab initio* method that allows one to compute the electronic density of the ground state, ρ_0, without computing the electronic wave function as Hartree-Fock and post-Hartree-Fock methods do. The DFT method is based on two theorems proposed by Hohenberg and Kohn [106]. The first theorem claims that all properties of a system can be determined if the ground state electronic density is known. Within this framework, the system energy E is then a density functional: $E = \mathcal{F}[\rho]$. The second theorem demonstrates that the electronic density that minimizes this functional is exactly the ground state density. This is equivalent to the variational principle for wave functions.

2.2.2 The Kohn-Sham approach

Thanks to Hohenberg and Kohn theorems, the total energy of the system $E_{HK}[\rho]$ can be written as follows:

$$E_{HK}[\rho] = T[\rho] + E_{Ne}[\rho] + E_{ee}[\rho] + E_{NC}[\rho], \tag{2.6}$$

where $T[\rho]$ is the kinetic energy, $E_{Ne}[\rho]$ the interaction potential energy between nuclei and electrons, $E_{ee}[\rho]$ the interaction potential energy between electrons and $E_{NC}[\rho]$ the non-classic contribution to the interaction between electrons.

However, among those terms, the kinetic energy of an interacting electron gas $T[\rho]$ and $E_{NC}[\rho]$ are unknown. Kohn and Sham suggested in 1965 [107] to replace the system containing interacting electrons by a fictitious system containing independent electrons moving in an external potential $V_S = \frac{\partial E_S}{\partial \rho}$. The energy $E_{KS}[\rho_S]$ of the non-interacting Kohn-Sham system, having the ρ_S electronic density, is therefore:

$$E_{KS}[\rho_S] = T_S[\rho_S] + E_S[\rho_S], \tag{2.7}$$

where $T_S[\rho_S]$ is the kinetic energy of the non-interacting system and $E_S[\rho_S]$ is the potential energy associated with the external potential V_S in which non-interacting electrons are moving. The total energy $E_{HK}[\rho]$ of equation 2.6 is then rewritten by introducing the exchange-correlation energy $E_{xc}[\rho]$:

$$E_{xc}[\rho] = T[\rho] - T_S[\rho] + E_{NC}[\rho], \tag{2.8}$$

which takes into account correlation effects, or the tendency of electrons having different spin to avoid each other (through the difference $T[\rho] - T_S[\rho]$) and the non-quantum contribution to the interaction between electrons (through the term $E_{NC}[\rho]$). By substituting the expression of $E_{xc}[\rho]$ into 2.6, we obtain:

$$E_{HK}[\rho] = T_S[\rho] + E_{Ne}[\rho] + E_{ee}[\rho] + E_{xc}[\rho]. \tag{2.9}$$

According to the second Hohenberg and Kohn theorem, the electronic density of the interacting system ρ and the electronic density of the non-interacting system are equal if $E_{HK}[\rho]$ and $E_{KS}[\rho]$ are equal. This is equivalent to:

$$E_S[\rho] = E_{Ne}[\rho] + E_{ee}[\rho] + E_{xc}[\rho]. \tag{2.10}$$

Kohn and Sham have therefore reduced a problem of N interacting electrons to a problem of N non-interacting electrons, moving in the V_S potential. The Schrödinger equation has then to be reduced for the fictitious system by developing the Kohn-Sham orbitals in wave functions. Therefore, one has to set a cutoff energy above which the Kohn-Sham orbitals are no longer developed.

2.2.3 Exchange correlation functionals

Nevertheless, the exchange correlation term $E_{xc}[\rho]$ has to be determined. An explicit form of this term is unknown. Therefore, one has to find approximations for this term. The first and most simple form of this term is the Local Density Approximation (LDA) [108]. In this approximation, the electronic density is considered as an uniform gas: the electronic density is homogeneous. The exchange correlation energy is therefore written as:

$$E_{xc}[\rho] = \int d\mathbf{r}\rho(\mathbf{r})\epsilon_{xc}[\rho(\mathbf{r})], \tag{2.11}$$

where $\epsilon_{xc}[\rho]$ is the exchange correlation energy for one electron in a homogeneous electron gas. Even though the LDA functional is adapted to the study of isolated molecules, it has weaknesses when describing condensed phases. In order to fulfill this problem, functionals with a gradient correction have been developed: the so-called Generalized Gradient Approximation (GGA) functionals. They account for the electronic density gradient in the

exchange correlation energy:

$$E_{xc}[\rho] = \int d\mathbf{r}\rho(\mathbf{r})\epsilon_{xc}[\rho(\mathbf{r}), \Delta\rho(\mathbf{r})]. \tag{2.12}$$

2.2.4 Running DFT calculations

DFT calculations were done using the VASP code. Once we have an expression for the exchange correlation functional, the ground state electronic density ρ_0 is computed by minimizing $E_{HK}[\rho]$. In order to do so, we have to solve the following Kohn-Sham differential equations:

$$\left(-\frac{1}{2}\nabla^2 + \frac{\partial E_{Ne}[\rho(\mathbf{r})]}{\partial\rho(\mathbf{r})} + \frac{\partial E_{ee}[\rho(\mathbf{r})]}{\partial\rho(\mathbf{r})} + \frac{\partial E_{xc}}{\partial\rho(\mathbf{r})} \right)\varphi_i = \epsilon_i\varphi_i, \tag{2.13}$$

where φ_i are mono electronic wave functions, or Kohn-Sham orbitals. Because $E_{ee}[\rho(\mathbf{r})]$ and $E_{xc}[\rho(\mathbf{r})]$ depend on the wave functions φ_i through the density ρ, the Kohn-Sham equations are not linear. Therefore, they need to be solved iteratively. The VASP code first performs electronic iterations which are Self Consistent Field (SCF) cycles in order to minimize the electronic energy for given atomic positions. Once the electronic energy is minimized for a given set of atomic positions, atomic nuclei are displaced in order to minimize the forces occurring on the atoms. The electronic energy is then minimized for the new set of atomic positions. DFT calculations consist on atomic iterations, including electronic iterations. The Kohn-Sham equations have therefore to be solved self-consistently. When the system is optimized, *i.e.* forces on the atoms are zeroed, different properties are computed.

We performed DFT calculations using the Vienna Ab-initio Simulation Package (VASP, [109–111]) and the GGA functional developed by Perdew, Burke and Ernzehof (PBE) [112]. The energy cutoff was set to 400 eV and we used a Brillouin zone with one k point. The k points number corresponds to the size of the reciprocal space in which calculations are made and depends on the precision level one wants to reach. Our surfaces being

actually very large, the corresponding Brillouin zone is small.

2.3 Classical molecular dynamics

When systems are large, it is impossible to use quantum calculations. One has to forget about the electronic details of the system and make hypotheses in order to use a less accurate method. In particular, when one wishes to erase the electronic details, the Born-Oppenheimer approximation is no longer necessary. Electrons are considered localized in the atom nucleus.

Several methods allow to probe atomic configurations. The most used ones are Monte-Carlo (MC) and Molecular Dynamics (MD). Classical molecular dynamic allows one to sample the phase space of a system, starting from an initial configuration $\{\mathbf{r}(0), \mathbf{v}(0)\}$. Discrete integration of Newton's motion equation generates a trajectory of atomic positions over the course of time. Generalization of Newton's second law states that the classical equation of motion of a system containing N particles, each particle experiencing a force $\mathbf{F}_i$ due to all the other particles in the system and possibly the external environment is:

$$\mathbf{F}_i = m_i \mathbf{a}_i = m_i \frac{\partial \mathbf{v}_i}{\partial t}, \tag{2.14}$$

where m_i is the mass of particle i, $\mathbf{a}_i$ its acceleration and $\mathbf{v}_i$ its velocity.

If we consider a macroscopic quantity A, it is computed by averaging its microscopic equivalent $a(t)$ over an infinitely long simulation:

$$\langle A \rangle = \lim_{\tau \to \infty} \frac{1}{\tau} \int_{t_0}^{t_0+\tau} a(t) \mathrm{d}t, \tag{2.15}$$

where τ is the simulation length and t_0 is the initial step of the simulation. Molecular dynamic has the advantage to give simultaneous access to equilibrium quantities, through their time averaged value, and to dynamical properties, through temporal correlation

functions. This aspect is not covered by other equilibrium methods such as Monte-Carlo. In order to use molecular dynamics correctly, a system has to be ergodic, *i.e.* the time average is equivalent to the ensemble average. This corresponds to a system that evolves for an infinite time and samples the full energy landscape.

There are three important features in a molecular dynamics simulation that have to be carefully chosen: (i) the algorithm to integrate the Newton's equations motion (ii) the interaction parameters to compute forces between particles and (iii) the statistical ensemble.

2.3.1 The velocity Verlet algorithm

In molecular dynamics, the Newton's equations of motion have to be numerically integrated. For this task, we need a numerical integrator. The *Verlet* algorithm is the simplest integrator algorithm. However, it does not explicitly computes the velocities. The *velocity Verlet algorithm* [113] is derived from the Verlet algorithm and includes explicit computation of particles velocity. This integrator generates phase space vectors at different discrete times that are multiple of a time step Δt. There is then a simple way to calculate the position of the particle i, $\mathbf{r}_i$ at a time $t + \Delta t$ by using a Taylor serie:

$$\mathbf{r}_i(t + \Delta t) \approx \mathbf{r}_i + \frac{\partial \mathbf{r}_i}{\partial t}\Delta t + \frac{\partial^2 \mathbf{r}_i}{\partial t^2}\frac{\Delta t^2}{2!} + \frac{\partial^3 \mathbf{r}_i}{\partial t^3}\frac{\Delta t^3}{3!} + \mathcal{O}(\Delta t^4). \tag{2.16}$$

Because $\frac{\partial \mathbf{r}_i}{\partial t} = \mathbf{v}_i$, $\frac{\partial^2 \mathbf{r}_i}{\partial t^2} = \mathbf{a}_i$, $\mathbf{F}_i = m_i \mathbf{a}_i$ and all terms above the second order in Δt are neglected, equation 2.16 can be rewritten as:

$$\mathbf{r}_i(t + \Delta t) \approx \mathbf{r}_i(t) + \mathbf{v}_i(t)\Delta t + \frac{\mathbf{F}_i(t)}{2m_i}\Delta t^2. \tag{2.17}$$

If we now start from $\mathbf{r}_i(t + \Delta t)$ and $\mathbf{v}_i(t + \Delta t)$, compute $\mathbf{F}_i(t + \Delta t)$ and use

$$\mathbf{r}_i(t) \approx \mathbf{r}_i(t + \Delta t) - \mathbf{v}_i(t + \Delta t)\Delta t + \frac{\mathbf{F}_i(t + \Delta t)}{2m_i}\Delta t^2 \tag{2.18}$$

to get $\mathbf{r}_i$(t). We now substitute 2.17 in 2.18, we get $\mathbf{v}_i(t + \Delta t)$:

$$\mathbf{v}_i(t + \Delta t) = \mathbf{v}_i(t) + \frac{[\mathbf{F}_i(t) + \mathbf{F}_i(t + \Delta t)]}{2m_i}\Delta t^2. \tag{2.19}$$

The velocity Verlet algorithm uses equations 2.17 and 2.19 to compute, at the same time step, particles position and velocity. It then evolves the system in time and computes a trajectory of the desired length. The time step Δt has to be carefully chosen. Δt must lower than the characteristic time of the phenomenon one wants to investigate. Therefore, Δt should be sufficiently small in order to maintain the integration numerically stable, and sufficiently long to correctly sample the space phase in a reasonable time. Δt is typically on the order of the femtosecond (10^{-15} second). In our case, $\Delta t = 1$ fs for all atom molecular dynamics simulations and $\Delta t = 10$ fs for coarse-grained molecular dynamics simulations. Our simulations are from 50 ns to 500 ns long.

2.3.2 Force field

A second important feature of molecular dynamics simulation is the choice of an appropriate force field. A force field is the ensemble of interaction potential chosen for a given system. The mathematical form of the interaction potentials as well as the parameters have to be carefully selected. As we do not use the electronic description, interactions between classical particles are empirically described by classical interaction potentials. The total potential energy of a system is defined as the sum of two contributions:

$$U = U_{nonbonded} + U_{bonded}, \tag{2.20}$$

where $U_{nonbonded}$ accounts for interactions between particles that are not chemically bonded and U_{bonded} describes the interactions between particles within the same molecule. Several forms of $U_{nonbonded}$ and U_{bonded} can be used, depending on the studied system.

Nonbonded interactions

For a sake of simplicity, we consider only two-body terms for the nonbonded interaction term. Four-body and higher terms are expected to be very small and are therefore neglected. Three-body terms are known to be relatively important in the liquid phase, however the calculation of quantity involving a sum over triplets of molecules will be computationally demanding. Three-body terms are therefore neglected. Considering two-body, *i.e.* pairwise interactions, is fortunately sufficient to lead to satisfactory results. N-body terms are implicitly taken into account in the two-body terms parametrization. Pairwise interactions are usually the sum of three components:

- coulombic interaction,
- dispersion,
- repulsion.

Firstly, the dispersion $U_{LJ}^{A}(r)$ and repulsion $U_{LJ}^{R}(r)$ (represented in figure 2.2) are taken into account as the sum of two terms in one potential, the Lennard-Jones (LJ) potential:

$$U_{LJ}(r) = U_{LJ}^{R}(r) + U_{LJ}^{A}(r), \text{with} \tag{2.21}$$

$$U_{LJ}^{R}(r) = \begin{cases} U_{LJ}(r) + \epsilon & r < r_{min} \\ 0 & r_{min} \leq r \end{cases}$$

$$U_{LJ}^{A}(r) = \begin{cases} -\epsilon & r < r_{min} \\ U_{LJ}(r) & r_{min} \leq r \end{cases}$$

The LJ potential is defined as the following:

$$U_{LJ}(r) = 4\epsilon\left[\left(\frac{\sigma}{r}\right)^{12} - \left(\frac{\sigma}{r}\right)^{6}\right], \tag{2.22}$$

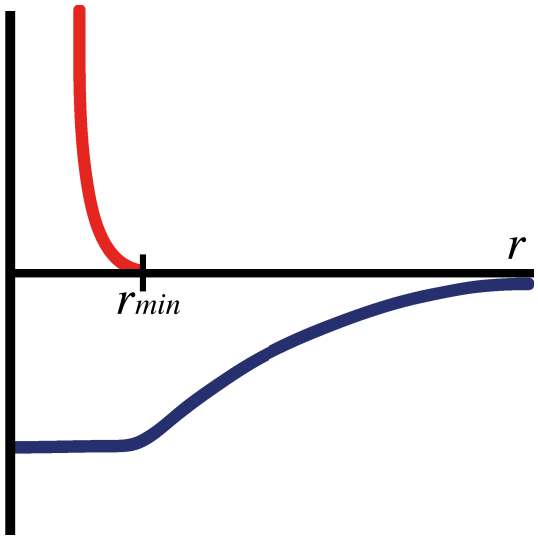

Figure 2.2 – Repulsive part of the LJ potential (red) and attractive part (blue).

where ϵ is the depth of the potential well, σ the length at which the potential value is minimum and $r_{min} = 2^{1/6}\sigma$ the finite distance at which the inter-particle potential is zero. For charged particles, the LJ potential is not enough to represent long-range interactions.

Secondly, the coulombic, or electrostatic, interaction accounts for interactions within two charged particles, or within one charged particle and a dipole, or within two dipoles. The coulombic potential reads:

$$U_{coul}(r) = \sum_i \sum_{j>i} \frac{q_i q_j}{4\pi\epsilon_0 r_{ij}}, \tag{2.23}$$

where q_i and q_j are the charges of respectively atoms i and j, r_{ij} the distance between atoms i and j and ϵ_0 the permittivity of free space. Polarization is not taken into account in our model.

2.3.3 Thermostat and barostat

As mentioned in section 2.1.1, all the thermodynamic ensembles are equivalent in the thermodynamic limit. Simple integration of the Hamilton's equations of motion leads to a microcanonical ensemble where the energy of the system is conserved. The natural ensemble of MD simulations is therefore the (N, V, E) ensemble. However, the work of Andersen generalized MD to simulations at "constant pressure and/or temperature" [114].

One may want to use (N, V, T) or (N, P, T) ensembles that are closer to experimental conditions because temperature and/or pressure are imposed. Within those ensembles, the energy is not conserved and therefore fluctuates. Although in the thermodynamic limit these fluctuations are small and can be neglected, it is not the case in finite size. In order to control the temperature or the pressure, one has to respectively use a thermostat or a barostat. While a thermostat corresponds to a thermal bath that exchanges energy with the system, a barostat relies on an external force that allows to reach the desired pressure for the system. There exists a wide range of thermostat and barostat whose use depends on the considered system and the targeted properties. Herein, we exclusively present the thermostat and barostat that were used, which are the ones developed by Nosé and Hoover [115, 116] and are rather widely used methods.

Thermostat

In the canonical (N, V, T) ensemble, energy fluctuates in order to fulfill the required Boltzmann distribution of energy due to the exchange of energy with the thermal bath. The role played by the thermostat is to mimic the effect of a thermal bath coupled with the system by acting on the kinetic energy and therefore the velocity of particles. There are several ways to fulfill the constraint on temperature.

The first one, which is the most simple one, rescales periodically the velocity of the particles. However, this method does not insure generation of a canonical phase space and can disturb the system dynamics. Another method is to periodically rescale part of the velocities, according to a collision frequency f_c. The probability that a particle undergoes a collision with another particle in a time Δt is $f_c \Delta t$. A random number between 0 and 1 is generated. If this random number is less that $f_c \Delta t$, the particle's velocity is then rescaled. The latter method introduces an additional variable to mimic the effect of the thermal bath.

Yet another method relies on the idea first developed by Nosé [115] and uses the sim-

plified formulation of Nosé's equations by Hoover [116]. Nosé introduces an extended Hamiltonian $\mathcal{H}_{\mathcal{N}}$. It contains a new coordinate s that insures that whether the kinetic energy fulfills the required temperature T of the canonical ensemble:

$$\mathcal{H}_{\mathcal{N}} = \sum_{i=1}^{N} \frac{\mathbf{p}_i^2}{2m_i s^2} + U(\mathbf{r}_1, \ldots, \mathbf{r}_N) + \frac{p_s^2}{2Q} + g k_B T \ln s, \tag{2.24}$$

where m_i is the particle mass, $\mathbf{r}_i$ the particle position, $\mathbf{p}_i$ the particle momentum, Q the time scale on which velocities are rescaled, p_s the new coordinate momentum and g the number of independent momentum degrees of freedom of the system. The resulting Hamiltonian $\mathcal{H}_{\mathcal{N}}$ has 6N + 2 degrees of freedom. One can tune the parameter Q and play on the relaxation time of the thermal bath. However, a simple Nosé-Hoover requires an additional conservation law that results in a distribution for the positions and momentum that is not Gaussian. The resulting phase space distribution is therefore non canonical. In order to correct the failure of Nosé-Hoover equations, one has to rather use a Nosé-Hoover chain that insures a Boltzmann distribution of momentum. See pp. 190-196 of reference [117] for more details on Nosé-Hoover chains.

Barostat

Performing simulations at constant temperature and pressure is necessary when one wants to be representative of experiments that are not done at constant volume. For instance, redox potentials, equilibrium constant and free energies of formation are experimental data reported at constant pressure and temperature. In order to maintain the desired pressure within the simulated system, one has to allow the fluctuations of the volume. The system is therefore coupled to an external force that compresses or expands the system in order to reach the required internal pressure of the system. This can be done by using the Nosé-Hoover barostat that is similar to the thermostat designated with the same name that we just described. The Nosé-Hoover barostat modifies the equations of motion in order to take into account the effect of the external force that modifies the particles position and velocities and the simulation cell volume in order to fulfill the required pressure.

2.4 Coarse-grained methods

As previously mentioned in chapter 2 an important limitation in computer simulation is computational time. From this restriction comes out the necessity to select the right method considering for instance the level of description and the quantity one wants to perform. Figure 2.3 is a graphical representation of the different time and length scales and the regarding methods that one would find in computer simulation of molecular systems. The work that is presented in this manuscript is related to the simulation of nanocomposite systems that are composed of polymers and silica nanoparticles. The typical size of nanoparticles is in the order of several tens of nanometer, corresponding to the NP's radius, and of polymer is from few to tens of nanometer, corresponding to the distance between cross-links. Over a first phase, we do not consider a system containing a large number of cross-links and of NP. Therefore, the typical order of magnitude of this system is of hundreds of nanometers. Regarding time scale, polymers are large molecules whose rearrangement can overlay a large range of time scale. Our model does not cover the reptation dynamic of polymer chains, which characteristic time can reach milliseconds or even seconds. In this work I limited myself to time scale up to hundreds of nanoseconds, that allow to observe chains reorganization but not reptation. Therefore, according to figure 2.3, the *coarse-grained molecular dynamics* (CGMD) is adapted to the investigated system. The overall idea of coarse-grained methods is to mask some of the atomic details in order to achieve larger systems for longer time scales. As there is a wide range of CG methods, we cut back in this section to CG methods applied to polymer science.

2.4.1 Coarse-graining in polymer simulations

The CG method one chooses logically depends on the addressed physical problem and the quantity one wants to compute. There exists a wide range of CG methods and we are not exhaustive in this chapter [118, 119]. We instead introduce the most widely used methods. These will be distinguished between the so-called *lattice* methods, where the CG model is defined on a lattice and *off-lattice* methods which consider space as a continuum.

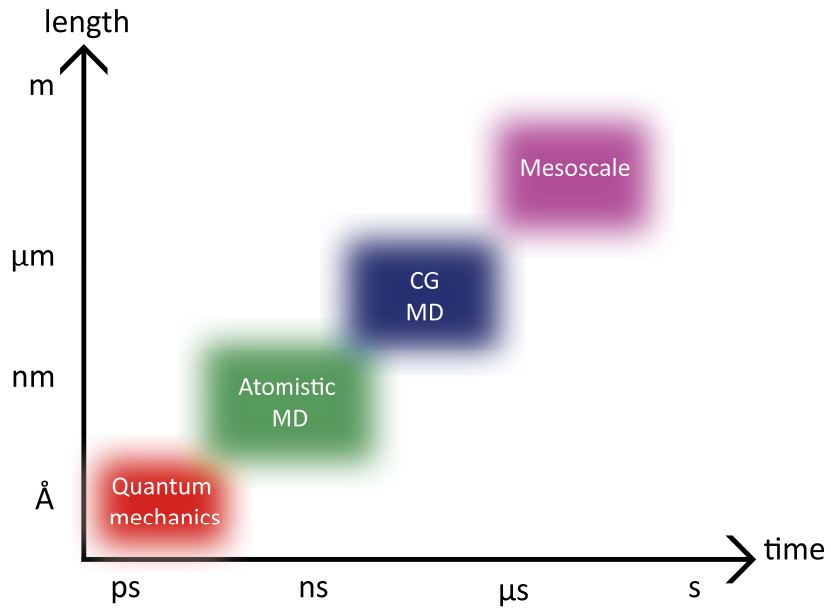

Figure 2.3 – Representation of different length and time scale in molecular simulations and the related methods.

Lattice models

In lattice models, a regular lattice is considered where effective polymer beads are placed on lattice points and a bond between two beads is a nearest-neighbor link on the lattice (see figure 2.4). The polymer's move is represented by a random walk on the defined lattice or by a self-avoiding walk on the lattice. Since two lattice nodes cannot be occupied by two polymer beads, this automatically creates an excluded volume interaction. The most simple lattice that one can use is a cubic lattice, as represented in figure 2.4. In such configuration, the polymer beads rotation is restrained to 0 or 90 degrees. This is an important idealization, but which does not trouble the computation of large-scale quantities. We now present some lattice algorithms.

In the pivot algorithm, one random link of the polymer chain is chosen and this link together with the rest of the chain is rotated to a new random orientation [120]. The move is accepted if the newly generated configuration does not violate the excluded volume constraint (see figure 2.4(a)). Such algorithm allows to efficiently and rapidly generate new configurations that are independent from one to the other. However, this algorithm does not allow the study of dynamical properties and cannot be used to generate dense

polymer systems.

The collective motion algorithm allows to simulate dense polymer systems and to introduce large reorganizations of polymer chains [121]. It rearranges the polymer chain by moving collectively several segments of it. For instance, a kink of a polymer chain is translated from one place on the polymer chain to another one (see figure 2.4(b)). The total motion involves several chain motions of the polymer chain and can extend to several chains. However, due to the fact that chains rearrangements are non local, this algorithm is difficult to parallelize.

We finally introduce the bond fluctuation model, which is in a sense intermediate between lattice models and off-lattice models [122–125]. This model is built on a lattice, and has the related benefits: it comprises the excluded volume constrain and allows efficient computation. Moreover, the bond that connects two beads can take a large range of values and therefore approximate a continuum behavior. In this model, a monomer corresponds to four occupied sites of the lattice. Two lattice sites cannot be occupied by two different monomers, which insures excluded volume constrain. The bond length does not have a fixed value, but varies between a bottom (d_b) and a top (d_t) value. Polymer chain moves consist in local jumps of the monomers. The algorithm works as follow: one random monomer is chosen and undergo a trial move. This move consists in a jump into one of the four lattice directions, with a distance of one lattice unit, to reach another lattice site (see figure 2.4(c)). This trial move is accepted if it satisfies two conditions: (i) the bond length must be between d_b and d_t and (ii) the excluded volume restriction must be respected.

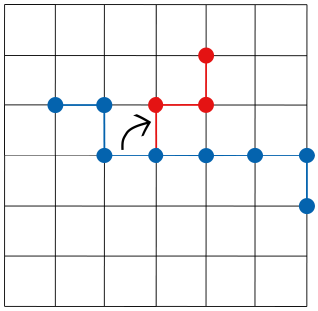

(a) Pivot algorithm.

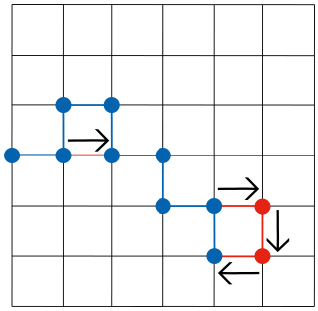

(b) Collective motion algorithm.

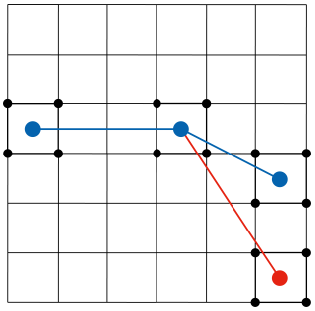

(c) Bond fluctuation algorithm.

Figure 2.4 – Representation of three lattice methods. The lattice is in black, initial configuration of the chain is in blue (beads are depicted as plain circles and bonds as solid lines), final configuration is in red and arrows indicate the direction of the move.

Off-lattice models

Off-lattice methods, as opposed to lattice models, are simulated on a continuum space and are referred to as *particle-based methods*. Here again, considering the large number of off-lattice methods that have been developed, we are not exhaustive but we rather present the most used models.

First of all, the *united atoms* is certainly the most popular particle-based CG model. Its basic idea is rather simple. Instead of explicitly taking into account all the atomistic details of polymeric chains, which is oftentimes not necessary and not computationally feasible to investigate polymeric systems, one can group several atoms into one bead. The bead size varies according to the desired description level, the system size and the quantities one wants to compute. One bead can map part of a monomer, one monomer or even several monomers of the polymer chain. These beads are then linked by bonds. The bonds can be rigid, as in the freely jointed chain model, where beads are considered as dots. In the pearl-necklace, beads are hard-sphere that cannot overlap and bond lengths freely vary between a bottom and a top length value [126, 127]. These conditions insure that chains cannot cross each other.

The mostly used off-lattice model is certainly the bead-spring model where neighboring

beads are connected by springs. Springs usually correspond to an anharmonic potential which is the finite extensibility nonlinear elastic (FENE) potential U^{FENE} [128–132]:

$$U^{FENE}(r_{ij}) = \begin{cases} -0.5kR_0^2 \ln[1 - (r_{ij}/R_0)^2] & r_{ij} \leq R_0 \\ \infty & R_0 < r_{ij}, \end{cases}$$

where r_{ij} is the bond distance between two neighboring beads and R_0 and k are constants that are chosen according to the ϵ and σ parameters of the LJ potential defined in equation 2.22 such as $R_0 = 1.5\sigma$ and $k = 30\epsilon/\sigma^2$. Nonbonded interactions between beads are described with the previously defined LJ potential.

Such bead-spring model is widely used in MD, but also in brownian dynamics (BD) simulations. BD is a modification of MD that allows to remove the detailed motion of solvent molecules by representing the solvent effect with random and dissipative force terms.

Even though the bead-spring model using the FENE potential is widely used with different types of polymeric systems [61, 133–135], it is usually used with rather large beads, that it to say beads that map together an important number of atoms. Using the FENE potential also requires a complete parametrization of both bonded and nonbonded interactions, which is usually a long stage. We instead used a more flexible model, that allows a rather fine coarse-graining of the atoms and that directly provides bonded and nonbonded interaction parameters: the Martini force field [136–139].

2.4.2 Martini force field

The Martini model is a CG force field for molecular systems whose first version dates back from 2004 and was developed by the Marrink group [136]. The Martini force field was originally developed with parameters for lipids only. Further versions [137, 138, 140] extended the model to proteins, peptides and is now extensively used for polymers. We

use the improved version by Marrink *et al* in 2007 [137]. The overall aim of the Martini CG approach is to provide a simple model that is computationally fast and easy to use, yet flexible enough to be applicable to a large range of biomolecular systems. The Martini force field has been successfully used for a variety of biomolecules, including lipids [136], sugars [141], proteins [138], and polymers such as polystyrene [142], polyethylene oxide and polyethylene glycol [143], polycaprolactam [144], and poly(methyl methacrylate) [145].

The Martini force field is based on a four-to-one mapping, meaning that one CG bead represents on average four heavy atoms and connected hydrogens. This choice is a compromise between computational efficiency and chemical representativeness. The Martini model has four main types of CG bead: polar (P), nonpolar (N), apolar (C) and charged (Q). Each particle type has several subtypes. This allows for a more detailed description of the underlying atomistic structure. There is a total of eighteen subtypes. For example, polar beads are distinguished by a number indicating the degree of polarity (from 1 for low polarity to 5 for high polarity). Nonpolar beads are distinguished by a letter indicating the hydrogen-bonding capability (*d* for donor and *a* for an acceptor of a hydrogen bond, *da* for both and 0 for none). The use of eighteen subtypes of beads allows one to set up a rather complicated molecule, with a limited number of building blocks. We used them to design the CG model of the polymers PAAm and PDMA, of the silica surface and of water.

In the Martini force field, interactions are treated in a simple manner. There are two kinds of interactions: bonded interactions between chemically connected sites and nonbonded interactions.

Nonbonded interactions within the Martini force field

Nonbonded interactions are described by a Lennard-Jones (LJ) 12-6 potential (see equation 2.22) and by Coulombic interactions. However, there are typically no Coulombic interactions explicitly considered for noncharged polymers [142–144].

The strength of the interaction, determined by the value of the LJ well depth ϵ_{ij}, depends on the interacting beads i and j. The ϵ_{ij} for normal beads (beads that map four or more atoms) are found in the interaction matrix given in the paper from Marrink and co-workers [137]. The interaction matrix is reproduced in figure 2.5. Each sign from O to IX refers to a different ϵ_{ij}, from 5.6 kJ/mol for O to 2.0 kJ/mol for IX. This interaction matrix directly gives the ϵ_{ij} that corresponds to the type of beads we consider among the eighteen bead type provided by the Martini force field.

TABLE 1: Interaction Matrix[a]

		Q				P					N				C				
	sub	da	d	a	0	5	4	3	2	1	da	d	a	0	5	4	3	2	1
Q	da	O	O	O	II	O	O	O	I	I	I	I	I	IV	V	VI	VII	IX	IX
	d	O	I	O	II	O	O	O	I	I	I	III	I	IV	V	VI	VII	IX	IX
	a	O	O	I	II	O	O	O	I	I	I	I	III	IV	V	VI	VII	IX	IX
	0	II	II	II	IV	I	O	I	II	III	III	III	III	IV	V	VI	VII	IX	IX
P	5	O	O	O	I	O	O	O	O	O	I	I	I	IV	V	VI	VI	VII	VIII
	4	O	O	O	O	O	I	I	II	II	III	III	III	IV	V	VI	VI	VII	VIII
	3	O	O	O	I	O	I	I	II	II	II	II	II	IV	IV	V	V	VI	VII
	2	I	I	I	II	O	II	II	II	II	II	II	II	III	IV	IV	V	VI	VII
	1	I	I	I	III	O	II	II	II	II	II	II	II	III	IV	IV	IV	V	VI
N	da	I	I	I	III	I	III	II	II	II	II	II	II	IV	IV	V	VI	VI	VI
	d	I	III	I	III	I	III	II	II	II	II	III	II	IV	IV	V	VI	VI	VI
	a	I	I	III	III	I	III	II	II	II	II	II	III	IV	IV	V	VI	VI	VI
	0	IV	IV	IV	IV	IV	IV	IV	III	III	IV	IV	IV	IV	IV	IV	IV	V	VI
C	5	V	V	V	V	V	V	IV	IV	IV	IV	IV	IV	IV	IV	IV	IV	V	V
	4	VI	VI	VI	VI	VI	VI	V	IV	IV	V	V	V	IV	IV	IV	IV	V	V
	3	VII	VII	VII	VII	VI	VI	V	V	IV	VI	VI	VI	IV	IV	IV	IV	IV	IV
	2	IX	IX	IX	IX	VII	VII	VI	VI	V	VI	VI	VI	V	V	V	IV	IV	IV
	1	IX	IX	IX	IX	VIII	VIII	VII	VII	VI	VI	VI	VI	VI	V	V	IV	IV	IV

[a] Level of interaction indicates the well depth in the LJ potential: O, $\epsilon = 5.6$ kJ/mol; I, $\epsilon = 5.0$ kJ/mol; II, $\epsilon = 4.5$ kJ/mol; III, $\epsilon = 4.0$ kJ/mol; IV, $\epsilon = 3.5$ kJ/mol; V, $\epsilon = 3.1$ kJ/mol; VI, $\epsilon = 2.7$ kJ/mol; VII, $\epsilon = 2.3$ kJ/mol; VIII, $\epsilon = 2.0$ kJ/mol; IX, $\epsilon = 2.0$ kJ/mol. The LJ parameter $\sigma = 0.47$ nm for all interacion levels except level IX for which $\sigma = 0.62$ nm. Four different CG sites are considered: charged (Q), polar (P), nonpolar (N), and apolar (C). Subscripts are used to further distinguish groups with different chemical nature: 0, no hydrogen-bonding capabilities are present; d, groups acting as hydrogen bond donor; a, groups acting as hydrogen bond acceptor; da, groups with both donor and acceptor options; 1−5, indicating increasing polar affinity.

Figure 2.5 – Martini's interaction matrix for ϵ_{ij} parameters, provided by reference [137].

In the case of small beads (beads that map two or three atoms), ϵ_{ij} is scaled to 75% of the standard value. The effective size of the particles is governed by the LJ parameter σ_{ij}. σ_{ij}, which is 0.47 nm for normal particles and 0.43 nm for small particles. The LJ potential is shifted to zero between 0.9 nm and 1.2 nm.

Bonded interactions within the Martini force field

Bonded interactions between two chemically connected beads are described by a harmonic potential $V_{bond}(r)$:

$$V_{bond}(r) = \frac{1}{2}K_{bond}(r - r_0)^2, \tag{2.25}$$

where r is the distance between two beads, K_{bond} the force constant of the harmonic bonding potential, and r_0 the equilibrium distance. Angles between three neighboring beads are governed by the potential $V_{angle}(\theta)$:

$$V_{angle}(\theta) = \frac{1}{2}K_{angle}[cos(\theta) - cos(\theta_0)]^2, \tag{2.26}$$

where θ is the angle between the three beads, K_{angle} the force constant and θ_0 the equilibrium angle. We decided not to use dihedral potential for the sake of simplicity. The Martini paper [137] provides general values for K_{bond}, K_{angle}, r_0 and θ_0. We find those values not adapted to our system, which is a rather fine grained model, *i.e.* containing small beads. We have thus reparametrized our CG model, on the basis of input from all atom simulations. Parameters for the bond and angle potentials were obtained by comparing distributions from all atom simulations with distributions from CG simulation. The parametrization stage will be explained in more details in the following chapter 3.

2.5 Numerical details

The DFT calculations that will be presented in this manuscript were done using the *Vienna Ab initio Simulation Package* (VASP) [109–111]. MD simulations were performed using the *Large-scale Atomic Molecular Massively Parallel Simulator* (LAMMPS) code [146, 147]. Calculations were performed using the computational resources of the Mathematical Department of the Technische Universität Berlin, of the Chemistry Department of the École normale supérieure, of the Curie supercomputer (CEA) and of the Occigen supercomputer (CINES).

Outcome of the chapter

The work presented in this manuscript is mostly based on statistical thermodynamics applied to coarse-grained molecular dynamics simulations using the Martini force field. Part of the work was carried out using quantum mechanics based on the density functional theory.

Chapter 3

Modeling nanocomposite materials

In the two previous chapters, we highlighted various difficulties that arise when dealing with nanocomposite systems. They are due to the complexity of such systems in which a large number of phenomena are coupled. It is therefore a challenging task to find the right method, model and level of description to simulate the system and compute key quantities.

The system we are interested in consists in a hydrogel interacting with silica NPs. The idea is to understand the strengthening mechanism of the hydrogel by the introduction of silica NPs. My approach is to couple the large-scale mechanical properties of the nanocomposite system to local interactions between polymer chains and silica NPs. This will therefore give insight into the link between the adsorption of polymers on the NPs surface and the resulting mechanical properties.

3.1 Density functional theory to model the polymers and silica

In order to investigate how the reinforcement of a PDMA hydrogel by the presence of silica NPs arises from the adsorption chemistry, I started with using quantum mechanics through the DFT method in order to probe the adsorption of PAAm and PDMA on silica NPs. We performed DFT calculations using the Vienna Ab-initio Simulation Package (VASP, [109–111]) and the GGA functional developed by Perdew, Burke and Ernzehof (PBE) [112].

3.1.1 The model

As already mentioned, DFT calculations require important computational resources. The system one wants to simulate has to be rather small, limited to hundreds of atoms. It is therefore not possible to simulate large reticulated polymer chains and amorphous silica. The first thing I did was to design a model for the polymers and for silica NPs that can be investigated with DFT and that is not too computationally demanding.

PAAm and PDMA

A simple and economical model for polymer chains is to consider few repeating units. We considered one and ten repeating units for PAAm and PDMA. These two kinds of polymer length will be referred as "monomer" for the polymer containing one repeating unit and as "decamer" for the one containing ten repeating units. Different chain types and lengths were relaxed using first an all atom MD simulation and then a DFT calculation. The MD simulation insures that the phase space is correctly probed and that polymers do not remain in a metastable state. The following DFT calculation is necessary to have a correct reference of the polymers for further adsorption energy calculations.

Silica surface

The model used for silica NPs is slightly more complicated. First, it is not possible to consider spherical nanoparticles with a radius from 5 to 15 nm. Instead, a flat silica surface is simulated. Moreover, when simulating surfaces with quantum mechanics, one has to consider a *slab* that is several layers wide in order to reproduce bulk properties of the solid far from the surface (see figure 3.1). There is above the slab a large vacuum in order to prevent interaction of the solid slab with itself thanks to PBC. Therefore, creating a surface is equivalent to creating a solid slab. Atoms that are in the middle of the slab should not feel the presence of a surface in order to insure that they correspond to bulk atoms of the solid. This condition requires that the created solid slab is thick enough and contains several atomic layers. Practically, atoms that are supposed to behave like bulk atoms are frozen (there are thereby equivalent to bulk atoms) and atoms that stand close

to the surface relax through the DFT calculation.

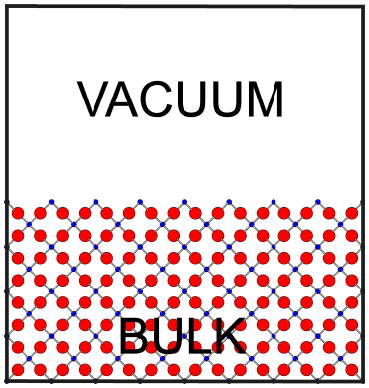

Figure 3.1 – Representation of a solid slab.

Silica surfaces exhibit several types of silanol terminations as one can see from figure 3.2) [148, 149]. There are isolated silanols that do not interact with other silanols of the silica surface, H-bonded silanols that interact *via* hydrogen bonds, vicinal silanols which are two silanols forming a siloxane Si–O–Si bridge and geminal silanols wherein one silicon atom bears two hydroxyls. The averaged silanol density of an amorphous silica surface is 5 OH/nm^2 [150–152]. However, computing an amorphous silica slab that reproduces the right silanol density and silanol terminations was out of range within the framework of the work we present in this manuscript, even if it has already been successfully realized using *ab initio* MD by some authors [153].

The authors of reference [154] propose to assimilate the amorphous silica surface to a heterogeneous surface including regions of 100 and 111 β cristobalite surfaces. The latter is reproduced in figure 3.3. 100 and 111 refer to Miller indices: hkl is the surface that results when cutting the β cristobalite crystal along the $h\mathbf{x} + k\mathbf{y} + l\mathbf{z}$ plane, where $\mathbf{x}$, $\mathbf{y}$ and $\mathbf{z}$ are lattice vectors (see figure 3.4).

β cristobalite is the crystalline structure whose density and refractive index are the closest from amorphous silica. The crystal thanks to its high symmetry, has the advantage to require a small simulation cell and necessitates reasonable computation time, which is not the case of the amorphous silica. The primitive cell of β cristobalite is cubic. Silicon

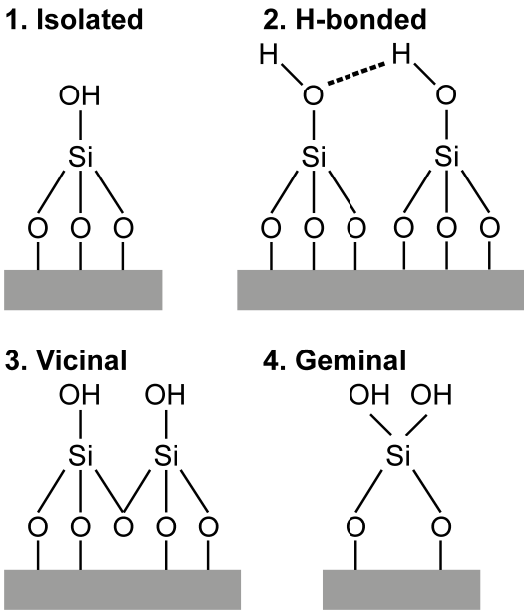

Figure 3.2 – Scheme of silanols on the surface of silica.

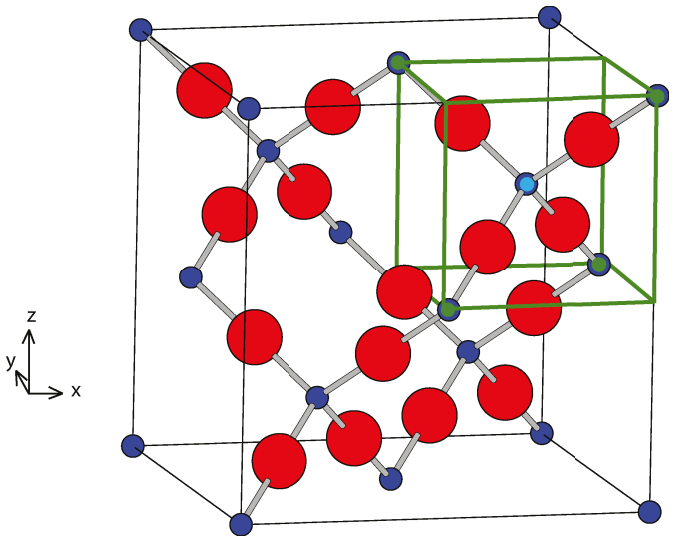

Figure 3.3 – β cristobalite primitive cell (black solid lines). Oxygen atoms are in red and silicon atoms are in blue.

atoms form a face-centered cubic elementary cell and occupy half of the tetrahedral sites, which is analogous to a diamond cell. One tetrahedral site is shown in figure 3.3: the silicon atom with the blue light circle is surrounded by four silicon atoms (the ones within the green cube) that form a tetrahedron. Finally, there is one oxygen atom in between two silicon atoms. This is the high temperature stable phase of silica but can be found at lower temperatures in a metastable state.

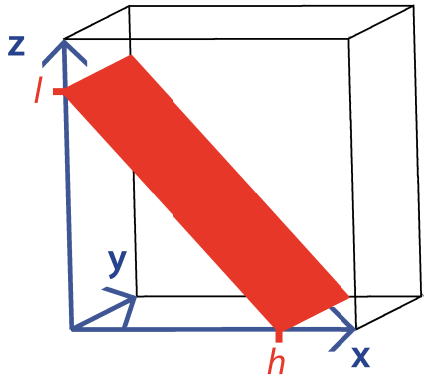

Figure 3.4 – Illustration of a h0l plane.

100 and 111 surfaces show two kinds of silanol terminations: the isolated silanol is on the 111 surface and geminal silanol is on the 100 surface. I have limited myself to the investigation of these two types of silanol termination, isolated and geminal.

First, the infinite β cristobalite crystal was relaxed using DFT calculations and PBC. A cell parameter of 7.35 Å was obtained, which is close to the theoretic value (7.27 Å) obtained by the authors of reference [155] and to the experimental value (7.17 Å). Si-O bond length equals 1.59 Å, which is again close to what is theoretically (1.6059 Å for the authors of reference [156]) and experimentally (1.611 Å for [157]) obtained. Si-O-Si angles equal 180 degrees and correspond to the theoretical value [156].

Then, surfaces have to be created from the infinite crystal. In order to do this, both 100 and 111 were constructed, respectively parallel to the (100) and (111) crystallographic planes in such a way that the external surfaces consist of oxygen atoms. The related (100) and (111) planes are shown in figure 3.5. 100 surface in figure 3.5(a) corresponds to an

infinite crystal that is sliced normal to the x direction and parallel to the y and z directions. 111 surface from figure 3.5(b) was created by slicing x, y and z axis at the same distance from the origin. The resulting slabs have two types of surfaces: one has oxygen terminations and the other one has silicon atoms terminations. Dangling bonds are then saturated with hydrogen atoms, which is what would happen when silica is surrounded by water. The surface finishing with Si-H groups is considered as a non-reactive surface, whereas the surface terminating with Si-OH groups is the reactive one. Afterward, polymer fragments will be added on the top of reactive surfaces. The created slabs are 3 layers width.

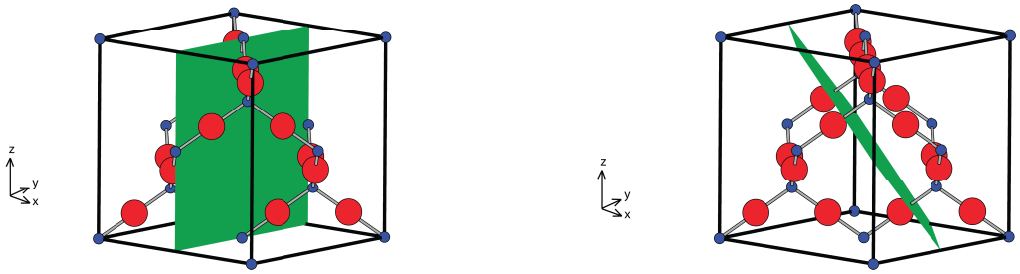

(a) Plan 100. (b) Plan 111.

Figure 3.5 – Planes in β cristobalite. Oxygen atoms are in red and silicon atoms are in blue.

The vacuum represented in figure 3.1 is essential to prevent the solid slab from interacting with itself due to PBC. If a polymer fragment is located on the reactive surface, the vacuum width has to be increased in order to prevent the polymer from interacting with the non-reactive surface. Therefore, there is a vacuum width of 10 Å for the system containing monomers (see figure 3.6) and a 25 Å vacuum width for the systems with 10 repeating units (figure 3.9(a)). When dealing with the polymer chains, surface dimensions have to be increased in order to prevent the polymer from interacting with itself through PBC is the x and y directions that are parallel to the surface. The surface is twice duplicated in x and y directions, leading to a 2x2 supercell when monomers are considered (see figure 3.6). The surface is duplicated 4 times in the x, y plan, leading to a 4x4 supercell when decamers are considered (figure 3.9(a)).

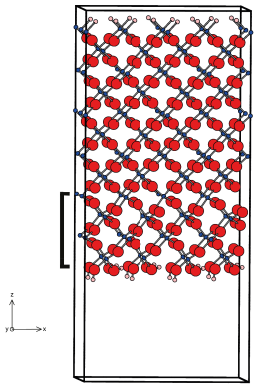

(a) 100 surface relaxed with 10 Å vacuum. The eight first atomic planes represent one layer (black square bracket). The surface is 216.6 $Å^2$ is the x, y plane and the cell length is 36.2 Å in z direction.

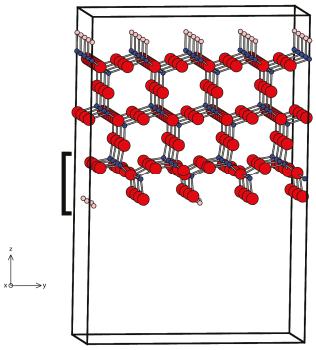

(b) 111 surface relaxed with 10 Å vacuum. The four first atomic planes represent one layer (black square bracket). The surface is 375.1$Å^2$ is the x, y plane and the cell length is 26.2 Å in z direction.

Figure 3.6 – 100 and 111 slabs. Oxygen atoms are in red and silicon atoms are in blue.

The slabs are finally relaxed using DFT calculations in the following manner: only the first layer is relaxed when the two deeper layers are frozen. It is worth noting that creating a solid slab has effects on structural parameters. Their evolution is summarized in table 3.1.

Infinite solid or slab	Cell	Si-O distance (Å)	Si-O-Si angle (degrees)
Infinite solid	Cubic	1,59	180
100	Cubic	1,63	154,3
111	Hexagonal	1,62	156,8

Table 3.1 – Evolution of structural parameters when solid slabs are created.

Introducing a surface modifies to a large extend Si-O-Si angles on the surface, whose value are reduced by 25 degrees. This is consistent with the fact that the studied solid is known to be flexible. The values we obtain for Si-O-Si angles and for Si-O distances are in good agreement with the ones from reference [156]. This article gives a theoretical value of 154.1 degrees and an experimental one of 146.7 degrees for Si-O-Si angles. It also provides a theoretical value of 1.6131 Å and an experimental one of 1.611 Å for Si-O distances. The designed model is therefore in very good agreement with theoretical and experimental values.

On surface 100, one can find geminal silanols that are hydrogen-bonded with a bond length of 1.7 Å, while isolated silanols of the 111 surface are separated by 5.2 Å. These observations are consistent with what was observed by the authors of reference [158] and [154]. Moreover, surface 100 has a silanol density of 7.39 OH/nm^2 which is close to the computed silanol density for this type of surface: the authors of reference [154] found a silanol density of 7.9 OH/nm^2. Surface 111 displays a silanol density of 4.53 OH/nm^2, again in good agreement with computed values of reference [154] and of reference [158] (4.55 OH/nm^2). Silanol density of 100 surface is higher than the one of amorphous silica (4.53 OH/nm^2), according to [154], whereas silanol density of 111 surface is below. Thereby, amorphous silica cannot be exclusively modeled as a 100 surface of a 111 surface. A system composed of a mixture of 100 and of 111 surfaces enables to recover the silanol density of amorphous silica. In this work, we consider 100 and 111 surfaces separately and not a combination, which would be even more complicated.

Adsorption of monomers on the silica surface

Once 100 and 111 silica surfaces are optimized using DFT calculations, PAAm and PDMA monomers are adsorbed on the surface. Because DFT is a static method, we started from different initial configurations of the monomers on the surfaces in order to probe the dependency of the monomer adsorption energy on its starting conformation. After DFT optimization, a hydrogen bond between the nitrogen of PAAm and a hydrogen of the surface and hydrogen bonds between monomers oxygen and hydrogens of the silica surfaces were observed. The related adsorption energy E_{ads} is computed using an energy difference:

$$\begin{aligned} E_{ads} = &\text{ energy of the relaxed polymer/surface system} \\ &- (\text{relaxed polymer energy} + \text{relaxed surface energy}) \end{aligned}$$

Figures 3.7 and 3.8 summarize the different monomer / surface configurations that were considered and the related adsorption energy. First, it is noteworthy that the range of

adsorption energies, on the order of several hundreds of meV, corresponds to weak adsorption. Moreover, the way monomers adsorb on surfaces indicates that the interaction occurs through hydrogen bonding. This corresponds to the experimental behavior found by the authors of reference [36, 37]. For PAAm, the highest adsorption energy (-0.72 eV) is given when PAAm monomer interacts with 111 surface by forming a first hydrogen bond between the oxygen of PAAm and a hydrogen of 111 surface and a second hydrogen bond between a hydrogen of PAAm and an oxygen of the 111 surface. As for PDMA, the highest adsorption energy (-0.66 eV) occurs when the oxygen of PDMA interacts with a hydrogen of the 111 surface. It is interesting to note that adsorption is stronger with the 111 surface than with the 100 surface. This is easily understood by the fact that hydrogens of 100 surface are already involved in hydrogen bonds within the surface and are consequently less available for interaction with the monomers, which is not the case of 111 surface. However, the difference of adsorption energy between PAAm and PDMA is rather slight and cannot be used to fully understand the discrepancy between PAAm and PDMA. I therefore used longer polymer chains, containing ten monomers in order to take into account part of the polymers flexibility.

Adsorption of decamers on the silica surface

As previously mentioned, decamers are first optimized using all atom MD and then DFT. They are then placed on 4x4 100 supercells and the resulting systems were optimized using DFT calculations. This was not done on the 111 surface.

The final structures obtained for decamers of PAAm and PDMA on the 100 surface are displayed in figures 3.9(a) for PAAm and 3.10(a) for PDMA. A zoom in the interfacial region is provided in figures 3.9(b) (PAAm) and 3.10(b) (PDMA). Adsorption of PDMA decamer on 100 surface has an energy of -0.40 eV, while PAAm decamer adsorbs with an energy of -1.42 eV. Figure 3.10(b) indicates that PDMA forms two relatively weak

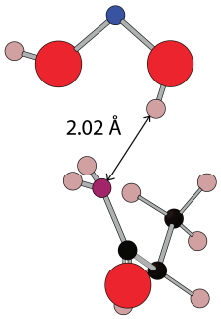

(a) N_{PAAm} ... H_{100}. $E_{ads} = -0,27$ eV.

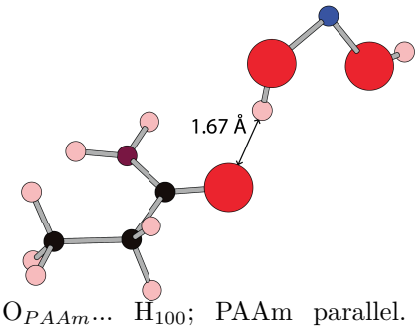

(b) O_{PAAm}... H_{100}; PAAm parallel. $E_{ads} = -0,57$ eV.

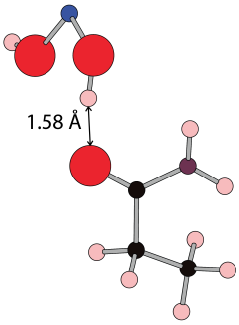

(c) O_{PAAm} ... H_{100}; PAAm normal. $E_{ads} = -0,55$ eV.

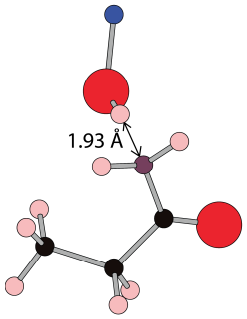

(d) N_{PAAm} ... H_{111}. $E_{ads} = -0,55$ eV.

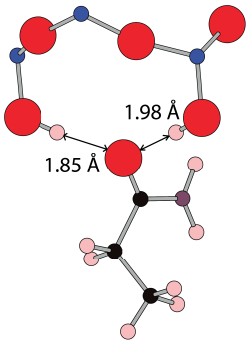

(e) two bonds O_{PAAm}... H_{111}. $E_{ads} = -0,70$ eV.

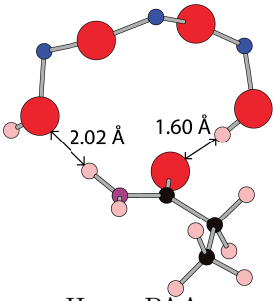

(f) O_{PAAm} ... H_{111}; PAAm parallel. $E_{ads} = -0,72$ eV.

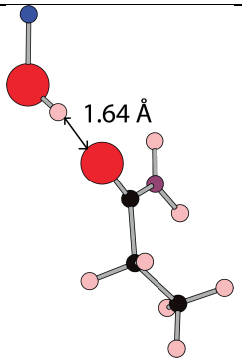

(g) O_{PAAm} ... H_{111}; PAAm normal. $E_{ads} = -0,58$ eV.

Figure 3.7 – PAAm adsorption on 100 and 111 surfaces and related adsorption energies E_{ads}. H_{100} is an hydrogen from the 100 surface and H_{111} is an hydrogen from the 111 surface.

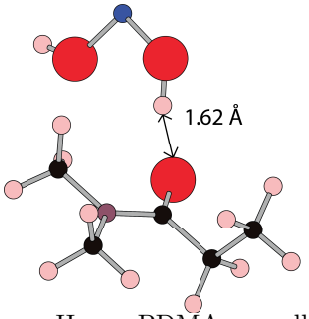

(a) O_{PDMA} ... H_{100}; PDMA parallel. $E_{ads} = -0,47$ eV.

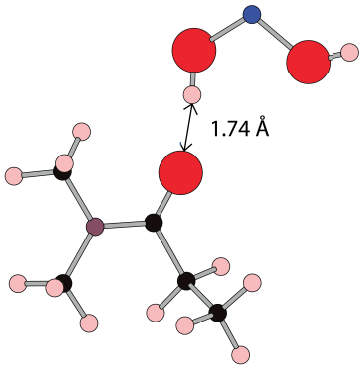

(b) O_{PDMA}... H_{100}; PDMA normal. $E_a = -0,35$ eV.

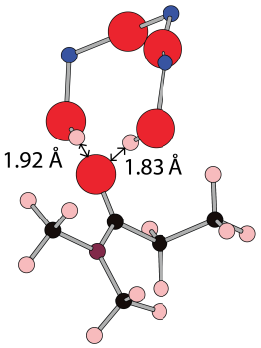

(c) two bonds O_{PDMA}... H_{111}. $E_{ads} = -0,54$ eV.

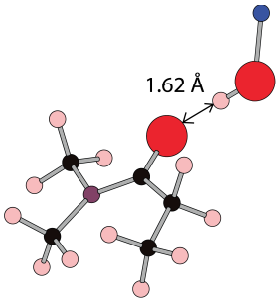

(d) O_{PDMA} ... H_{111}; PDMA parallel. $E_{ads} = -0,22$ eV.

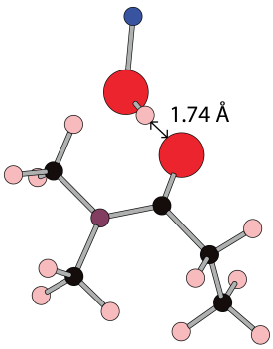

(e) O_{PDMA} ... H_{111}; PDMA normal, into the surface. $E_{ads} = -0,66$ eV.

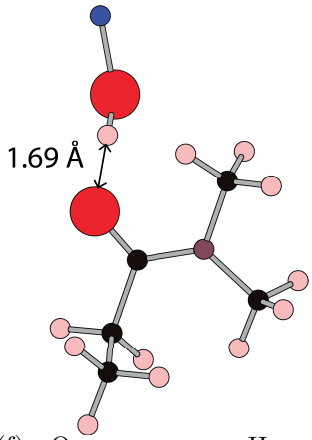

(f) O_{PDMA} ... H_{111}; PDMA normal, under the surface. $E_{ads} = -0,45$ eV.

Figure 3.8 – PDMA adsorption on 100 and 111 surfaces and related adsorption energies E_{ads}. H_{100} is an hydrogen from the 100 surface and H_{111} is an hydrogen from the 111 surface.

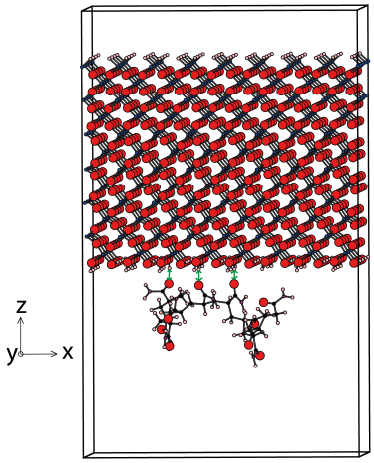

(a) PAAm decamer adsorbed on 100 silica surface with E_{ads} = -1.42 eV. Interactions through hydrogen bonds are depicted with a green arrow. The surface is 866,5 Å^2 and the cell length in the z direction is 47,7 Å.

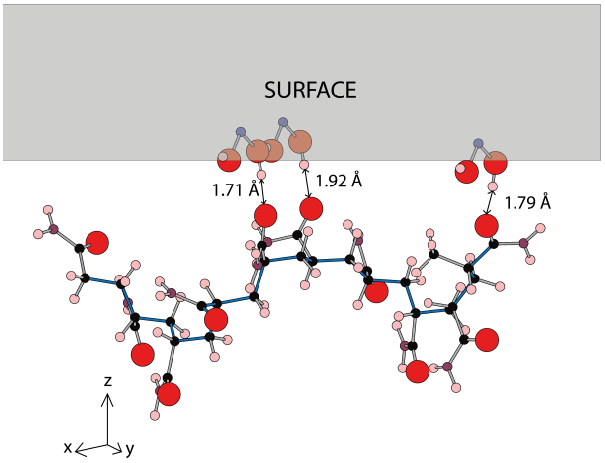

(b) Zoom on PAAm decamer adsorbed on 100 silica surface. Polymeric chain is in blue and surface is represented by a gray rectangle. Only silanol terminations interacting with PAAm are shown.

Figure 3.9 – Decamer of PAAm on the 100 surface.

hydrogen bonds with the silica surface (1.88 and 2.48 Å), whereas figure 3.9(b) highlights the formation of three stronger hydrogen bonds between PAAm and the surface. There is now a rather significant difference between PAAm and PDMA with regard to their adsorption energy on the silica surface which could lead to important consequences on the reorganization of polymer chains. PDMA, by not being strongly adsorbed on the silica surface, is more labile and allows the material to efficiently recover its mechanical properties and dissipate energy when put under mechanical constraint. However, this result could strongly depend on the initial configurations of PAAm and PDMA on the surface. Because of a lack of time, only one configuration of PAAm and of PDMA on the surface were tested.

The results obtained using DFT calculations allow some conclusions on the interaction strength between silica and PAAm versus PDMA. However, they highlight the crucial necessity of a broader model that includes more effects, such as longer chains, chains reorganization and the effect of water. There have been attempts to include water into the DFT calculations, first with explicit water molecules and then with implicit water. I

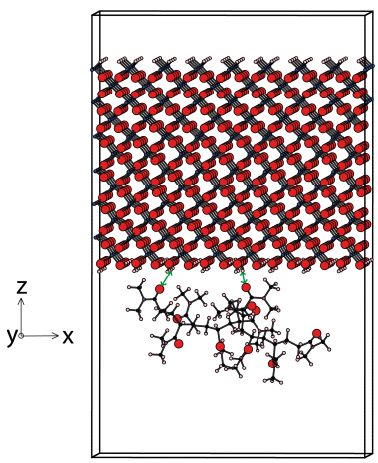

(a) PDMA decamer adsorbed on 100 silica surface with E_{ads} = -0.40 eV. Interactions through hydrogen bonds are depicted with a green arrow. The surface is 866,5 Å^2 and the cell length in the z direction is 47,7 Å.

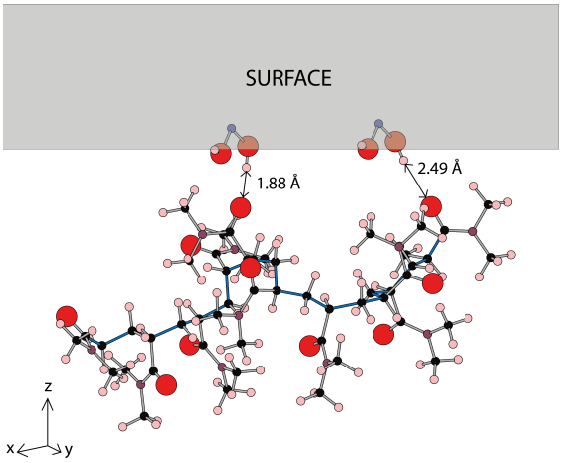

(b) Zoom on PDMA decamer adsorbed on 100 silica surface. Polymeric chain is in blue and surface is represented by a gray rectangle. Only silanol terminations interacting with PAAm are shown.

Figure 3.10 – Decamer of PDMA on the 100 surface.

tried to add explicit water molecules, using *ab initio* MD, to the system. Unfortunately, computing adsorption energies of polymers surrounded by water on the surface turned out to be not accurate enough. A post doctoral researcher of our group at the ENS tried to use VASPSOL to include implicit water into the system [159, 160]. This implicit solvent method includes two terms in the electronic Hamiltonian in order to reproduce some features of water: a cavitation term and an electrostatic term. However, the results were not conclusive and the attempt to combine DFT calculations with water was put aside. Those trials highlight the high necessity to design a model and find a method able to probe larger scales.

3.2 A coarse-grained model for silica

As previously discussed in chapter 2, CG is a convenient method when one wants to probe large systems containing multiple components for long time scales. The CG model we used (see section 2.4.2 of chapter 2) was developed by Marrink and coauthors and is well adapted to the system we want to investigate.

The first step, when designing a CG model, is to find a CG representation of the all atom model. This process is the so-called *mapping* of chemical groups onto CG beads, represented in figure 3.11. In my CG model, one monomer is mapped onto two CG beads: one bead for the backbone chain (gray circle in figure 3.11) and one for the side chemical function (red circle in figure 3.11). The "C" bead (C for Chain) accounts for two carbon atoms of the backbone chain of PAAm and PDMA. The "A" bead (A for Amide), represents the side groups of PAAm and PDMA. For PAAm, the side group is an amide function. For PDMA, it is a dimethylacrylamide function. Therefore a C bead is similar for PAAm and PDMA, whereas an A bead differs between PAAm and PDMA, with an A_{PDMA} bead being bigger than an A_{PAAm} bead. The second step is to associate the corresponding type of bead, using the 18 subtypes we mentioned in section 2.4.2 of chapter 2. According to Martini's type of particles, a C bead is a bead of type C_1: it is an apolar bead with a low degree of polarity. A_{PAAm} is a bead of type N_{da}: a nonpolar bead which can donate hydrogen bonds (through NH_2) or accept hydrogen bonds (through oxygen). A_{PDMA} is a bead of type N_a which can only accept hydrogen bonds. We mentioned in section 2.4.2 that Martini is a four-to-one mapping. Therefore, CG beads that map four or more atoms are considered as "normal" beads, their σ_{ij} equals 0.47 nm and ϵ_{ij} is the value indicated on the interaction matrix in figure 2.5. Beads that map less than four atoms are "small" beads, their σ_{ij} equals 0.43 nm and ϵ_{ij} is scaled to 75% of the standard value presented in the interaction matrix (figure 2.5). C bead is a small bead because it maps only two carbon atoms and connected hydrogens. An A_{PAAm} bead maps three heavy atoms: it is also a small bead. A_{PDMA} is a normal bead because it maps four heavy atoms.

3.3 Parametrization of the polymers

The Martini force field relies on two types of interactions: bonded and nonbonded interactions. The latter were simply determined from the interaction matrix provided in the Martini's paper and reproduced in figure 2.5 [137]. Bonded interaction parameters were derived from all atom MD simulations.

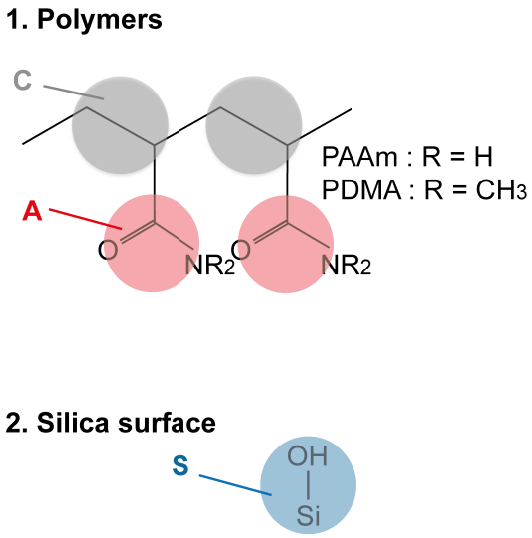

Figure 3.11 – Coarse-grained mapping of the polymer and the silica surface.

3.3.1 Parametrization of nonbonded interactions

The LJ interaction parameters ϵ_{ij} used for the system are presented in table 3.2, for self and cross interactions. There is no A_{PAAm}/A_{PDMA} interaction because simulated systems contain either PAAm or PDMA. P_4 stands for a water bead designed within the framework of the Martini force field. Water models will be discussed in the following section 3.4.

Explicit solvent	C	A_{PAAm}	A_{PDMA}	S	P_4
C	2.625	2.042	2.71	2.042	2.3
A_{PAAm}	2.042	3.375	—	3.375	4.5
A_{PDMA}	2.71	—	4.0	4.5	4.5
S	2.042	3.375	4.5	3.0	4.5
P_4	2.3	4.5	4.5	4.5	4.5

Table 3.2 – Interaction parameter ϵ_{ij} (kJ.mol^{-1}) matrix with explicit solvent.

3.3.2 Parametrization of bonded interactions

In section 2.4.2, potentials that govern the behavior of bonds ($V_{bond}(r)$) and angles ($V_{angle}(\theta)$) were presented. We briefly recall them:

$$V_{bond}(r) = \frac{1}{2} K_{bond}(r - r_0)^2 \tag{3.1}$$

is a harmonic potential occurring between two chemically bonded beads, where r is the distance between two beads, K_{bond} is the force constant of the harmonic bonding potential, and r_0 is the equilibrium distance.

$$V_{angle}(\theta) = \frac{1}{2} K_{angle}[cos(\theta) - cos(\theta_0)]^2 \tag{3.2}$$

describes angles, where θ is the angle between the three beads, K_{angle} is the force constant and θ_0 is the equilibrium angle. The four parameters K_{bond}, K_{angle}, r_0 and θ_0 are unknown. They are determined by comparing distributions from all atom simulations with distributions from CG simulations.

We performed all atom simulations, using the LAMMPS code [146], [147] and the CHARMM22 force field [161] (the time step was set to 1 fs). The CHARMM force field is widely used for all atom simulations and is adapted to the studied system. Along the all atom simulation lengths and angles between the center of mass of the groups of atoms that are mapped onto one CG bead are computed. The resulting all atom histograms of bond length r and of the angle θ are the dashed lines in figure 3.12. The CG histograms are the solid lines in 3.12. Both histograms are normalized. They indicate the probability of finding a bond at a given distance or an angle at a given value.

All atom and coarse-grained simulations are done with a system containing five polymer chains of twenty monomers. The averaged value of the all atom histograms is used to optimize the equilibrium bond length r_0 and angle θ_0 of the CG potentials $V_{bond}(r)$ (Eq. 3.1) and $V_{angle}(\theta)$ (Eq. 3.2). r_0 and θ_0 are tuned in such a way that the averaged value of the CG histogram matches the averaged value of the all atom histogram. The coupling constants K_{bond} and K_{angle} are optimized by comparing the width of the CG histogram with the corresponding width of the all atom histogram. End-to-end distances (the distance between the two extremities of a polymer chain) and radius of gyration between all atom and CG simulation are finally compared to validate our CG model. We find, for the radius of gyration, an average value of 7.1 $\pm$ 0.3 Å for the all atom system

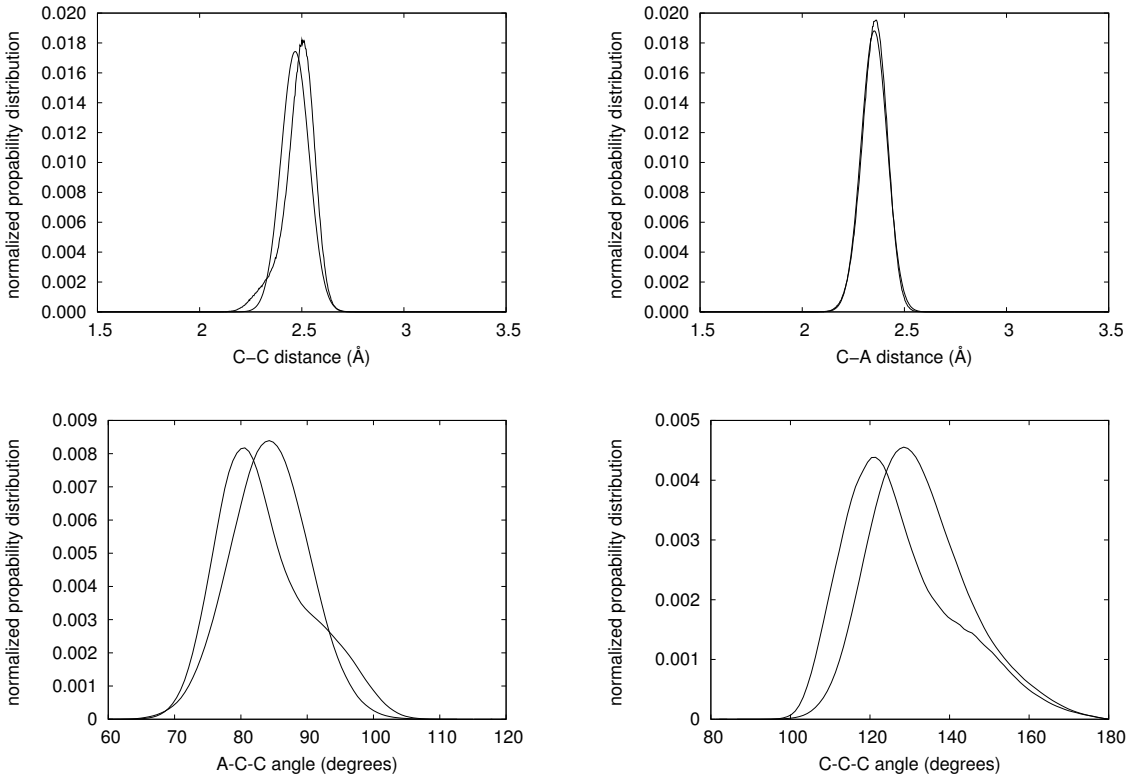

Figure 3.12 – Comparison between all atoms (dashed line) and coarse-grained (solid line) bonds and angles distribution.

and of 7.3 ± 1.0 Å for the coarse-grained system. The values of the radius of gyration are in good agreement between all atom and coarse-grained systems. As for the end-to-end distance, the average value is 15.07 ± 2.53 Å in the all atom system and 13.21 ± 3.33 Å in the coarse-grained system. End-to-end distances also show good agreement between all atom and coarse-grained simulations. The final K_{bond}, K_{angle}, r_0 and θ_0 parameters are summarized in table 3.3. For the sake of simplicity and to have a CG model that differs as little as possible between PAAm and PDMA, K_{bond}, K_{angle} and θ_0 are the same for PAAm and PDMA. Only A_{PDMA}–C differs. This arises from the comparison between all atom and CG distributions.

3.4 Solvent model

There are two ways to simulate water within the Martini framework: either explicitly or implicitly.

Bonds	K_{bond} (kJ.mol^{-1}.nm^2)	r_0 (nm)
C–C	566.7	0.249
A_{PAAm}–C	666.7	0.237
A_{PDMA}–C	666.7	0.271
Angles	K_{angle} (kJ.mol^{-1})	θ_0 (degrees)
C–C–C	116.7	127.5
A_{PAAm}–C–C	233.3	85.5
A_{PDMA}–C–C	233.3	85.5

Table 3.3 – Bonded interaction parameters for bonds and angles, for PAAm and PDMA.

3.4.1 Explicit solvent

The Martini model of explicit water comes down to mapping four water molecules onto one bead (P_4 beads, according to the type of beads) [137]. The use of the explicit Martini water in a system containing polymer chains has already been done with polystyrene [142], polyethylane oxide and polyethylene glycol [143]. The interaction parameter ϵ between two water beads is proposed to be 5.0 kJ.mol^{-1}. However, it has been reported that water, modeled as P_4 particles, has a freezing temperature that is too high compared to real water. This is linked to the use of a Lennard-Jones 12-6 potential for nonbonded interactions, which overemphasizes the structuration of water in layers [139]. This is particularly observed in systems where a nucleation site is already present (such as a solid surface in my case). We noted, for a system containing a surface and 2064 water beads at the normal water density, a freezing temperature around 360 K. To avoid this problem, we decreased the ϵ interaction parameter of water beads to 4.5 kJ.mol^{-1}. With this new interaction parameter, water close to the surface does not freeze at 300 K (see figure 3.13). Because the interaction parameters given by Martini for water were modified and do not strictly use the water from Martini, we use the term "solvent" instead of "water" for the rest of the manuscript.

3.4.2 Implicit solvent

However, using an explicit solvent is computationally expensive, especially in the system we investigate where experimental hydrogels are composed of 90 % of water in weight.

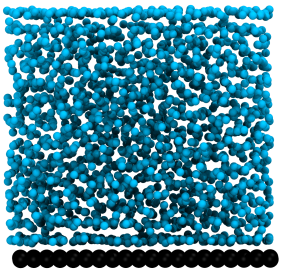

Figure 3.13 – Snapshot of a simulation cell containing solvent (blue beads) and a surface (black beads) at 300 K.

Almost all of the considerable computational time is spent on calculating interactions involving solvent beads. The simplest model to overcome this problem is not to simulate "real" solvent, but to instead simulate the solvent as a continuum which includes the important features of the solvent one absolutely needs to investigate the desired properties of a solute. Such model is an implicit solvent.

There is a wide range of implicit solvents employed in polymer science [162] such as Brownian dynamics (BD) [122], dissipative particle dynamics (DPD) [163] or lattice-Boltzmann (LB) [164]. Both BD and DPD are molecular dynamics methods that account for the effect of solvent by considering random and dissipative force terms. BD replaces Newton's equation by a Langevin equation:

$$\mathbf{F}_{ij}^{BD} = \mathbf{F}_{ij}^{C} - \gamma \mathbf{p}_i + \sigma \xi_i, \tag{3.3}$$

where $\mathbf{p}_i$ is the particle momenta, $\mathbf{F}_{ij}^{C}$ is the conservative force acting on particle i due to particle j, γ is a friction coefficient, σ is a noise amplitude and ξ is a Gaussian random noise term. In BD, the short time motions of solvent molecules are removed from the simulation and their effects on the polymer are represented by dissipative ($-\gamma\mathbf{p}$) and random ($\gamma\xi$) force terms. In DPD, the interaction between two particles i and j is a sum

of three force terms:

$$\mathbf{F}_{ij}^{DPD} = \mathbf{F}_{ij}^{C} + \mathbf{F}_{ij}^{D} + \mathbf{F}_{ij}^{R}, \tag{3.4}$$

where $\mathbf{F}_{ij}^{C}$ is a conservative force term, $\mathbf{F}_{ij}^{D}$ is a dissipative force term and $\mathbf{F}_{ij}^{R}$ is a random force term [165, 166]. The DPD method was first introduced by Hoogerbrugge and Koelman in 1992 to efficiently compute the hydrodynamic behavior of fluids [163]. DPD is based on the idea that solvent is considered through point particles that represent lumps of solvent containing many particles. DPD, by considering a dissipative and a random force term, is close to BD. However, in DPD, the particles number and their momentum are conserved: it allows to simulate the hydrodynamic behavior, in addition to simple diffusion. Another solution is to build a temperature dependent force field that reproduces the LCST or UCST polymer behavior along with the temperature [167, 168] or to take into account the solvent through parametrization of the CG model on all atom simulations at the right solvent density [169–173].

In this work, we do not account for the random force due to the solvent as in BD or in DPD. The implicit solvent we use consists of tuning the interaction parameters to take into account the effect of explicit solvent. Indeed, the interactions of a "solvophilic" bead with other beads would be screened by the presence of a solvation shell in explicit solvent. Therefore, the interaction parameter of solvophilic beads is reduced to take into account the screening due to solvent. On the contrary, there is a depletion of solvent molecules around a "solvophobic" bead: the interaction parameter of solvophobic beads is increased in an implicit solvent model. MD simulations were performed with the implicit solvent CG model developed by Marrink and co-workers called Dry Martini [174]. This implicit solvent developed within the Martini framework has extensively been used to study systems containing polymers with molecular dynamics [175–179]. Such implicit solvent is easy to use and computationally inexpensive. Dry Martini provides new ϵ_{ij} interaction parameters that are gathered in table 3.4.

Table 3.4, compared with table 3.2, shows that ϵ between two A_{PAAm} beads is decreased

Implicit solvent	C	A_{PAAm}	A_{PDMA}	S
C	3.375	2.042	2.71	2.042
A_{PAAm}	2.042	2.042	—	2.042
A_{PDMA}	2.71	—	2.3	2.71
S	2.042	2.042	2.71	1.725

Table 3.4 – Interaction parameter ϵ_{ij} (kJ.mol^{-1}) matrix with implicit solvent.

with Dry Martini that with the normal Martini. This is consistent with the solvophilic nature of A_{PAAm}: their interactions are screened by the presence of a solvation shell. This screening is well reproduced by Dry Martini. On the opposite, ϵ between two C beads, which is a solvophobic bead, is increased with Dry Martini, compared to the normal Martini.

Outcome of the chapter

In this chapter we presented the most precise, but also smallest system one can use to investigate the polymer / silica surface interface. Indeed DFT is an appropriate choice when one wants to probe the chemistry of the adsorption of a small polymer fragment on a model silica surface. DFT indicates that both PAAm and PDMA adsorb on silica by forming hydrogen bonds with the surface. However, this description level, which does not consider the effect of water and the entropy, is not totally satisfactory. This is the reason why we use CGMD. First, the CG model was built from the atomistic structure of PAAm, of PDMA, of the silica surface and of water. Then, the CG model was parametrized, based on inputs from all atom MD simulations and confirmed by the comparison of radius of gyration and of end-to-end distances. Endowed with a robust CG model and two solvent models, we study adsorption of PAAm and of PDMA in the following chapters.

Part II

Results

Chapter 4

On the role played by the solvent

The system we are interested in is composed of three components, namely polymer, silica surface and solvent. As explained in section 3.4.2 of part I, the use of an explicit solvent has a high computational cost. We will show in the present section why it is crucial to use explicit solvent instead of an implicit one, and the features of the solvent that prevent us from using an implicit solvent. First, results are presented for a system containing an explicit solvent, and then compared with results obtained from a system interacting through an implicit solvent to validate – or not – the use of an implicit solvent. In this section we focus on local quantities at the interface between polymer chains and silica surface. On the one hand, we investigate the structure of the polymer chains on the silica surface and the strength of the interactions occurring at the interface. On the other hand, we probe the dynamical behavior of the polymer chains in the vicinity of the silica surface in the direction which is normal to the silica surface. Finally the solvation of polymer beads when the system interacts through an explicit solvent is examined.

4.1 Explicit solvent

4.1.1 The system

We use systems containing 50% of solvent in weight. This is a compromise between the wish to be as close to experimental systems as possible (which contain around 90 % of water [1]) and the computational cost that the simulation of an explicit solvent implies. Using 50% of solvent in weight insures to have a large enough number of solvent beads in the simulation cell in order to capture essential features of the solvent. We use the explicit

solvent described in section 3.4.1 of part I. 24 chains containing 90 monomers and 200 beads for the surface are considered. As we work with a percentage in weight, the PAAm system contains 960 solvent beads and PDMA system contains 1340 solvent beads. A snapshot of the simulation cell containing PAAm, the silica surface and solvent beads is shown in figure 4.1. The simulation cell dimensions are: l_x, l_y = 63 Å, l_z = 80.9 Å for PAAm and l_z = 103.4 Å for PDMA. The system was first equilibrated during 5 ns in the NPT ensemble at a pressure of one atmosphere and a temperature of 300 K, then during 5 ns in the NVT ensemble with the Nosé-Hoover thermostat (relaxation time of 100 fs) and barostat (relaxation time of 1 000 fs). We then performed production simulations using the NVT ensemble during 50 ns. The results we present are averaged over 10 independent simulations of 50 ns. As A beads interact more strongly with the surface than C beads and are different between PAAm and PDMA, we focus on A beads for the rest of this section.

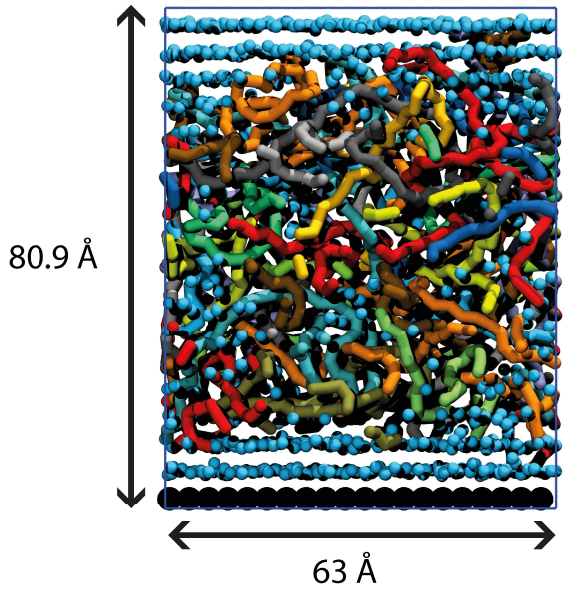

Figure 4.1 – Snapshot of a simulation cell containing 24 PAAm chains of 90 monomers each (one color corresponds to one chain), 200 silica beads (black) and 960 solvent beads (light blue).

4.1.2 Polymer structure on the surface

First of all, it is interesting to characterize the structure of the polymer chains close to the silica surface. Thus, I have computed the normalized histogram $P(d)$ of the distance d

between the surface and the polymer A beads. The free energy profile of the A beads along the direction normal to the surface is then $F(d) = -k_B T ln[P(d)]$, plotted in figure 4.2 for one simulation with PAAm (solid line) and one simulation with PDMA (dashed line). The surface introduces a symmetry breaking that forces the polymer beads to organize in layers. At small d, there is a well corresponding to a high stability of the polymer beads: they form a first layer in the direct vicinity of the surface, then a second layer. Beyond that second layer, there is no more influence of the surface on the polymer beads. Both PAAm and PDMA beads have a similar structuration close to the surface. Figure 4.2 is computed by folding the simulation cell in two and averages are done on two surfaces in order to improve statistics.

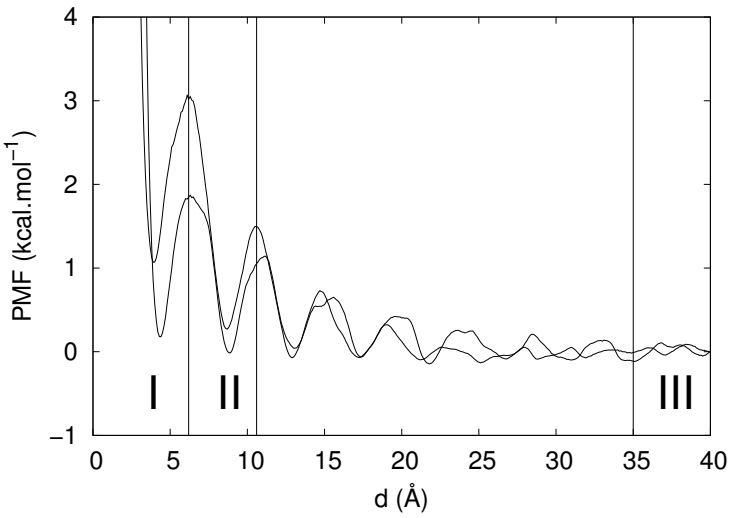

Figure 4.2 – Potential of mean force of PAAm (solid line) and of PDMA (dashed line) both in explicit solvent.

In order to be convinced that the structure we observe in figure 4.2 for one simulation with PAAm and one simulation with PDMA is meaningful and reproducible, we superimpose the PMF obtained with nine independent simulations starting from different initial configurations of PDMA (figure 4.3(a)) and of PAAm (figure 4.3(b)). These two figures highlight the good reproducibility of the PMF between independent simulations. It is noteworthy that the plot in figure 4.3(b) is noisy for $d < 7$ Å. It indeed corresponds to the region I where we observe only few A_{PAAm} beads coming in the vicinity of the surface, leading to noise in the corresponding PMF.

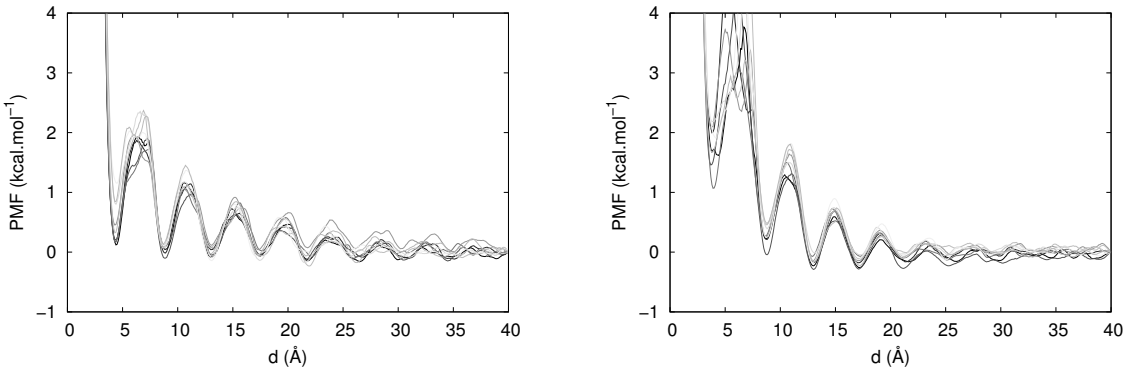

(a) Potential of mean force of PDMA A beads. (b) Potential of mean force of PAAm A beads.

Figure 4.3 – Potential of mean force of PDMA A beads and PAAm A beads collected in nine independent simulations. .

From the structure presented in figure 4.2 we define different regions of stability I, II and III such as represented in figure 4.2. Region I is defined as the first layer near the surface: it starts close to the surface and ends at the first maximum. In region I, A beads are well dispersed on the silica surface, as illustrated in figure 4.4. Region II starts just after the region I and ends at the second peak of the probability distribution. This second layer is less structured than the first layer. Region III corresponds to a bulk-like region where there is no interaction between the polymer and the surface and is defined by a slab of 10 Å in the middle of the simulation cell.

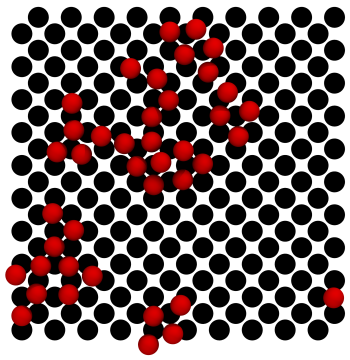

Figure 4.4 – Top view of A_{PDMA} beads (red beads) on silica surface (black beads) in region I.

4.1.3 Polymer interaction with the surface

The difference in free energy between the first well and the first peak in figure 4.2 corresponds to the free energy barrier ΔF_B that beads have to overcome to move away from the surface. It characterizes the local exchange of A beads, or the ability to detach an A bead from the surface. This barrier, averaged over ten independent simulations, turns out to be higher for PDMA (2.1($\pm$0.3) kcal.mol^{-1}) than for PAAm (1.6($\pm$0.6) kcal.mol^{-1}). It is thus harder for an A bead of PDMA to leave the first adsorption layer to move to the second layer or to the bulk.

System	Region I	Region II	Region III
A beads of PAAm	-2.8	-0.1	0.0
A beads of PDMA	-4.2	-0.3	0.0
Solvent beads	-4.6	-0.3	0.0

Table 4.1 – Interaction energy between beads and the surface (in kcal.mol^{-1}).

It is worth comparing ΔF_B with the interaction energy between A beads and the surface in region I. The latter equals 2.8 kcal.mol^{-1} per bead for PAAm and 4.2 kcal.mol^{-1} per bead for PDMA (see the two first rows of table 4.1). This is consistent with the interaction parameters presented in section 3.3 of chapter 3. The results obtained for the free-energy barrier and for the interaction energy between A beads and the surface in region I are then consistent. We conclude that there is a slight difference between PAAm and PDMA when their behavior in the vicinity of the surface is considered. A beads of PDMA interact more strongly with the surface, making it more difficult for them to leave the first adsorption layer. It is relevant to note the different range of adsorption energy between DFT calculations (section 3.1.1 of chapter 3) and CGMD results presented here. In section 3.1.1, the highest adsorption energy computed using DFT of a monomer of PAAm, interacting through its amide function, on the surface is -0.72 eV, equivalent to 16.6 kcal.mol^{-1}. The highest adsorption energy of a monomer of PDMA on the surface is -0.66 eV, being 15.2 kcal.mol^{-1}. CGMD therefore drastically underestimates the adsorption energy of a

monomer on a surface. This is consistent with the fact that coarse-grained models are known to lead to rather "soft" potential interaction that lead to a smaller adsorption energy [180]. We have computed with quantum DFT calculations an interaction energy of -16.6 kcal.mol^{-1} between one PAAm monomer and the silica surface (figure 3.7) and an interaction energy of -15.2 kcal.mol^{-1} between one PDMA monomer and the silica surface (figure 3.8). Considering the same system and replacing atoms by coarse-grained beads leads to the same range of interaction energy: -1.12 kcal.mol^{-1} between PAAm and the surface, and -0.43 kcal.mol^{-1} between PDMA and the surface. To that extent, our CG model reproduces results obtained with quantum DFT.

4.1.4 Dynamical properties of the polymers on the surface

We investigate the structure of PDMA and PAAm in the vicinity of the surface and their interaction with the surface. Polymer structure accounts for the symmetry breaking introduced by the surface. Interaction strengths correspond to the interaction parameters we selected. One of our first hypotheses is that PDMA hydrogel glues better on the silica nanoparticles than PAAm and makes a stronger system due to the PDMA ability to rearrange on the surface of the silica nanoparticles and to dissipate energy under stress [181, 182]. We therefore think that interesting mechanical properties of PDMA are linked to its ability to reorganize in the vicinity of the silica surface and to efficiently attach and detach from the surface. Thus, dynamical properties of PAAm and PDMA chains in the vicinity of the silica surface, surrounded by an explicit solvent, are investigated.

Our approach

Computing dynamical quantities such as mean square displacement of individual polymer beads or of the polymer center of mass is, in this system, not relevant due to the fact that polymer chains are rather constrained and the move of individual beads is restrained. Moreover, we are interested in small moves of the polymer chains close to the surface in the direction normal to the surface that are not reachable by computing the mean square displacement. We do not focus on displacements of the polymer chains in the direction

which is parallel to the surface because that would be equivalent to studying shear behavior, which is not the purpose of this work. Therefore, we developed a method to compute dynamical properties of polymer chains in the vicinity of the surface.

The overall idea of this method is to quantify the ability of the polymer beads to move close to the surface. By "move", we mean to detach from or to attach to the surface. First, we consider what we call "active beads" which are beads that cross regions over the course of the simulation (regions being defined in figure 4.2). Polymer beads undergo two kinds of events: whether they leave the region I (close to the surface) or else they reach region I. Beads that leave region I go from region I to beyond region II. Beads that reach region I arrive in region I from outside region II. The number of active beads is in the first row of table 4.2. Since the number of active beads is rather small for both PAAm and PDMA and to be sure that active beads are not only tail beads but are rather well dispersed along the polymeric chain, we checked where are located the active beads (see figure 4.5). Figure 4.5 shows the position of active beads along polymer chains that are folded in two, averaged over the 24 chains and over the course of the simulations: position 1 is the end of the chain and position 45 is right in the middle of the chain. The figure shows an excess of active beads at the end of the chains, but also active beads all along the chains. Therefore, we are confident that the dynamical behavior of polymer chains is due to the motion of the whole polymer chain rather than small motions of end beads. It is also noticeable from figure 4.5 that PDMA has more active beads than PAAm, which is confirmed by the values in the first row of table 4.2.

Dynamic

Second row of table 4.2 is the number of non-active beads, which are beads that stay close to the surface during the whole course of the simulation. The averaged number of events that beads undergo is presented in the third row of table 4.2. The number of occurrences of the event "bead leave" divided by the simulation time is the frequency of this event and is shown in the fourth row of the table. We compare the datas between A beads of PAAm

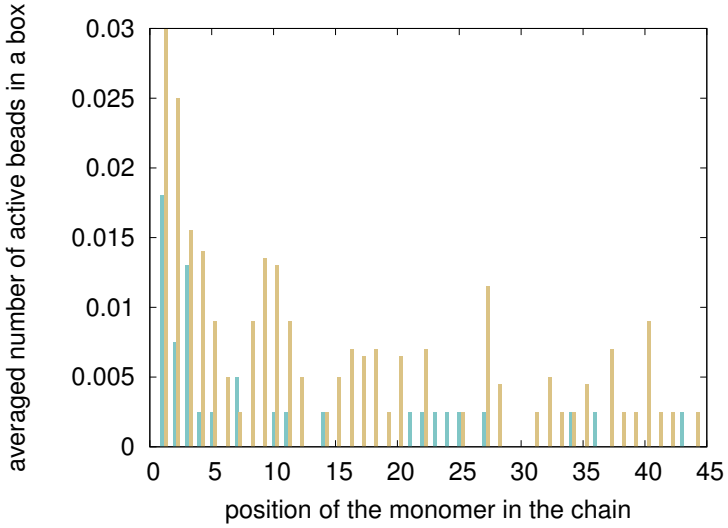

Figure 4.5 – Distribution of active beads in PAAm (blue) and PDMA (orange). Position 1 is the extremity of the chain; position 45 is the middle of the chain.

Dynamic	A beads of PAAm	A beads of PDMA
Number of active beads	4.1(±1.7)	13(±5.8)
Number of non-active beads	8(±5.8)	44(±18.2)
Averaged number of events per active bead	1.5(±0.6)	2.5(±0.7)
Frequency of the event "bead leave" (Ghz)	0.1	0.4

Table 4.2 – Dynamic of PAAm and PDMA A beads.

and of PDMA. The numbers displayed in table 4.2 were averaged over ten independent simulations. One can see from table 4.2 that PDMA has more active beads than PAAm and that these active beads undergo more events than the active beads of PAAm. Not only they undergo more events, but their frequency is also higher. Therefore A beads of PDMA are slightly faster than A beads of PAAm. It is interesting to comment on the number of non-active beads, which is different between PAAm and PDMA. One could think that this difference is due to the fact that PDMA has more non-active beads, which are beads that stay for a long time (at least longer than our simulations, which are 50 ns long), that it gives experimentally a stronger system. However, the number of non-active beads in the second row of table 4.2 is related to the fact that PAAm is better solvated than PDMA close to the surface, and that solvent beads prevent PAAm beads from approaching the surface. This behavior will be extensively studied in section 4.1.5.

However, we see in table 4.1 that A beads of PDMA interact more strongly with the

surface than PAAm. The fact that PDMA has a stronger interaction with the surface, but moves faster in the vicinity of the surface is surprising. This is certainly due to the fact that the interaction energy between A_{PAAm} and the surface is low below the interaction energy of the solvent beads and the surface (first and third rows of table 4.1): PAAm is then replaced by solvent beads near the surface. This is not the case for A_{PDMA}, which has an interaction energy with the surface in the same range as the interaction energy between the solvent beads and the surface (second and third rows of table 4.1). Explicit solvent apparently plays an important role in this system by competing with the polymer chains with regard to the adsorption on the silica surface.

4.1.5 Polymer solvation

In order to fully understand what is the role played by the explicit solvent in this system, one has to properly characterize the solvation of the polymer chains by solvent beads and the way solvent beads behave close to the surface and interact with it. We quantify the solvation of PAAm and PDMA by computing the number of first solvent neighbors of PDMA and PAAm in regions I, II and III. To do so, we count the number of solvent beads that stand at a certain distance d_{shell} from A beads, where d_{shell} corresponds to the radius of the first solvation shell of A beads. This procedure is done for A beads of PAAm and of PDMA and in regions I, II and III. N_{PAAm} is the number of solvent first neighbors of A beads of PAAm and N_{PDMA} is the number of solvent first neighbors of A beads of PDMA. The ratio N_{PAAm}/N_{PDMA} is presented in table 4.3 in order to compare the solvent behavior around PAAm and PDMA.

Region	N_{PAAm}/N_{PDMA}
Full cell	1.4
Region III	2.1
Region II	0.7
Region I	0.8

Table 4.3 – Ratio of first solvent neighbors of PDMA and PAAm.

One can first note that the ratio of first neighbors of PDMA and of PAAm in the full

simulation cell is about 1.4, which gives the number of solvent beads for PDMA divided by the number of solvent beads for PAAm. This "full cell" ratio, that we use as a reference, is compared with the ratio in regions I, II and III. In region III, the ratio goes up to 2.1, meaning that A_{PDMA} has more first solvent neighbors than A_{PAAm}. The value of the ratio is above 1.4: there is an "excess" of solvent beads for PDMA, or a default of solvent beads for PAAm in the bulk-like region (region III), compared to the full cell ratio. The tendency is well understood when we move toward the surface, in regions I and II, where the ratio lowers to 0.7 (region II) or 0.8 (region I). There is clearly, as one can see from figure 4.6, a large excess of solvent beads close to A_{PAAm} beads in the vicinity of the surface (left side of the figure 4.6), compared with the cell containing PDMA (right side of the figure 4.6). It is worth noting that we started the simulation of the systems containing PAAm and PDMA from the same initial configuration and led to different configurations of the solvent around the polymer. Therefore, in the cell containing PAAm, solvent beads leave the bulk-like region to reach the interface with the surface resulting in a default of solvent beads in region III and an excess of solvent beads in regions I and II. In the PAAm system, solvent beads go in between the polymer chains and the surface, preventing PAAm chains from adsorbing to the surface. For PAAm, there is a competition between solvent beads and PAAm beads with regard to the adsorption on the surface. However, there is also an attraction between PAAm beads and solvent beads.

The attraction between PAAm and solvent is confirmed by the study of the part of the interaction energy between A beads and solvent among the interaction energy between A beads and all the other beads, which is summarized in table 4.4. Indeed, as PAAm and PDMA do not interact with the same strength with the surrounding beads, we cannot directly compare A/all interaction energy between PAAm and PDMA. The first row of table 4.4 shows that, in region I, the part due to A/solvent interactions among the A/all interactions is higher for PAAm than for PDMA. Therefore, A_{PAAm} interacts more forcefully with solvent beads than A_{PDMA} close to the wall.

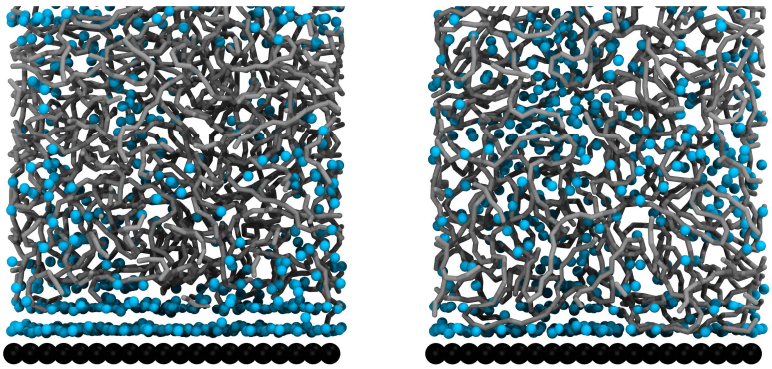

Figure 4.6 – Snapshot of half a simulation cell. Surface is in black, solvent in blue and polymer chains are in gray. PAAm is on the left side and PDMA on the right.

System	Part of the interaction energy in region I (%)
PAAm	31.1
PDMA	20.3

Table 4.4 – Part of the interaction energy between A and solvent beads among the interaction energy between A beads and every other beads.

We presented in section 4.1 the dynamical properties, interaction energies and solvation of PAAm and PDMA in the vicinity of the surface. Our results show that PDMA A beads are moving more and faster than A_{PAAm} in the vicinity of the surface. Moreover, solvent beads prevent A_{PAAm} beads from approaching the surface by better solvating A_{PAAm} and surface beads than in the case of PDMA. These results highlight an important difference between PAAm and PDMA and explain part of the experimental behavior: PAAm is better solvated than PDMA and this solvation appears to be responsible for the non-adsorption of PAAm on the silica surface. At this stage, it turns out that solvent is an important feature of the system. Nevertheless, it is interesting to investigate the manner the solvent prevents PAAm from adsorbing on the silica surface, and not PDMA. One can wonder if this behavior is driven by interactions (solvent/polymer versus solvent/surface interaction) or by the presence of solvent beads and the implied steric effect.

4.2 Implicit solvent

To address the question of the role played by the solvent in our system, we compare the use of an explicit solvent with the use of an implicit solvent. Explicit solvent is a computationally demanding method. When using it, most of the computational time is spent calculating solvent-solvent interactions. For this reason, using an implicit solvent which drastically reduces computational time is an appealing solution. There is a wide range of implicit solvents [162] employed in polymer science, such as Brownian dynamics (BD) [122], dissipative particles dynamics (DPD) [163] or lattice-Boltzmann (LB) [164]. See section 3.4.2 of part I for details about BD, DPD and LB methods. In this work, we use the implicit solvent CG model developed by Marrink and co-workers called dry Martini [174] that has extensively been used to study systems containing polymers with molecular dynamics [175–179].

4.2.1 The system

We use the implicit solvent described in section 3.4.2 of chapter 3. We still consider 24 chains containing 90 monomers and 200 beads for the surface. A snapshot of the simulation cell containing PAAm and the silica surface is shown in figure 4.7. The simulation cell dimensions are : l_x, l_y = 63 Å, l_z = 51.4 Å for PAAm and l_z = 55.8 Å for PDMA. The system was first equilibrated during 5 ns in the NPT ensemble at a pressure of one atmosphere and a temperature of 300 K, then during 5 ns in the NVT ensemble with the Nose-Hoover thermostat (relaxation time of 100 fs) and barostat (relaxation time of 1000 fs). We then performed production simulations using the NVT ensemble during 50 ns. The results we present are averaged over 5 independent simulations of 50 ns. We still focus on A beads for the rest of this section.

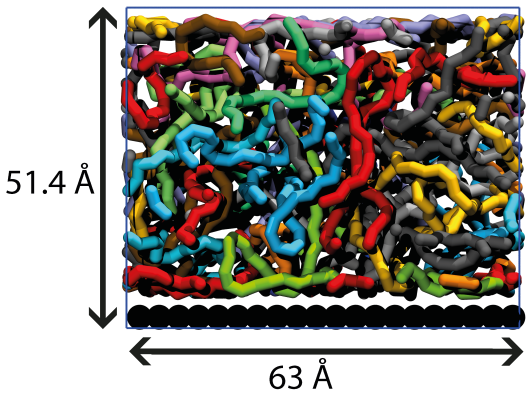

Figure 4.7 – Snapshot of a simulation cell containing 24 chains of 90 monomers of PAAm (one color corresponds to one chain) and 200 silica beads (black).

4.2.2 Polymer structure on the surface

We first examine the structure of the polymer chains close to the silica surface. As already presented in section 4.1.2, we compute the normalized histogram $P(d)$ of the distance d between the surface and the polymer A beads. The free energy profile of the A beads along the direction normal to the surface is then $F(d) = -k_B T ln[P(d)]$, plotted in figure 4.8 for one simulation with PAAm (solid line) and one simulation with PDMA (dashed line).

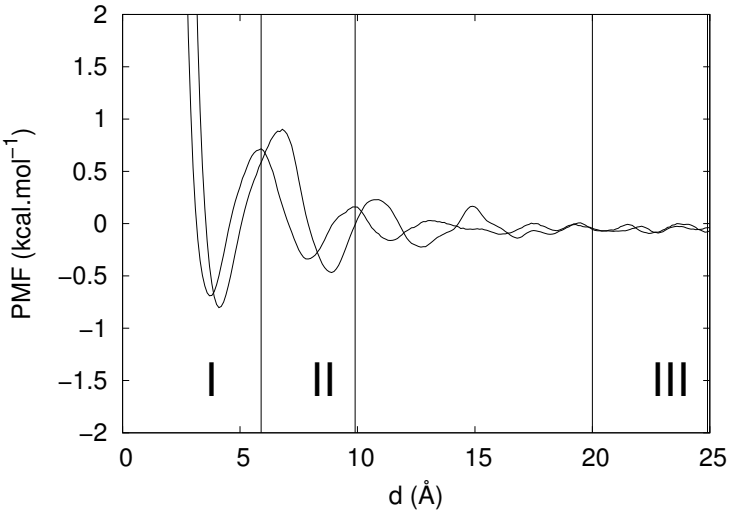

Figure 4.8 – Potential of mean force of PAAm (solid line) and of PDMA (dashed line). Implicit solvent.

One can see from figure 4.9 that there are more A beads in region I when the system interacts through an implicit solvent than when it interacts through an explicit solvent (figure 4.4). This is easily explained by the fact that polymer beads prefer to interact with the surface than with void, in the case where an implicit solvent is used.

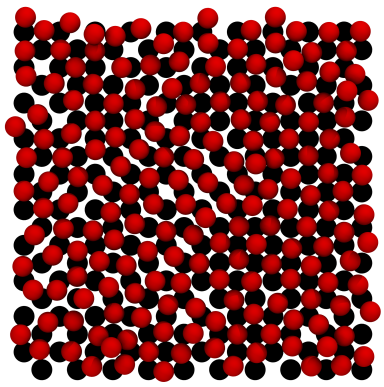

Figure 4.9 – Top view of A_{PDMA} beads (red beads) on silica surface (black beads) in region I.

Here again, we superimpose the PMF obtained with five independent simulations starting from different initial configurations of the PDMA (figure 4.10(a)) and of PAAm (figure 4.10(b)) to be sure that the structure we observe in figure 4.8 for one simulation with

PAAm and one simulation with PDMA is meaningful and reproducible. These two figures highlight the good reproducibility of the PMF between independent simulations. One can note that the PMF plot of PAAm interacting through an implicit solvent (figure 4.10(b)) is less noisy than the one of PAAm interacting with an explicit solvent (figure 4.3(b)) for $d < 7$ Å . It is due to the fact that the silica surface is more available for A_{PAAm} when the solvent is implicit rather than explicit.

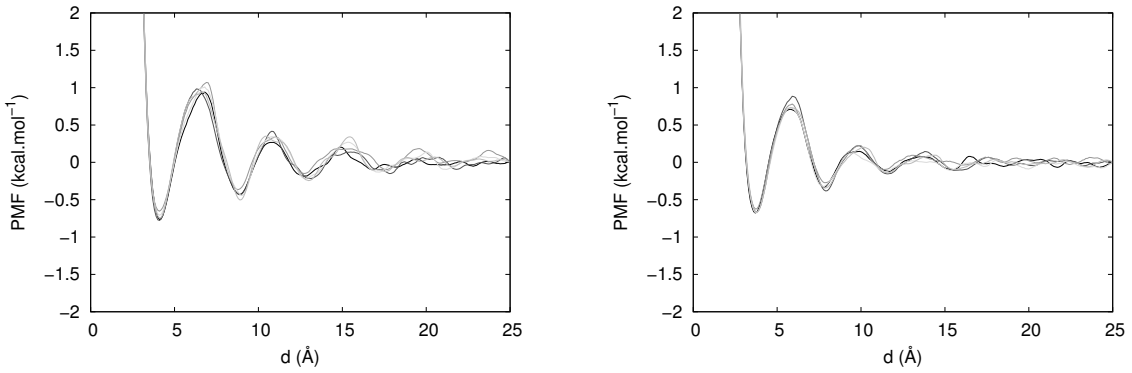

(a) Potential of mean force of PDMA A beads. (b) Potential of mean force of PAAm A beads.

Figure 4.10 – Potential of mean force of PDMA A beads and PAAm A beads interacting through an implicit solvent collected in five independent simulations. .

4.2.3 Polymer interaction with the surface

First, ΔF_B turns out to be slightly higher for PDMA (1.7 kcal.mol^{-1}) than for PAAm (1.4 kcal.mol^{-1}). It is thus a little harder for an A bead of PDMA to leave the first adsorption layer to move to the second layer or to the bulk. This is consistent with interaction energies displayed in table 4.5, which show that the interaction between A beads and surface beads in region I is stronger in the system containing PDMA. It is noteworthy that the range of interaction energies given in table 4.5 with an implicit solvent is lower than values given in table 4.1 with an explicit solvent, but the ranking is the same.

System	Region I	Region II	Region III
A beads of PAAm	-0.9	-0.2	0
A beads of PDMA	-1.6	-0.3	0

Table 4.5 – Interaction energy between beads and the surface (in kcal.mol^{-1}).

Dynamic	A beads of PAAm	A beads of PDMA
Number of active beads	38.8(±12.3)	21.4(±13.1)
Number of non-active beads	446	427
Averaged number of events per active bead	1.9(±0.4)	3.8(±2.0)
Frequency of the event "bead leave" (Ghz)	1.0	0.8

Table 4.6 – Dynamical quantities of PAAm and PDMA A beads interacting through an implicit solvent.

As explained in section 3.4.2 of Part I, the implicit solvent we use consists in tuning the interaction parameters between beads in order to reproduce the effect of a solvent. In our case, both A_{PAAm}, A_{PDMA} and S beads are solvophilic; their interaction parameters are then decreased and the resulting interaction energy is lower than when an explicit solvent is used. At this stage, implicit and explicit solvent models give the same results: A beads of PDMA interact more strongly with the surface, making it more difficult for them to leave the first adsorption layer.

4.2.4 Dynamical properties of the polymers on the surface

In order to know whether the implicit solvent reproduces dynamical properties of PAAm and PDMA, we follow the same procedure as in the previous section for the system containing an explicit solvent. We consider active beads, which are beads that cross regions, and investigate their dynamics. We therefore have an insight into the number of events beads undergo and the frequency of the event "bead leaves the surface". These results are summarized in table 4.6.

First of all, both PAAm and PDMA have rather few active beads over the course of the simulations, compared to the system in which the solvent is explicit. This is due to the fact that the system interacting through an implicit solvent is more constrained than the system containing an explicit solvent. Concerning non-active beads, table 4.6 shows that difference between PAAm and PDMA is small and PAAm has slightly more non-active beads than PDMA. Knowing that experimentally, PAAm does not glue on silica nanoparticles whereas PDMA does, we conclude that non-active beads do not play an important role as far as adsorption of polymer chains on silica surface is concerned. One

can see from table 4.6 that PAAm has more active beads than PDMA (first row), which is the opposite of what is observed when the solvent is explicit 4.2, but that PDMA active beads undergo more events than PAAm active beads (third row). The consequence is that the dynamical properties of A beads of PAAm and A beads of PDMA are the same: the resulting frequency of the event "bead leaves" is the same for PAAm and PDMA for instance (fourth row).

4.3 Conclusion

The system containing an explicit solvent yields results that correspond to the observed experimental behavior. The reproducibility of experimental behavior is even more significant in the following chapters 5 and 6 of part II. As far as the use of the implicit solvent is concerned, we conclude that it reproduces energetical features, such as interaction energy ranking and free energy barrier ΔF_B. However, dynamical properties are poorly captured by an implicit solvent. This is due to the fact that proper solvent beads and the related steric effect they imply are lacking in the implicit description of solvent. Therefore, the solvent plays a role by screening – or not – interactions, but also by moving freely (compared to polymer chains) and replacing polymer beads on the surface of the silica surface, and also by competing with polymer beads with regard to the interaction with the silica surface. The latter characteristics are not included in an implicit solvent. Therefore, we decided to continue using an explicit solvent.

Outcome of the chapter

To understand why PAAm does not glue on silica surface, whereas PDMA does, one has to consider the effect of solvent which not only interacts with both polymer and surface, but which also prevents – or not – polymer chains from adsorbing on silica surface thanks to its lability compared to polymer chains. To that extent, the use of an implicit solvent, which does not capture all the important features of the solvent, is not an option in our system.

Chapter 5

Stability of a polymer chain on silica surface

In the previous chapter, we focused on the interfacial area between a silica surface and a rather dense polymer solution. Dynamics as well as interaction energies and polymer solvation were discussed. We then decided to investigate the mechanisms occurring when PAAm and PDMA are detached from a silica surface. However, we soon realized that it is difficult to rigorously study the detachment of a dense polymer solution. We therefore decided to model a diluted polymer system. In the present chapter we probe, by the mean of free energy methods, the detachment of PAAm and PDMA from a silica surface. All along this chapter, infinitely diluted polymer chains are considered: one chain stands on the silica surface, surrounded by solvent beads. This gives us insight into the energy one has to provide to remove PAAm or PDMA from a silica surface, how PAAm and PDMA detach from silica, and what the important features are.

5.1 Computing free energy

The free energy is directly related to the canonical partition function Q_{NVT} through $F = -k_B T \ln Q_{NVT}$. Different thermodynamic quantities are therefore obtained from derivation of the free energy. Furthermore, more than free energy F, free energy difference ΔF is a central quantity that is important to be able to evaluate. Free energy differences are indeed of particular interest: they give for instance information on the hydrophobic or hydrophilic nature of a solute, on a system stability as a function of a given reaction coordinate and on the solvation free energy of a solute. Nonetheless, free

energy of a system along a reaction coordinate is not directly accessible from one standard molecular dynamics simulation. Free energy is a state function, thus it does not depend on the reaction path that is used to evaluate it. A consequence is that it exists a wide range of methods to calculate free energy differences. We will present some of the main ones and the one we selected: *umbrella sampling*. We use this method to study the relative stability of one PAAm and one PDMA chain on the silica surface, surrounded by a solvent. We also investigate the free energy barrier that PAAm and PDMA have to respectively overcome in order to detach from the silica surface.

We consider a polymer chain adsorbed on a silica surface. The center of mass of the polymer chain is stabilized at a certain distance from the surface. Moving the polymer chain toward or away from the surface has a high energetic cost which prevents the polymer chain from moving too close or far from the surface. Therefore, using a simple force field does not yield sufficient sampling of higher energy regions. Using simple molecular dynamic does not provide the free energy profile of the polymer chain as a function of the position of its center of mass.

5.2 Free energy methods

5.2.1 Reaction coordinate

It is of first importance, when dealing with free energy, to introduce the notion of *reaction coordinate*. The latter are generalized coordinates that are helpful when investigating the free energy evolution of a system. The reaction coordinate can be a simple Cartesian coordinate, $\mathbf{r}$, a combination of two coordinates, $|\mathbf{r}_1 - \mathbf{r}_2|$, an angle, a center of mass position ($\mathbf{R} = (m_1\mathbf{r}_1 + m_2\mathbf{r}_2)/(m_1 + m_2)$), or a radius of gyration. The reaction coordinate has to be carefully chosen and depends on which system and which of its parameters are studied. In our system, we consider the distance between the center of mass of the polymer chain and the surface as the reaction coordinate.

5.2.2 Free energy perturbation theory

We first consider the problem of transforming a system from one state A to another state B with respective energies $U_A(\mathbf{r}_1, \mathbf{r}_2, ..., \mathbf{r}_N)$ and $U_B(\mathbf{r}_1, \mathbf{r}_2, ..., \mathbf{r}_N)$. The two related free energies are then $F_A = -k_BT \ln Q_A$ and $F_B = -k_BT \ln Q_B$, where Q_A and Q_B are the related canonical partition functions:

$$Q_A = \frac{Z_A(N,V,T)}{N!\lambda^{3N}}, \text{and} \tag{5.1}$$

$$Q_B = \frac{Z_B(N,V,T)}{N!\lambda^{3N}}, \tag{5.2}$$

where N is the particle number, $\lambda = \sqrt{\beta h^2/2\pi m}$ (h is the Planck constant and m the particle mass), $Z_A(N,V,T)$ and $Z_B(N,V,T)$ are the configurational partition functions for states A and B in the canonical ensemble:

$$Z_A = \int d^N\mathbf{r} \exp\Big(- \beta U_A(\mathbf{r}_1, ..., \mathbf{r}_N)\Big), \tag{5.3}$$

$$Z_B = \int d^N\mathbf{r} \exp\Big(- \beta U_B(\mathbf{r}_1, ..., \mathbf{r}_N)\Big), \tag{5.4}$$

with $\beta = 1/k_BT$. The difference of free energy between states A and B is therefore:

$$\Delta F_{AB} = F_B - F_A = -k_BT \ln\left(\frac{Q_B}{Q_A}\right) = -k_BT \ln\left(\frac{Z_B}{Z_A}\right). \tag{5.5}$$

However, the right member of equation 5.5 is not easy to calculate because molecular dynamics allows to compute averages of microscopic functions but not directly partition functions. We then have to modify the expression of Z_B:

$$\begin{aligned} Z_B &= \int d^N\mathbf{r} \exp\Big(- \beta U_B(\mathbf{r}_1, ..., \mathbf{r}_N)\Big) \qquad (5.6)\\ &= \int d^N\mathbf{r} \exp\Big(- \beta U_B(\mathbf{r}_1, ..., \mathbf{r}_N)\Big) \exp\Big(- \beta U_A(\mathbf{r}_1, ..., \mathbf{r}_N)\Big) \exp\Big(\beta U_A(\mathbf{r}_1, ..., \mathbf{r}_N)\Big)\\ &= \int d^N\mathbf{r} \exp\Big(- \beta U_A(\mathbf{r}_1, ..., \mathbf{r}_N)\Big) \exp\Big(- \beta\Big(U_B(\mathbf{r}_1, ..., \mathbf{r}_N) - U_A(\mathbf{r}_1, ..., \mathbf{r}_N)\Big)\Big), \end{aligned}$$

and

$$\frac{Z_B}{Z_A} = \left\langle \exp\Big(-\beta\Big(U_B(\mathbf{r}_1,...,\mathbf{r}_N) - U_A(\mathbf{r}_1,...,\mathbf{r}_N)\Big)\Big)\right\rangle_A, \tag{5.7}$$
$$\Delta F_{AB} = -k_B T \ln\left\langle \exp\Big(-\beta(U_B - U_A)\Big)\right\rangle_A,$$

which corresponds to the *free energy perturbation* formula [183]. In this approach, states A and B have to be very close, as state B is averaged over A ensemble. If this is not the case, $U_B - U_A$ becomes large, and hence $\exp\Big(-\beta(U_B - U_A)\Big)$ becomes small. Moreover, when doing an average in ensemble A ($<>_A$), we explore B configurations in the A ensemble. Statistics of the A ensemble have to be representative of B. Otherwise, B is really small in the A ensemble average, and therefore ΔF_{AB} converges slowly. For this reason, the free energy perturbation theory can be used when states A and B are really close.

We are interested in probing the free energy required for PAAm and PDMA respectively to detach from the surface. We start from a configuration where the polymer chains are adsorbed on the surface and end with a drastically different configuration where the polymer chains are detached from the surface. Hence, the free energy perturbation theory, which requires similar starting and final states, is not adapted to our problem.

5.2.3 Thermodynamic integration

Thermodynamic integration considers intermediate states to smoothly, continuously switch the system from state A to state B. The system is fully relaxed at each step of the path between A and B. In order to switch the system between A and B, we introduce a parameter κ that varies between 0 (initial configuration, state A) and 1 (final configuration, state B) and switching functions, $f(\kappa)$ and $g(\kappa)$ defined as:

$$U(\mathbf{r}_1,...,\mathbf{r}_N,\kappa) = f(\kappa)U_A(\mathbf{r}_1,...,\mathbf{r}_N) + g(\kappa)U_B(\mathbf{r}_1,...,\mathbf{r}_N). \tag{5.8}$$

We need $U(\mathbf{r}_1, ..., \mathbf{r}_N, 0) = U_A(\mathbf{r}_1, ..., \mathbf{r}_N)$ and $U(\mathbf{r}_1, ..., \mathbf{r}_N, 1) = U_B(\mathbf{r}_1, ..., \mathbf{r}_N)$. A simple choice for $f(\kappa)$ and $g(\kappa)$ is then $f(\kappa) = 1 - \kappa$ and $g(\kappa) = 1$. This choice leads to an expression for the free energy difference:

$$\Delta F_{AB} = \int_0^1 \langle U_B - U_A \rangle_\kappa d\kappa. \tag{5.9}$$

One disadvantage of this method is that only states A and B, when κ equals respectively 0 and 1, have a physical meaning. Since intermediate states are unphysical, this method requires to run numerous simulations to accurately compute intermediate, non-physical states.

5.2.4 Umbrella sampling method

Umbrella sampling is a free energy method that allows to probe regions of the free energy curve that would not be available at room temperature (unconstrained simulation) or with simple molecular dynamics. The method was first developed by Torrie and Valleau in 1974 [184, 185]. The overall idea of the method is to restrain the reaction coordinate, rather than constraining it [117], by applying a bias potential. Umbrella sampling is, to that extent, different from thermodynamic integration or from the blue moon method [117], which both constrain the reaction coordinate of interest. In our case the reaction coordinate is the position of the center of mass of the polymer with respect to the surface. Here the bias potential is an harmonic potential:

$$V_{US}(r_{COM}) = \frac{1}{2} K (r_{COM} - r_0)^2, \tag{5.10}$$

which is added to the Martini force field. K is a strength constant, r_{COM} is the position of the center of mass (COM) of the polymer chain and r_0 is its equilibrium position. The new interaction potential is then:

$$V(r_{COM}) = V_{bonded}(r_{COM}) + V_{nonbonded}(r_{COM}) + V_{US}(r_{COM}). \tag{5.11}$$

This modified potential is used in a molecular dynamics simulation. The bias potential is used to restrain the reaction coordinate within a small interval in order to enhance sampling in this region. We then run several molecular dynamic simulations of 10 nanoseconds at several $V_{US}(r_{COM})$ bias potential, for different equilibrium position r_0, and finally unbiase and recombine the results of the various biased simulations to obtain the final free energy profile. However recombining the results is not an easy task. There exist several methods to do so which are not optimal computationally because they do not use all the data from the simulations and can lead to important errors [184–188]. The Weighted Histogram Analysis Method (WHAM) is an efficient extension to the umbrella sampling method [189] because it provides a free energy value by taking into account all the data from the simulations and provides an estimation of the uncertainty. We use the implementation of WHAM provided by the Grossfield Laboratory [190].

Therefore, I performed umbrella sampling calculations to sample the free energy of the center of mass of the polymer chain as a function of its distance D to the silica surface. This method was used to compare the behavior of PDMA and of PAAm in implicit and explicit solvent with regard to the silica surface. All along the following sections, r_{COM} is the instantaneous position of the polymer COM, r_0 is its equilibrium position that is fixed and D is the average distance between the polymer COM and the surface which is computed along the MD simulations with the bias potential $V_{US}(r_{COM})$. Last but not least, the COM equilibrium position of the polymer is constrained in the x, y, z directions.

5.3 Investigating the detachment of a polymer chain from the silica surface

5.3.1 The system

The system we consider contains one silica surface, one polymer chain of PAAm or of PDMA (90 monomers) and a solvent, implicit in a first part (sections 5.3.2 and 5.3.3) and explicit in a second part (section 5.3.4). We have highlighted in section 4 that the implicit solvent reproduces some of the features of the system, such as interaction energies, but not all, like steric hindrance due to the solvent. It is interesting to know whether the use of an implicit solvent instead of the explicit solvent reproduces the free energy profile of the polymer COM.

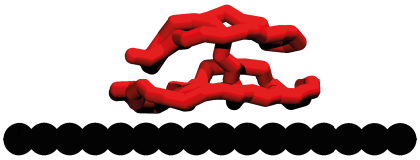

Figure 5.1 – Snapshot of the initial configuration of the polymer chain on the silica surface.

We first use the umbrella sampling method and the implicit solvent model presented in section 3.4.2 at 300 K to plot the evolution of the free energy as a function of the distance between the silica surface and the polymer COM, D in section 5.3.2. Then, we study the same system at 500 K in section 5.3.3 in order to have a point of comparison to compare systems containing an explicit solvent at 500 K in section 5.3.4. We start from a stable configuration of PAAm and PDMA close to the silica surface (see figure 5.1) and then restrain the polymer COM closer and further from the surface. For each value of the equilibrium position of the polymer COM r_0, a 10 ns simulation was performed and the evolution of the polymer COM position along the simulation was collected. We then use the WHAM algorithm to combine the results obtained for different r_0 and plot the

free energy profile of the polymer as a function of its distance with the silica surface D. r_0 is the target equilibrium distance between the polymer COM and the silica surface, whereas D is the resulting distance averaged over each 10 ns MD simulations. When r_0 corresponds to a stable state of the polymer chain on the surface, r_0 and D are close. However, when r_0 is a hard-to-reach stage for the polymer chain, r_0 and D differ.

5.3.2 Implicit solvent, 300 K

We consider a simulation cell with $l_x = l_y = l_z = 63$ Å, containing 200 surface beads S and one polymer chain of 90 monomers. We start from the initial configuration presented in figure 5.1 and restrain the polymer COM at different r_0, for PAAm and PDMA. For each value of r_0, we compute the histogram distribution of the distances between the polymer COM and the surface D. The resulting succession of histograms is displayed in figure 5.2. From this sequence, we compute the free energy profile in figure 5.3.

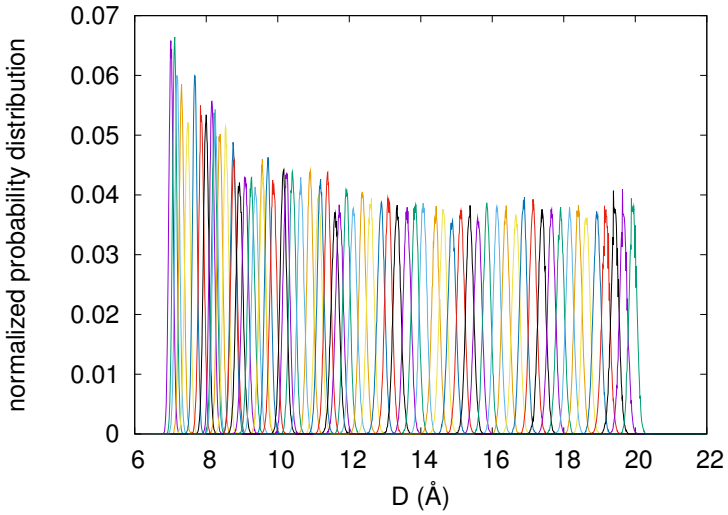

Figure 5.2 – Histogram distributions as a function of distances D.

Both polymers detach from the surface above 20.5 Å. Above this distance, polymer beads are desorbed from the silica surface. Moreover, one can directly see from figure 5.3 that the free energy difference ΔF_{COM} between the "unbound" state (where the whole polymer

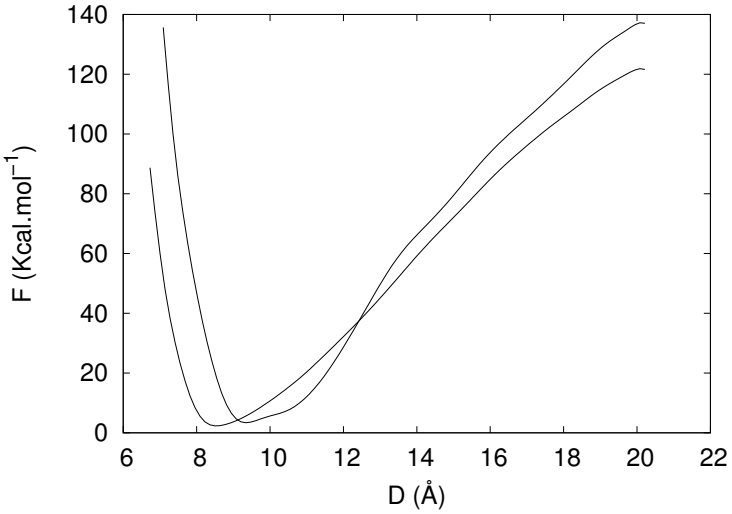

Figure 5.3 – Free energy profile for PAAm (solid line) and PDMA (dashed line) in an implicit solvent at 300 K.

chain is detached from the surface) and the state where the free energy equals zero, is higher for PDMA (136 kcal.mol^{-1}) than for PAAm (122 kcal.mol^{-1}). Thus, it is more difficult to detach one PDMA chain from the surface than one PAAm chain from a silica surface. Figure 5.3 corresponds to the experimental behavior in the sense that PDMA is more difficult to detach from the surface [38] than PAAm [36]. However, it shows that PAAm is actually adsorbed on the silica surface when it is experimentally difficult to glue a PAAm hydrogel on silica nanoparticles [36].

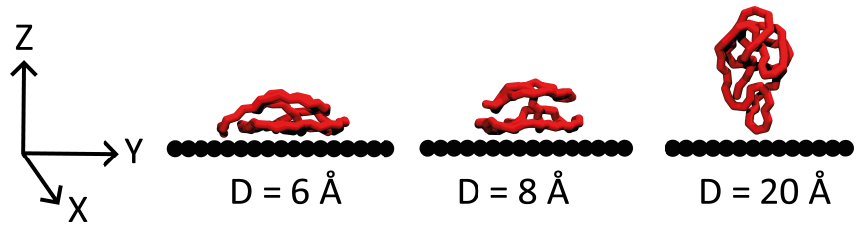

Figure 5.4 – Evolution of the polymer shape as D increases.

Figure 5.4 shows the evolution of the polymer shape as D increases. There is a wide range of polymer conformations along the distance between the polymer COM and the silica surface. The evolution of the polymer shape raises curiosity: the polymer chain switches from a pancake shape to a funnel. In order to investigate the evolution of the shape of PAAm and PDMA as a function of D, we compute the three components of inertia moment in

the directions x, y and z (where z is normal to the surface and x, y is the surface plan) along all the 10 ns simulations. We then calculate the ratio $R = 2I_{zz}/(I_{xx} + I_{yy})$. This ratio allows us to know whether the polymer chain is elongated in the z direction ($R > 1$) or in the x, y plan ($R < 1$). The evolution of R as a function of the distance between the polymer COM and the surface is shown in figure 5.5. When the distance between polymer COM and surface is below 12 Å, R is below 1, meaning that the polymer chain is spread on the surface. Above 12 Å the polymer chain elongates along the z direction. It is worth noting that, up to 16 Å, PDMA (dashed line) is slightly less elongated along the z direction than PAAm, meaning that PDMA prefers to interact with the surface compared to PAAm. Above 16 Å, the PAAm curve fluctuates because only few beads from the PAAm chain still interact with the surface, and its shape is not well defined.

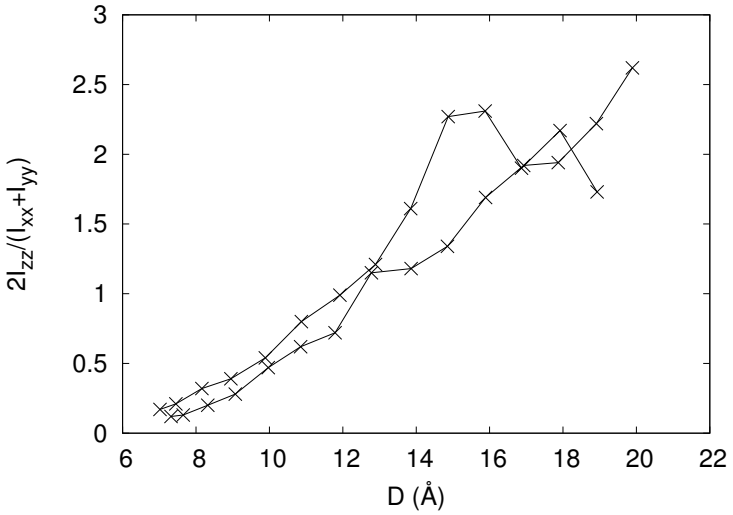

Figure 5.5 – Evolution of the shape of PAAm (solid line) and PDMA (dashed line) along the direction normal to the surface. Implicit solvent at 300 K.

Therefore, even if the use of an implicit solvent reproduces some of the experimental features, like the difficulty to detach the PDMA chain from the silica surface, which is highlighted by the high free energy barrier (136 kcal.mol^{-1}) and the interesting shape that PDMA adopts to enlarge the number of beads that interact with the surface, it fails to reproduce the important difference of behavior between PAAm and PDMA. In order to reproduce the divergence between PAAm and PDMA, the use of an explicit solvent might be necessary.

In the following section one polymer chain on the silica surface surrounded by 2000 solvent beads is simulated. Herein, we consider a system where polymer chains are infinitely diluted. However, as mentioned in section 3.4.1, the explicit solvent model developed by Marrink and co-workers within the Martini force field [137] has the tendency to freeze at too low temperature when a nucleation site is present in the system, which is the case in our model where a silica surface is present. In this situation, the authors of reference [137] propose to change solvent beads for "non-freezing" beads, which are larger beads whose aim is to introduce a symmetry breaking within the system. However, we decided not to use those beads because we would not completely control their behavior and their influence on the polymer behavior. We instead increase the temperature up to a point where solvent beads do not freeze: 500 K. Temperature has an impact on the free energy profile. So we had to compute the free energy profile of the system with an implicit solvent at 500 K to be able to compare it with the free energy profile of the system containing an explicit solvent at 500 K. This will also allow us to rationalize the impact of temperature on the system containing an implicit solvent, by comparing the free energy profile at 300 K and at 500 K.

5.3.3 Implicit solvent, 500 K

Simulation cell is the same as described in the previous section 5.3.2. Figure 5.6 is the free energy profile of PAAm and PDMA on the silica surface, surrounded by an implicit solvent at 500 K. It remains more difficult to detach PDMA than PAAm from the silica surface, as seen in the previous section 5.3.2. For PDMA the free energy barrier ΔF_{COM} is 93 kcal.mol^{-1} (at 20.5 Å) with an implicit solvent at 500 K against 136 kcal.mol^{-1} with an implicit solvent at 300 K. As for PAAm, the free energy barrier is of 82 kcal.mol^{-1} (20.5 Å) at 500 K against 122 kcal.mol^{-1} at 300 K. A lowering of the free energy barrier is expected at 500 K, compared to 300 K. PDMA detaches further from the surface than at 300K.

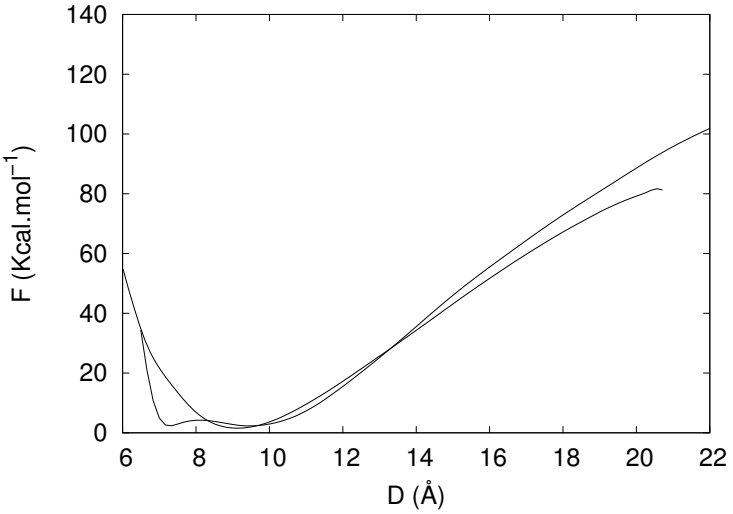

Figure 5.6 – Free energy profile for PAAm (solid line) and PDMA (dashed line) in an implicit solvent at 500 K.

As for the shape (figure 5.7), we observe the same behavior than at 300 K: PDMA is slightly more elongated along z direction than PAAm.

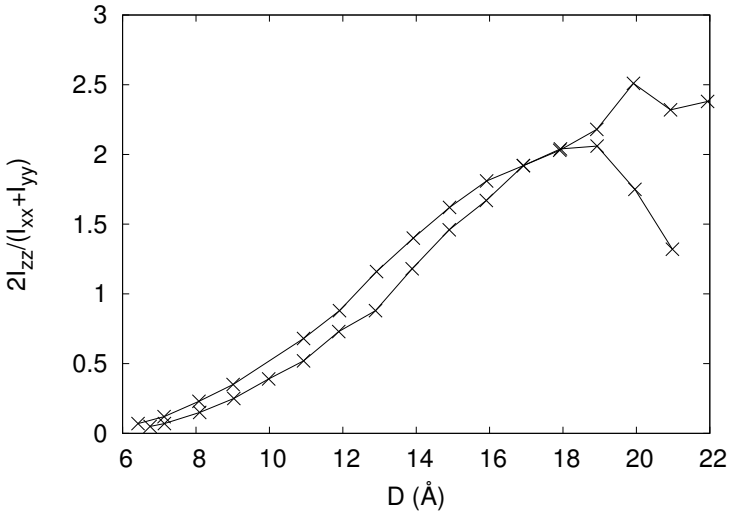

Figure 5.7 – Evolution of the shape of PAAm (solid line) and PDMA (dashed line) along the direction normal to the surface. Implicit solvent at 500 K.

Moreover, one can see from figure 5.6 that there is a high-stability region for PDMA at $D = 7.2$ Å. Figure 5.8 shows the side (figure 5.8(a)) and top (figure 5.8(b)) view of the PDMA chain on the silica surface at $D = 7.2$ Å. We see that the polymer chain is flat like a crepe on the surface and forms a spiral. This is a preferred configuration for PDMA because it optimizes the number of beads which interact with the surface.

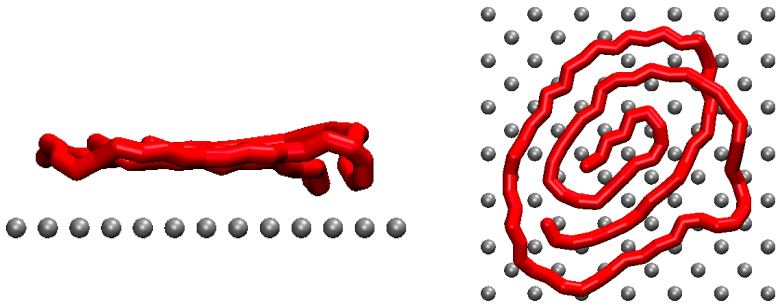

(a) Side view. (b) Top view.

Figure 5.8 – Side and top view of the PDMA chain on silica surface at D equals 7.2 Å. Only the backbone chain (C beads) is represented. Implicit solvent at 500 K.

Free energy profile at 500 K is then consistent with what was observed at 300 K but still shows a shortcoming of the implicit solvent model. PAAm is actually able to adsorb on silica surface and is difficult to detach from it, which is contradictory with the experimental behavior [36].

5.3.4 Explicit solvent, 500 K

To know whether the solvent plays an important role during the detachment of a polymer chain from the surface, we use the umbrella sampling method on a system containing an explicit solvent. The aim is to probe whether the solvent will stabilize PAAm or PDMA with regard to the surface and will be able to reproduce the experimental behavior. The simulation cell we use has different dimensions as described in sections 5.3.2 and 5.3.3: $l_x = l_y = 63$ Å and $l_z = 63.4$ Å. Moreover, it contains 2 000 additional solvent beads.

We see from figure 5.9 that solvated PAAm is not stabilized by the presence of the surface. PAAm is well solvated: the chain is more stabilized when being solvated than when being adsorbed on the silica surface. There is still an energy well for PDMA, but further from the surface (around 13 Å from the surface) and not as deep as with implicit solvent (figure 5.6). Moreover, the free energy difference ΔF_{COM} between the "unbound" state (where the whole polymer chain is detached from the surface) and the state where the free energy equals zero is smaller for PDMA solvated at 500 K than for PDMA with im-

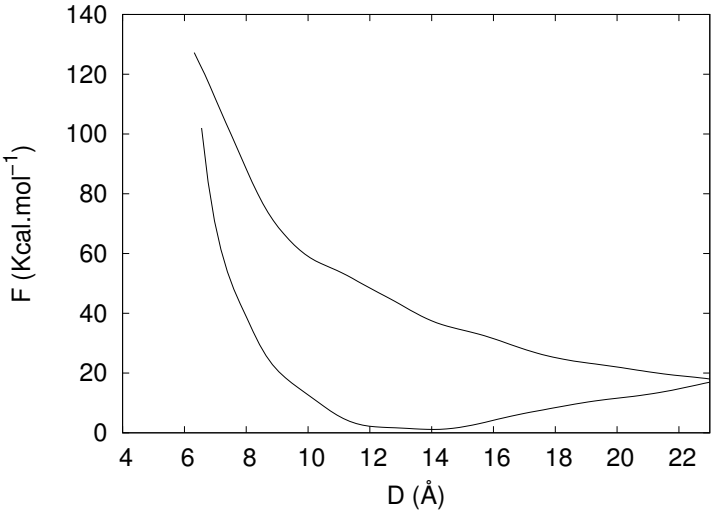

Figure 5.9 – Free energy profile for PAAm (solid line) and PDMA (dashed line) in an explicit solvent at 500 K.

plicit solvent at 500 K, meaning that the explicit solvent stabilizes PDMA and makes the detachment easier. It is worth noting that PDMA chains detach further from the surface than with the implicit solvent. PDMA chain in implicit solvent detaches at 20.5 Å from the surface, whereas PDMA in explicit solvent detaches at 26 Å. PAAm chain in implicit solvent detaches at 20.5 Å from the surface, whereas PAAm in explicit solvent detaches at 16 Å. This is a major difference between PDMA and PAAm in explicit solvent: PAAm is well solvated and detaches easily from the surface, whereas PDMA interacts as much as possible with the surface and is hard to detach from the surface.

Moreover, when we start from the configuration where the polymer COM is constrained at 12.5 Å from the surface and let the system evolve for 100 ns, we find that PAAm moves away from the surface whereas PDMA stays close to the surface (figure 5.10(a) and 5.10(b)). This result corresponds to the experimental behavior where PDMA is adsorbed on the silica surface and is really hard to detach from the surface [38] whereas PAAm does not adhere on the silica surface [36].

The fact that PAAm desorbs readily from the surface, whereas PDMA is difficult to detach from the surface can be visualized in figure 5.11 that shows the evolution of the polymer chains shape. Figure 5.11 indicates that PAAm almost keeps the same shape,

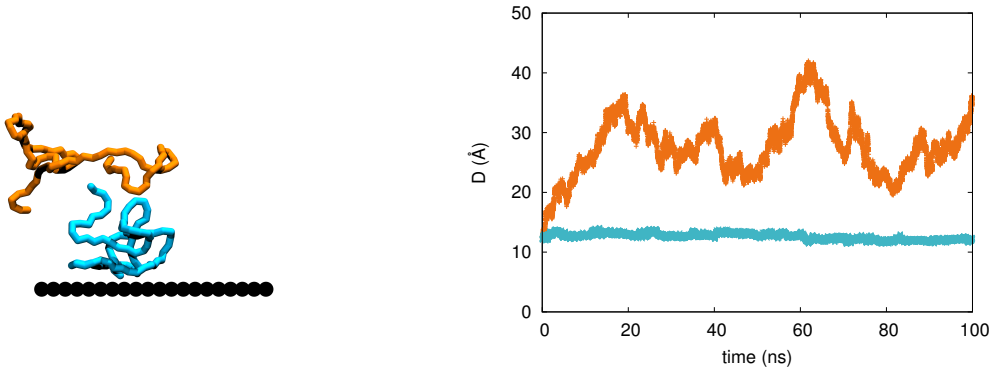

(a) Final configuration of PAAm (orange) and PDMA (blue), without-constraint evolution. PAAm and PDMA are only superimposed to take the snapshot.

(b) Distance between the center of mass of the polymer chain and the silica surface along the simulation. PAAm is in orange and PDMA in blue.

Figure 5.10 – Without-constraint evolution of PDMA and PAAm.

spread on the x, y plan, when we constrain its COM at different distances from the surface. This is due to the fact that PAAm detaches from the surface for short distances and strongly interacts with the solvent (or prefers to interact with the solvent than with the surface). On the opposite, PDMA is really elongated because it keeps some beads attached to the surface, even when we constrain its center of mass far from the surface.

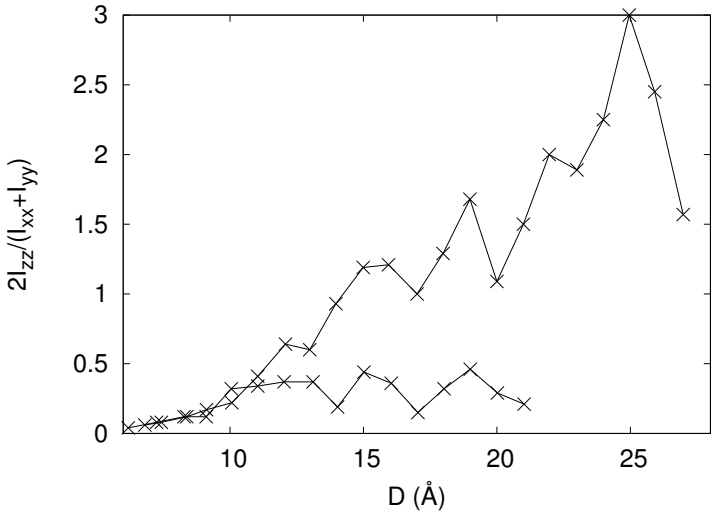

Figure 5.11 – Evolution of the shape of PAAm (solid line) and PDMA (dashed line) along the direction normal to the surface. Explicit solvent at 500K.

In order to get a better insight into the detachment process of PDMA from the silica surface, we compute the number of adsorbed polymer beads on the silica surface (figure

5.12). We see, for PDMA, that above 16 Å the number of adsorbed beads on the surface is constant, oscillating around height beads adsorbed on the surface. The flat part of the curve shows that there is a constant number of adsorbed beads on the surface as we continue pulling on the polymer chain. On this part, the polymer chain changes its shape both to satisfy the constraint on its COM and to keep some beads on the surface. We may wonder whether this behavior has an entropic or energetic origin.

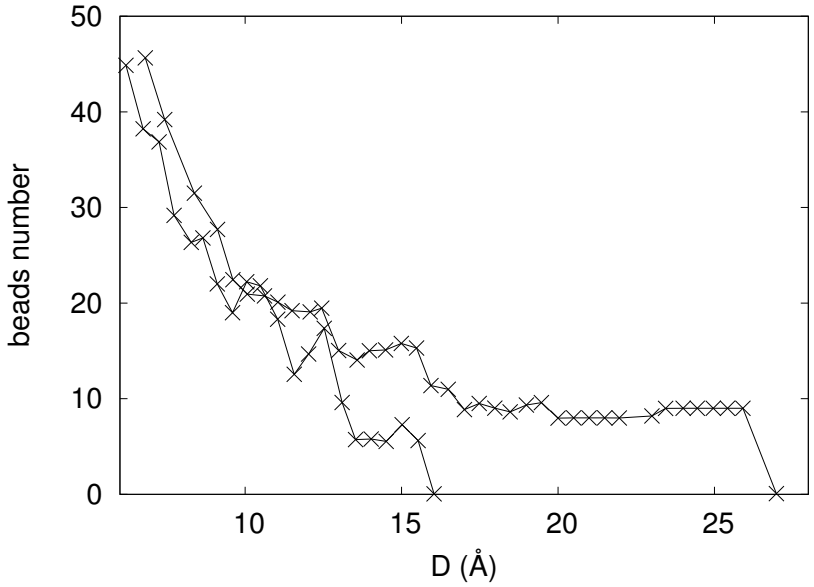

Figure 5.12 – Number of adsorbed beads close to the surface for PAAm (solid line) and PDMA (dashed line).

Figure 5.15 shows the evolution of total potential energy and entropy of the systems containing PAAm (figures 5.13(a) and 5.13(c)) or PDMA (figures 5.13(b) and 5.13(d)) when the polymer center of mass moves away from the surface. The total potential energy (enthalpic term, considering that kinetic energy is equal in both systems) of systems containing PAAm and PDMA both decrease with D, even though it decreases faster for PAAm than for PDMA. The opposite of the entropy multiplied by the temperature has the same shape for PAAm and PDMA but is sharper for PAAm.

At first glance, it is difficult to distinguish PAAm and PDMA with regard to their enthalpic or entropic behavior. In order to understand what is the role played by entropy

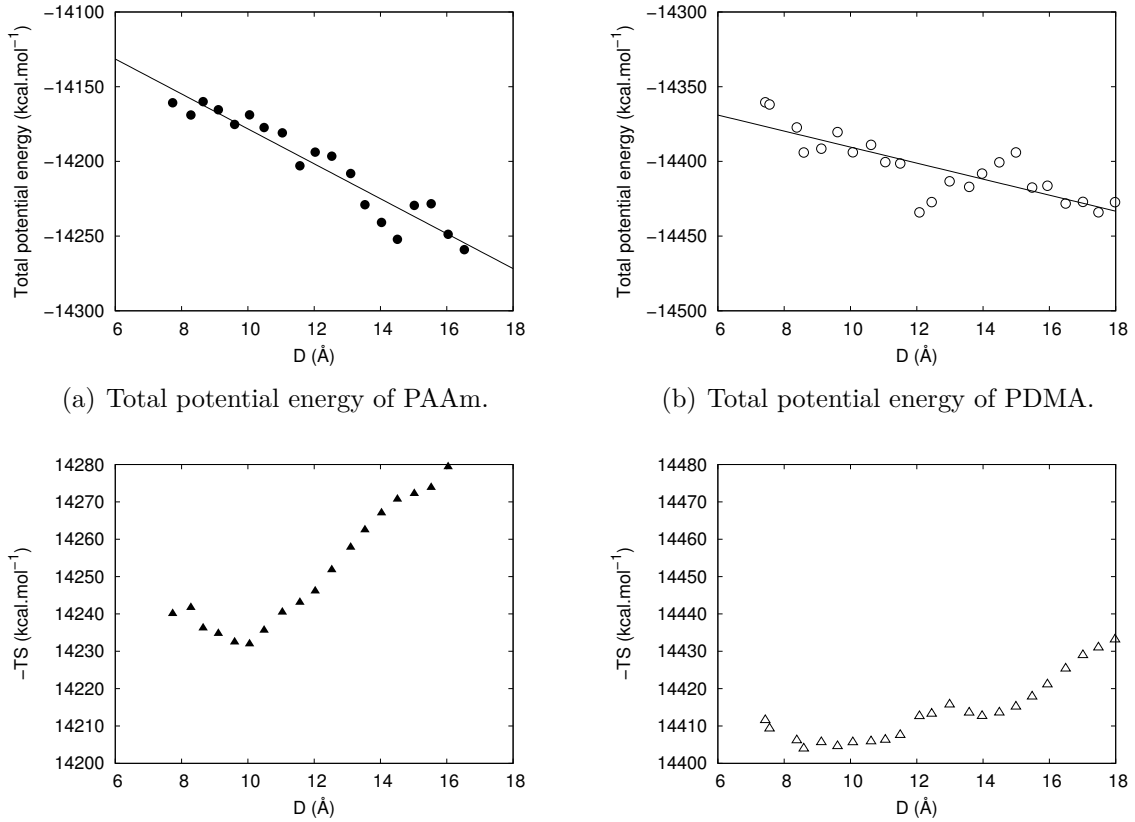

(a) Total potential energy of PAAm.

(b) Total potential energy of PDMA.

(c) Entropy (-TS) of PAAm.

(d) Entropy (-TS) of PDMA.

Figure 5.13 – Energetic behavior of systems containing PAAm and PDMA. Cross: experimental datas. Dashed line: fitting lines.

and enthalpy, and which one is responsible for the well in the free energy profile of PDMA, we mixed the entropy and the potential energy of PAAm and PDMA in figure 5.14. Top part of figure 5.14 is $F = U_{PAAm} - TS_{PDMA}$; the bottom part is $F = U_{PDMA} - TS_{PAAm}$. The bottom figure has the well, whereas the top part decreases uniformly. In other words, $U_{PDMA} - TS_{PDMA}$ has a well and $U_{PDMA} - TS_{PAAm}$ has also a well: U_{PDMA}, associated with TS_{PDMA} or with TS_{PAAm} results in the presence of a well. This is therefore the slope of the potential energy of PDMA that is responsible for the presence of a well. Hence, the potential energy drives the behavior of the system.

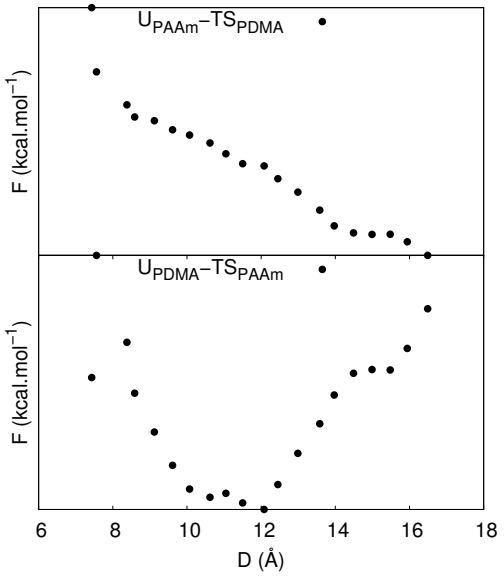

Figure 5.14 – Free energy from mixed potential energy and entropy between PAAm and PDMA.

It is interesting to look at the different component of the potential energy. The figure 5.15 shows the different component of the potential energy: polymer/surface, polymer/polymer, polymer/solvent and surface/solvent interaction energies. One can see from the figure 5.15 that in the system containing PDMA and PAAm, the polymer/surface interaction energy tends to zero as the polymer moves away from the surface (as expected...) and the surface/solvent decreases due to the fact that more solvent beads are in contact with the surface when the polymer moves away from the surface. One can note different behaviors with regard to the polymer/polymer and polymer/solvent in-

teraction energy. Close to the surface, PDMA/solvent interactions are destabilized with regard to PDMA/PDMA interactions whereas PAAm/solvent interactions are stabilized with regard to PAAm/PAAm interactions. It means that PAAm is better solvated than PDMA. As we move away from the surface, PDMA/solvent interactions are stabilized and PDMA/PDMA interactions decrease. This is due to the particular shape adopted by PDMA far from the surface (see figure 5.11): it is strongly extended, therefore it increases polymer/solvent interactions and reduces polymer/polymer interactions. If we now compare polymer/polymer interactions between PAAm and PDMA, the decrease in interaction energy is more significant for the PDMA/PDMA interaction than for the PAM/PAM interaction. Therefore, polymer/polymer interactions are responsible for the different behavior between PAAm and PDMA.

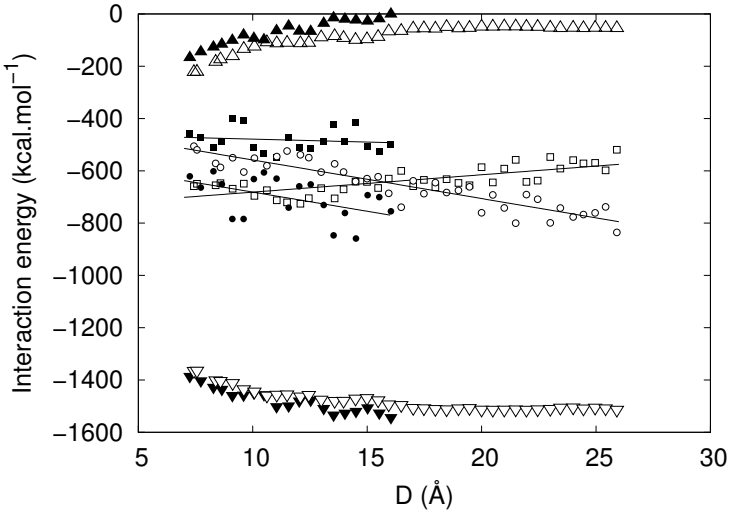

Figure 5.15 – Interaction energies for PAAm (solid line and black symbols) and PDMA (dashed line and open symbols). Polymer/surface (▲ for PAAm and △ for PDMA), polymer/polymer (■ for PAAm and □ for PDMA), polymer/solvent (● for PAAm and ○ for PDMA) and surface/solvent (▼ for PAAm and ▽ for PDMA) interaction energies are represented.

5.4 Link with interaction parameters

In this section we investigate what are precisely the interaction parameters responsible for the different behavior of PDMA and PAAm.

5.4.1 Method

In order to uncouple the participation of different interaction parameters, we change one-by-one the interaction parameters of PAAm for the one of PDMA to know what is the role played by each interaction parameter. We made this study for a larger system containing one polymer chain of 2000 monomers, which corresponds to what is experimentally used (see chapter 7). The solvent is explicit and polymer chains are infinitely diluted. The resulting system contains 2000 monomers, being 4000 beads for the polymer chain, 800 beads for the silica surface and 24469 solvent beads for PAAm and 24169 solvent beads for PDMA. The different number of solvent beads is due to the fact that PDMA A beads, being bigger than PAAm A beads, they occupy a larger volume, which cannot be neglected when the polymer chain is 2000 monomers long. In order to have the same solvent density in the system containing PAAm and PDMA, we had to reduce the number of solvent beads for PDMA.

(a) Final configuration of PDMA.

(b) Final configuration of PAAm.

Figure 5.16 – Snapshot of the final configuration of PDMA and PAAm after a without-constraint 500 ns evolution. Silica surface is in black, solvent beads are in blue and polymer chain is in red.

We first build the system and let it evolve for 500 ns. Snapshots of the final configurations of PDMA and PAAm are shown in figure 5.16 (figure 5.16(a) for PDMA and figure 5.16(b) for PAAm. The same initial configuration, close to the final state of PDMA, was used for PDMA and PAAm. The simulation cell lengths are $l_x = 126$ Å, $l_y = 126$ Å and $l_z = 200$ Å for PDMA and PAAm. The cell length in the z direction is large enough so that polymer chains do not interact with the bottom surface implied by the use of pe-

riodic boundary conditions. The final configurations of PDMA and PAAm are similar to what is observed when polymer chains contain 90 monomers (figure 5.10): PDMA remains collapsed and adsorbed onto the silica surface, whereas PAAm is more unfolded and gets away from the surface. The idea of the following sections is to know which parameters allow PDMA to remain shrunk and adsorbed on the surface. So we start from the final configuration of PDMA (figure 5.16(a)) and use bonded and nonbonded interaction parameters of PAAm. Then, we modify one-by-one PAAm parameters to the ones of PDMA and see which one leads to the stable state of PDMA (figure 5.16(a)) and not to that of PAAm (figure 5.16(b)).

5.4.2 Contribution of interaction parameters

In this section, we compare and evaluate the contribution of bonded and nonbonded parameters to the final behavior of PDMA and PAAm. With this aim in mind, we compare the global configuration and the structure of the polymer beads along the direction normal to the surface through the PMF. It should be recalled that A bead is the chemical group of the polymer chain, C bead is the backbone chain and S bead is a surface bead.

Bonded interaction parameters.

Table 5.1 shows the bonded interaction parameter between C and A beads, which is the only one that differs between PAAm and PDMA. We remind that one of the main interest of our model is that few parameters differ between PAAm and PDMA.

	PDMA		PAAm	
Bonds	k (kcal.mol^{-1})	r_0 (Å)	k (kcal.mol^{-1})	r_0 (Å)
C-A	80.0	2.71	80.0	2.37

Table 5.1 – Bonded interaction parameters differing between PDMA and PAAm.

Nonbonded interaction parameters.

Table 5.2 shows nonbonded interaction parameters differing between PAAm and PDMA.

	PDMA		PAAm	
	ϵ (kcal.mol^{-1})	σ (Å)	ϵ (kcal.mol^{-1})	σ (Å)
A-A	0.96	4.7	0.81	4.3
C-A	0.65	4.7	0.49	4.3
A-S	1.08	4.7	0.81	4.3

Table 5.2 – Nonbonded interaction parameters differing between PDMA and PAAm.

Looking for the interaction parameters responsible for divergences between PAAm and PDMA.

Table 5.3 presents the results obtained when one or two bonded or nonbonded parameters from PAAm are modified (first column), a snapshot of the final configuration (second column) and the corresponding PMF of A beads as regards their distance with the surface d. The corresponding PMF (solid line in each row of table 5.3) is compared with the PMF of PDMA whose snapshot is shown in figure 5.16(a) (dashed line).

We first change the bonded interaction parameter for C-A bond of PAAm for the one of PDMA: $r_0 = 2.37$ Å is replaced by 2.71 Å (see table 5.1). The results are presented in the first row of table 5.3. It is worth noting that the polymer chain has the same type of configuration as PAAm in figure 5.16(b) and the corresponding PMF does not fit with the dashed line of PDMA. It is actually too noisy for small d because there are a rather small number of beads that approach the surface. The polymer chain is completely unfolded and well swelled like PAAm would typically be. We then change the interaction parameters (ϵ and σ) between A and S beads of PAAm for the ones of PDMA (see table 5.2). The resulting conformation presented in the second row of table 5.3 is also close to the one of PAAm. However, the corresponding PMF is now closer to the PMF of PDMA: it is less noisy than in the previous case for small d, meaning that there are more A beads coming in the vicinity of the surface. Therefore, the interaction parameters between A and S beads are responsible for the adsorption of the beads on the surface. Because the polymer chain is unfolded and swelled, the solvent prevents the polymer chain from adsorbing on the surface, even if the polymer chain is stabilized close to the surface. If we

now change PAAm C-A interaction parameters for the ones of PDMA, we see in the third row that the polymer shape is similar to the PDMA spherical shape observed in figure 5.16(a), but is not adsorbed on the surface (the resulting PMF is noisy for small d). The spherical, shrunk shape adopted by PDMA is then due to the interaction parameters between C and A beads: intramolecular interactions are favored with respect to intermolecular interactions with the surface or the solvent. The interaction between polymer and solvent remains stronger than with the surface (see interaction table 3.2 in section 3.3.1 of Chapter 3), leading to a desorption of the polymer chain. We now change the interaction parameters between two A beads: the shape is unfolded, like for PAAm, and the PMF is noisy for small d. We now change two types of interactions: C-A and A-S. Changing C-A interaction enables the polymer to fold by decreasing its interactions with the solvent. It is therefore available to interact with the surface. This is what is shown in the fifth row: the polymer chain adopts the same shape as PDMA and the two PMF are in good agreement.

5.5 Conclusion

In this chapter, and by the mean of the umbrella sampling free energy method, we were able to reproduce the experimental behavior regarding the adsorption or not of one PAAm and one PDMA chains on a flat silica surface. Once again, we demonstrated that the use of an explicit solvent is required when dealing with our system. We were able to understand that the difference in the free energy profiles between PAAm and PDMA is due to the potential energy, and more precisely to the internal interaction energy. We went deeper and decided to uncouple the interaction parameters to know precisely and without any doubt, what is the role played by each of them. We concluded that the interaction between C and A beads in PDMA are responsible for its folded and not swelled state while adsorption of PDMA on silica surface is due to the interaction between A and S beads. It it worth noting that for PDMA to adsorb on the surface, both types of interaction operating together are needed. Having only PDMA A-C interaction will lead to a folded sphere that moves apart from the surface while having PDMA A-S interaction alone leads

Modified Parameter	Snapshot	Corresponding PMF
C-A bond	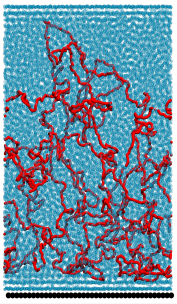	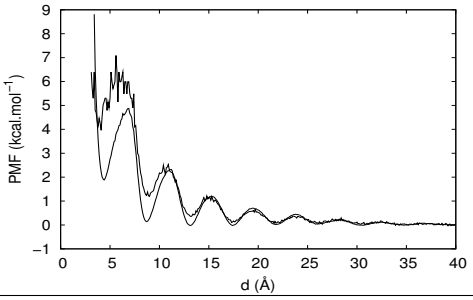
A-S	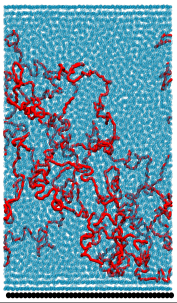	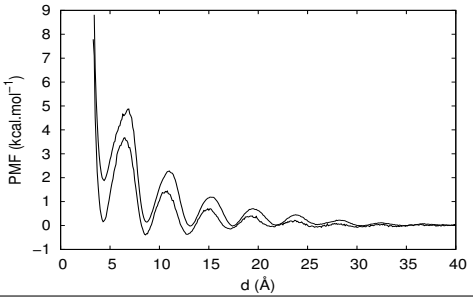
C-A	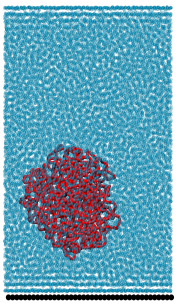	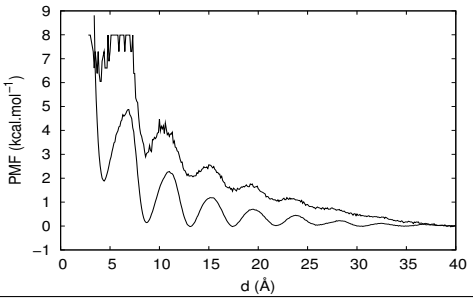
A-A	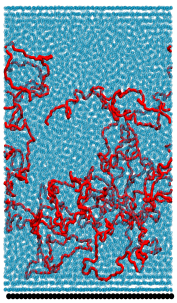	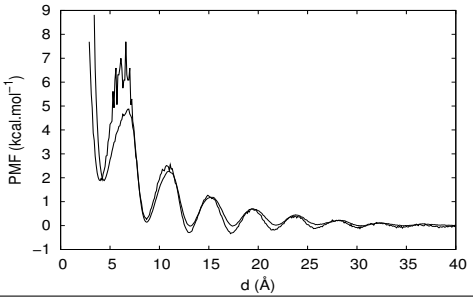
C-A and A-S	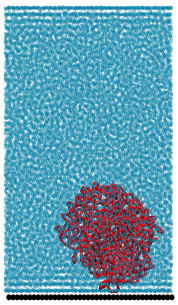	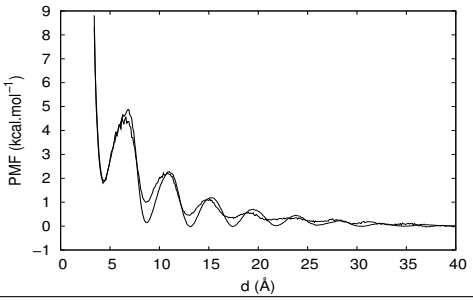

Table 5.3 – Results when one of PAAm parameters is modified.

to a well solvated unfolded chain that interacts quite favorably with the surface but also with the solvent.

Outcome of the chapter

Intramolecular interactions between C and A beads, but also intermolecular interactions between A and S beads are responsible for the stability of a PDMA chain in the vicinity of the silica surface.

Chapter 6

Detaching a polymer chain from two surfaces

In the previous chapter 5 we investigated the stability of explicitly solvated polymer chains on a flat silica surface. We demonstrated that the interaction between the polymer chain and the surface and in between the polymer chain are crucial to the adsorption of PDMA on silica. In this chapter, we probe the interface between surface/polymer/solvent and highlight the structure and dynamic of this interface. Moreover, we show that more than one polymer chain on a silica surface, constraining one polymer chain between two silica surfaces, is a promising device that enables us to investigate interesting features of polymer chains.

6.1 Presentation of the models

Herein we first introduce the two models we will be discussing all along this chapter. On the one hand, we consider one long polymer chain containing 2000 monomers on a silica surface. On the other hand, the same polymer chain is constrained in between two silica surfaces. The latter gives us insight into the polymer behavior when submitted to pressure.

6.1.1 One polymer chain on the silica surface

We first employ the system described in section 5.4 of chapter 5. The system contains 800 beads for the silica surface, 4000 beads for a 2000 monomers polymer chain and

24469 solvent beads for PAAm and 24169 solvent beads for PDMA. The dimensions are $l_x = 126$ Å, $l_y = 126$ Å and $l_z = 200$ Å for PDMA and PAAm. The final and stable configurations are shown in figure 7.16. Simulations are 250 ns long. We first describe and deeply discuss this system.

6.1.2 One polymer chain between two surfaces

We investigate the mechanism of detachment of PAAm and PDMA in between two flat silica surfaces that are driven apart step by step. At the beginning, the two surfaces are 200 Å apart. In this work, periodic boundary conditions are applied in the x, y directions, but not is the z direction. We start with the same initial configuration displayed in figure 7.16(a) for PAAm and PDMA. The initial configuration was generated by increasing the temperature of the system up to 1 000 K in the canonical ensemble and modifying the interaction parameters of the polymer in order to obtain this state. Temperature was then slowly cooled down to 500 K. Afterwards, PAAm and PDMA evolve for 500 ns to reach the final configurations shown in figure 7.16(b) for PDMA and in figure 7.16(c) for PAAm. This step requires a very long simulation time because polymer chains are moving slowly due to large rearrangement of the chains.

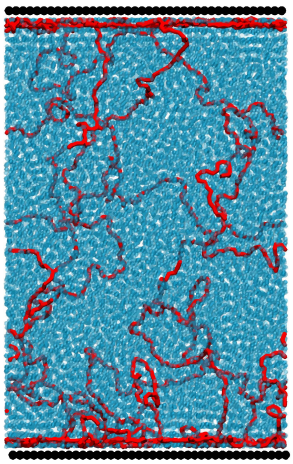

(a) Initial configuration for PAAm and PDMA.

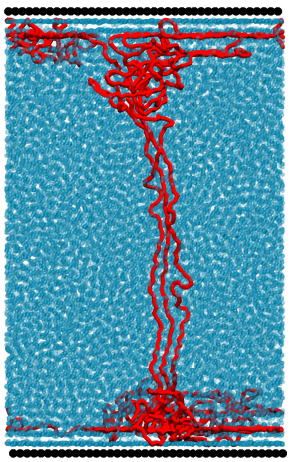

(b) Final configuration of PDMA.

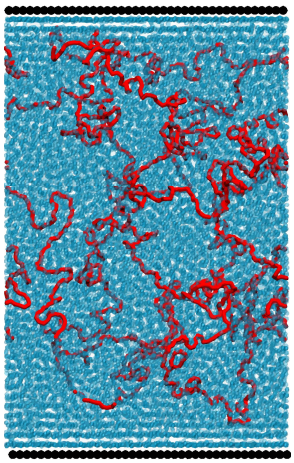

(c) Final configuration of PAAm.

Figure 6.1 – Snapshots of the initial and final configurations of PDMA and PAAm between two flat silica surfaces. The silica surface is in black, solvent beads are in blue and the polymer chain is in red.

We change the interaction parameters for the ones of PDMA or PAAm and adapt the number of solvent beads in order to obtain the bulk density of water. The resulting number of solvent beads is the same as previously presented: 24469 solvent beads for PAAm and 24169 solvent beads for PDMA. We checked that the density was correct by computing the bulk solvent density in several small volumes where there is no polymer beads. Then, both systems containing PAAm and PDMA were simulated for 250 ns.

On the one hand, one will notice that PAAm adopts the same behavior as previously observed: it desorbs from the surface and remains far from the surface surrounded by the solvent. It is therefore not relevant to probe the detachment of PAAm between two surfaces as the distance between two surface increases. On the other hand, the configuration adopted by PDMA is really interesting. The initial configuration of figure 7.16(a) leads to figure 7.16(b), and not to what was previously observed when PDMA stands on one silica surface (see figure 5.16(a)). Figure 7.16(b) shows that PDMA remains attached to both top and bottom surfaces, while attempting to adopt its huddled shape. This conclusion is of particular interest: not only the shrunk behavior of PDMA is its most stable state, but it stays attached to both surfaces. This makes the system really astonishing and interesting to deal with.

6.2 Quantification of the adsorption

Now that different polymer configurations have been introduced, the aim of the next section is to characterize PDMA and PAAm adsorption when chains are standing on one silica surface. We first probe the structure and dynamic of individual polymer beads and then study trains formed by polymers when adsorbed on the silica surface.

6.2.1 Structure of the adsorption of one polymer chain on the silica surface

We first consider the system containing one polymer chain surrounded by an explicit solvent adsorbed on one silica surface. It corresponds to the snapshots of figure 5.16. In order to compare the structure of the polymer chain in the vicinity of the surface, we plotted the PMF of PAAm and PDMA A beads as a function of their distance to the surface d in figure 6.2. The figure highlights the fact that for small d, there are almost no A_{PAAm} beads that come close to the surface while A_{PDMA} beads are present and well structured in this region. It is noticeable that the first well in the PDMA profile is not as deep as the second one which can be explained by the following way: PDMA, in order to increase its intramolecular interactions, adopts this spherical shape that favors polymer/polymer interactions instead of polymer/surface interactions. Finally, when $d = 15$ Å and above, PAAm and PDMA have the same profile.

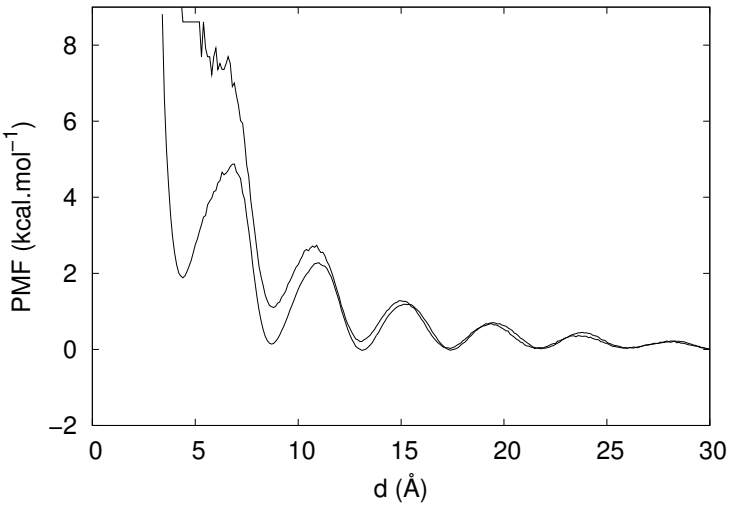

Figure 6.2 – Potential of mean force of A beads of PAAm (solid line) and PDMA (dashed line).

If we now zoom in on the interface and use the different stability regions defined in chapter 4, we can count the beads that are active (their "activity" equals 1): they go from region I to beyond region II or the opposite (see figure 4.2) and the beads that are not active (activity equals 0): they remain in one of the regions. Figure 6.3 shows the activity

– or lack of activity – of polymer beads. Herein, in order to probe the activity of the chain and not only of A beads that correspond to side groups, we consider the activity of C beads corresponding to the backbone chain. Activity of C beads is plotted as a function of the monomer number along the polymer chain. Figure 6.3 brings out the high level of activity of PAAm C beads compared to PDMA. This result seems to claim that PAAm monomers come more frequently close to the surface than PDMA monomers. However, this statement is not in agreement with the noisy part of the plot in figure 6.2 for PAAm for small d, which shows that PAAm A beads (and therefore monomers) do not remain for a long time in the vicinity of the surface. This result can be explained by the different conformations of PDMA and PAAm. PAAm is unfolded and moves more freely than PDMA, which is shrunk. PDMA has therefore only few active monomers, but they stay for a long time in region I. Indeed, 33 C beads stay on average 52.7 ns in region I, whereas PAAm has 564 active C beads that stay 0.1 ns in region I. PAAm active beads are random beads that come at one point close to the surface and then move away as rapidly as they approached the surface.

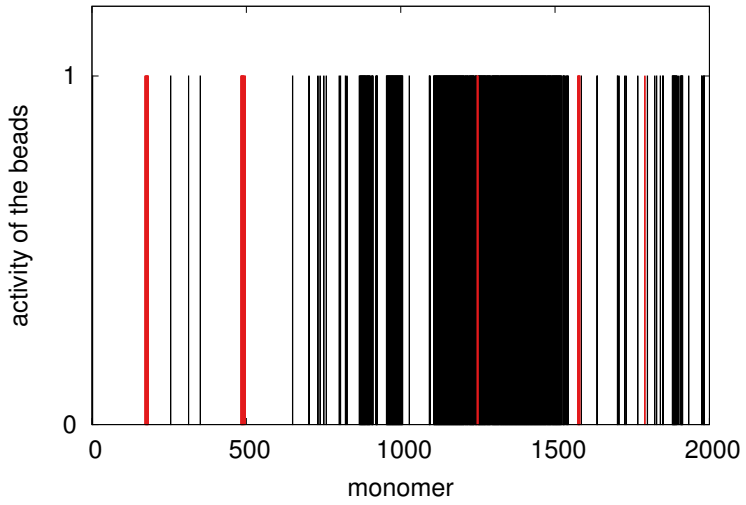

Figure 6.3 – Activity of the monomers of PAAm (black) and PDMA (red).

6.2.2 Trains length

These considerations show that considering the activity, 0 or 1, of the monomers is not sufficient. One also needs to take into account the residence time of beads in region I or the

length of *trains* that approach the surface. A train is a sequence of successive monomers with centers inside the adsorbed layer (*i.e* in region I) and is depicted in figure 6.4.

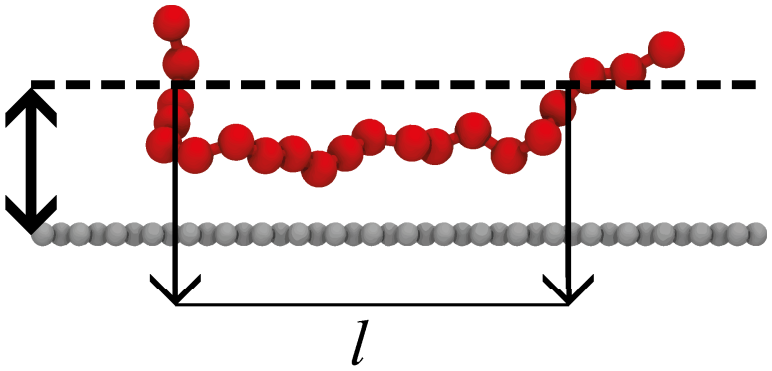

Figure 6.4 – A train of length l (in red) on a flat surface (in gray).

Here again we consider C beads because we are interested in the length of the backbone chain that adsorbs on the silica surface. The histogram of train length for PAAm and PDMA is shown in figure 6.5. It underlines the fact that PAAm only has really short trains coming in region I that are one or two monomers long. Moreover, those short trains stay for a very short time (around 0.1 ns) in region I. On the contrary, PDMA has longer trains that are up to nine monomers long which remain for tens of nanoseconds (around 50 ns) in region I. This highlights a different behavior between PAAm and PDMA. On the one hand, PAAm appears to have more active monomers than PDMA, but it appears that PAAm monomers that reach the surface stay for a short time and therefore do not participate in the efficient adsorption of the PAAm chain on the silica surface. On the other hand, PDMA only has a few monomers that reach the silica surface, but they form long trains on the surface and stay there for 50 ns on average. Thus, PDMA monomers contribute to an efficient adsorption of PDMA on the silica surface.

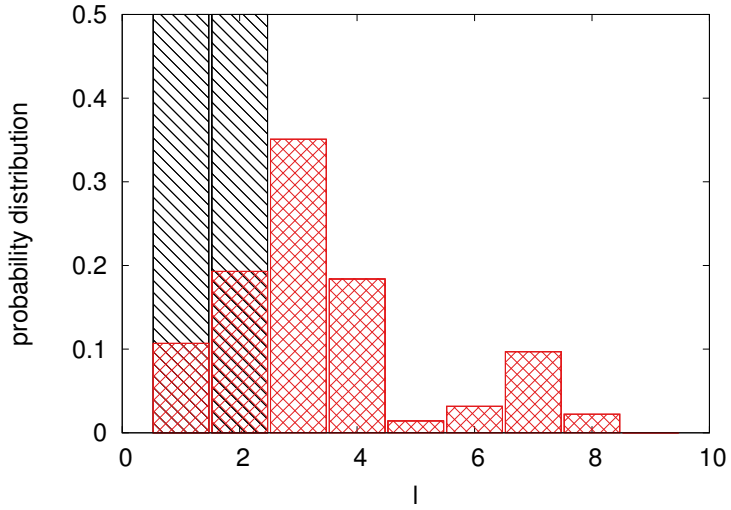

Figure 6.5 – Histogram distribution of trains length for PDMA (red) and PAAm (black).

6.3 Quantification of the detachment

6.3.1 Differences between one polymer chain placed on a surface and shared between two surfaces

Over a first phase, we compare different quantities between two situations of PDMA: (i) the first situation (1S) where the polymer lays on a flat silica surface (l_z = 200 Å), shown in figure 6.6(a)) and (ii) the second situation (2S) where the polymer is shared between two silica surfaces (l_z = 200 Å, see figure 6.6(b)). In this study the distance between the two silica surfaces does not vary. We do not consider the two situations for PAAm because the chain adopts the same type of configuration in both situations: figure 5.16(b) is the final configuration of PAAm, starting from a state where PAAm is placed on the silica surface and figure 7.16(c) is the final state, starting from a configuration where PAAm is shared between two silica surfaces.

Figure 6.7 compares the PMF of A_{PDMA} beads for the two situations (1S) and (2S). Both PMF have, as expected, their peaks and wells aligned. Moreover, the first well is not as deep as the second one for the two curves. It is nevertheless less the case for the second situation where PDMA is forced to spread on the surface due to its initial configu-

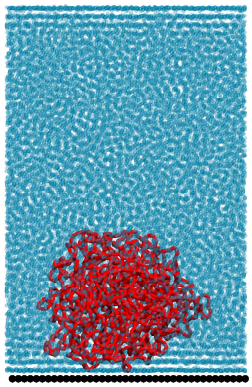

(a) Snapshot of the first situation (1S): PDMA (in red) placed on a flat silica surface (in black), surrounded by explicit solvent (in blue).

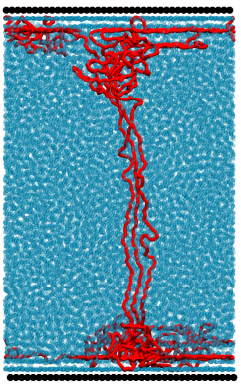

(b) Snapshot of the second situation (2S): PDMA (in red) shared between two flat silica surfaces (in black), surrounded by explicit solvent (in blue).

Figure 6.6 – PDMA on one silica surface (left figure) and in between two silica surfaces (right figure).

ration. The fact that the PMF plot of the first situation is higher than its minimum value for large d is consistent with the spherical shape adopted. In the same way, PDMA being more flat in the second situation, its free energy is smaller for small d than for larger ones.

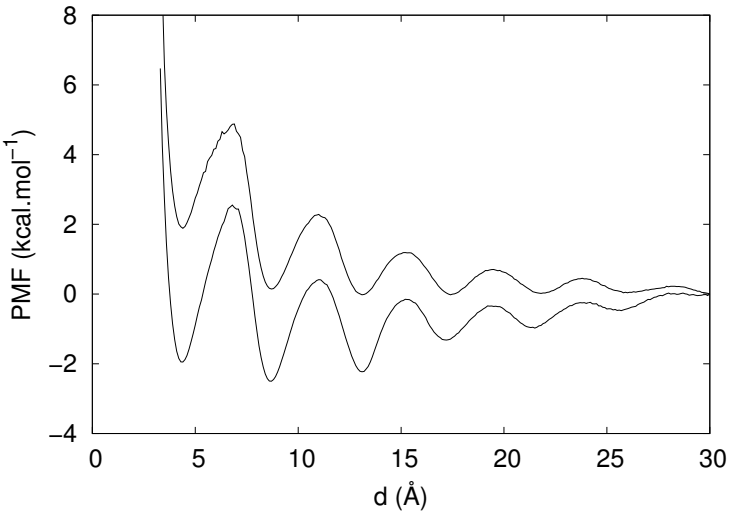

Figure 6.7 – Potential of mean force of PDMA A beads in situation (1S) (dashed line) and situation (2S) (solid line).

Train dynamic in the two situations (1S) and (2S) is then investigated. Because we are interested in moves of the polymer chain, we still focus on C beads that give insight into the backbone chain behavior. The resulting dynamical quantities in situation (1S) and (2S) are summarized in table 6.1. The first row of the table indicates the number of

active beads in the system: in other words, the averaged number of C beads that cross the previously defined regions. This number is significantly higher in situation (2S) than in situation (1S). In the first situation (1S), PDMA is actually really stable; whereas in second situation (2S), PDMA shrinks in order to improve intramolecular interactions but also increases its interactions with the surface. Therefore, the second situation raises the ability of PDMA to adsorb on the silica surface, which is confirmed by the following rows of table 6.1.

Dynamical quantity	Situation 1	Situation 2
Number of active beads	33	711
Number of beads stuck on the surface	1	104
Mean time for the beads to leave Region I (ns)	22	4
Residence time of active beads in Region I (ns)	53	36

Table 6.1 – Dynamical quantities of PDMA in situation (1S) and (2S).

The second row shows indeed that PDMA has more beads that remain for at least 250 ns on the silica surface: being more spread than when PDMA adopts its spherical shape, its monomers adsorb readily on the silica surface and stay for rather long times close to the surface. The third row is the time required by C beads to leave region I and to go beyond region II. This time lapse is definitely shorter in the second situation, meaning that monomers are moving more freely. This idea is confirmed by the fourth row which corresponds to the residence time of C beads in region I: it is still shorter in the second situation (2S).

Figure 6.8 is the distribution of residence times of active C beads (which are C beads that cross regions). In situation (1S) (red bars), there is no probability for the beads to have a residence time that is above 150 ns. Whereas in situation (2S), there are more blue bars covering a large range of residence times (from less than 1 ns to almost 250 ns). The beads that remain stuck close to the surface are not taken into account in this figure. If

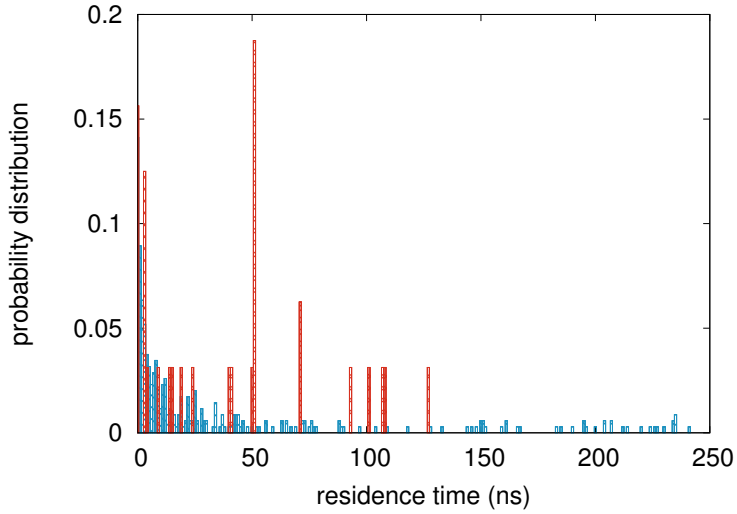

Figure 6.8 – Histogram of residence times of PDMA active C beads for situation (1S) (red) and situation (2S) (blue).

we now concentrate on figure 6.9, which represents the residence time of all C beads of the PDMA chain in region I, in both situations (1S) (red bars) and (2S) (blue bars), it becomes clear that the second situation (2S) leads to a system where motions are free: there are more beads that approach or leave region I and there is a wide range of residence time of C beads close to the surface.

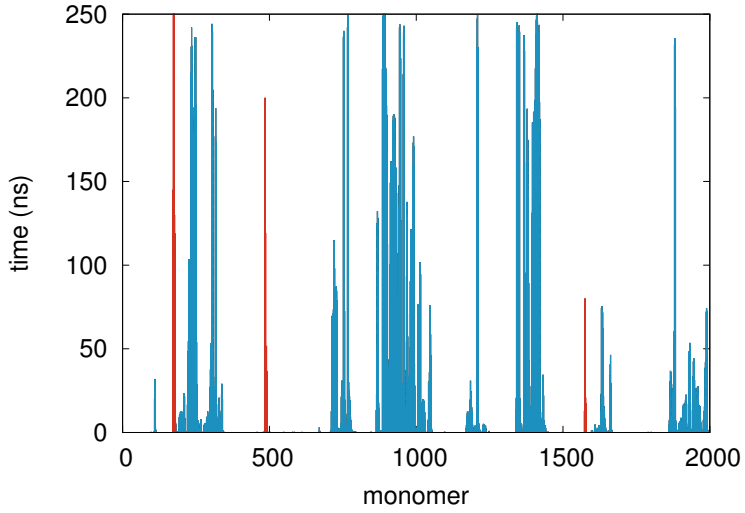

Figure 6.9 – Residence time in region I for each PDMA C bead, in situation (1S) (red) and in situation (2S) (blue).

Consequently, PDMA adopts two fairly different behaviors in situations (1S) and (2S). On the one hand, PDMA is well adsorbed on the silica surface, but has no particular

dynamic due to the fact that it corresponds to its most stable state. On the other hand, when we constrain PDMA to share between two silica surfaces, it attempts to shrink, but fulfils the requirement to adsorb on both silica surfaces. This constrained configuration implies an increase of the dynamical properties of PDMA.

6.3.2 When the two silica surfaces are taken away

Distance between the two silica surfaces is now step-by-step enlarged and consequences on the dynamic of the PDMA chain and its interaction strength with the surfaces are probed. We consider figure 7.16(b) as the initial configuration. Starting from this state we increase the distance between the two silica surfaces D_S by 5 Å, adjust the number of solvent beads in order to conserve the right bulk density, equilibrate the system in the NVT ensemble and use a 250 ns production run in the same ensemble.

Figure 6.10 is a comparison of the residence time of C beads when D_S equals 200 Å (in blue) or 285 Å (in red). There is a drastic decrease of the number of C beads that approach the surfaces. Moreover, the large majority of beads that remains close to the surfaces when $D_S = 285$ Å stays there for very long times, almost for the whole simulation time. Those beads play an essential role when preventing the PDMA chain to detach from the surfaces. The red large band around the 900th monomer corresponds to monomers adsorbed on the top surface and the red band at the 1400th monomer matches with monomers adsorbed on the bottom surface. Such large bands indicate that PDMA interacts with the surfaces by constituting long trains that remain on the silica surface for long times. Those assumptions are confirmed by the study of different quantities that follows.

Figure 6.10 highlights the fact that when we pull apart the two silica surfaces, only a few beads remain adsorbed on the surfaces and those beads are strongly adsorbed on the surfaces and remain there for long times. Figure 6.11(a) shows N_{stuck}, the number of beads that stay in region I for the whole simulation time, 250 ns. N_{stuck} decreases continuously as the two surfaces are pulled apart but shows a faster decrease when D_S is close to 200

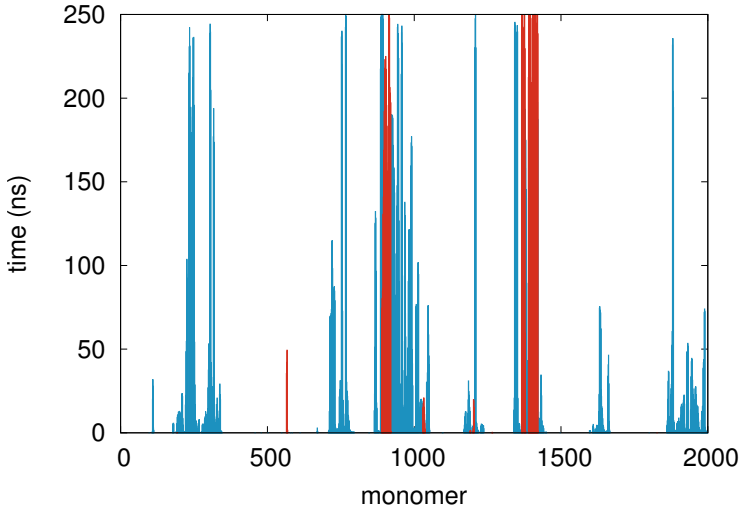

Figure 6.10 – Residence time, per PDMA C bead, close to the surface (nanoseconds). In blue: initial configuration, distance between the two surfaces = 200 Å. In red: distance between the two surfaces = 285 Å.

Å. This reveals a first mechanism of the desorption of PDMA chain that occurs through a diminution of the number of monomers that are strongly adsorbed on the surfaces. At the same time, the number of beads that are far from the surfaces increases rapidly for small D_S (figure 6.11(b)). This indicates a fast change of the behavior of the polymer as soon as the distance between the two surfaces is increased. The particular shape of the curve in figure 6.11(b) is connected with the number of active beads, that drastically decreases for small D_S, as shown in figure 6.12(a). Figures 6.11(a), 6.11(b) and 6.12(a) show that the behavior of the PDMA monomers changes radically as soon as D_S is increased: when looking at the evolution of the number of active beads and the number of beads that never approach the surfaces, there is a large gap between the initial configuration when $D_S = 200$ Å and when D_S increases. The number of beads that remain close to the surfaces does not undergo this large gap, and instead decreases continuously. It is thus really difficult to detach those beads from the surfaces. Therefore, when pulling apart two surfaces, there are two phenomena occurring. On the one hand, for small D_S, active beads that are not strongly adsorbed on silica surfaces move away from the surfaces easily. On the other hand, when D_S increases, beads that are stuck to the surfaces slowly desorb, step-by-step.

We now want to quantify the dynamic of the beads. First of all, figure 6.12(b) shows

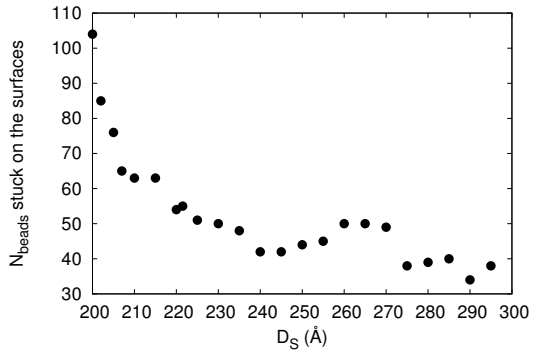

(a) Number of beads that remain in region I for 250 ns at least.

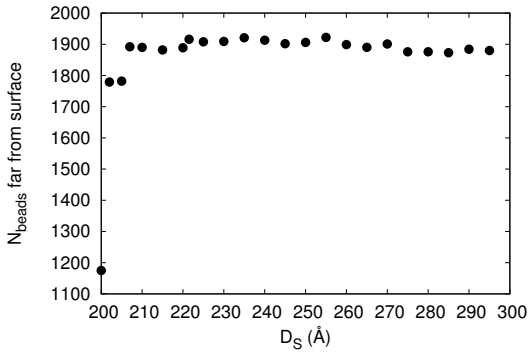

(b) Number of beads that never approch the surfaces for 250 ns at least.

Figure 6.11 – Number of PDMA beads that remain close to of far from surfaces during the whole simulation time (250 ns).

the evolution of the number of events per active beads (that are beads crossing regions) as D_S increases. The shape of this curve is interesting: it first increases, then is constant, and finally has a noisy rise. When D_S is below 210 Å, the number of events per active beads slightly increases because, as described before, most of the active beads are leaving the surface, so their activity is enhanced. As D_S is between 210 Å and 250 Å, the evolution of the number of events per active beads is rather constant: in this range of D_S, PDMA does not change its behavior. When D_S is above 250 Å, the number of active beads increases in a noisy way with no clear trend.

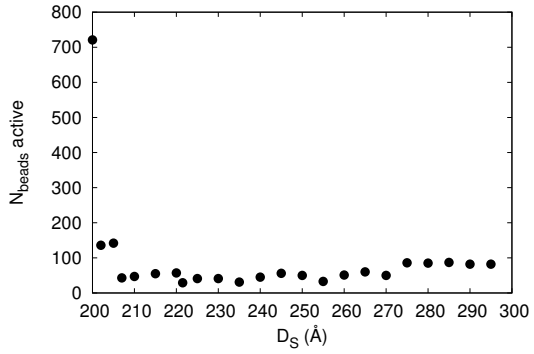

(a) Number of active beads.

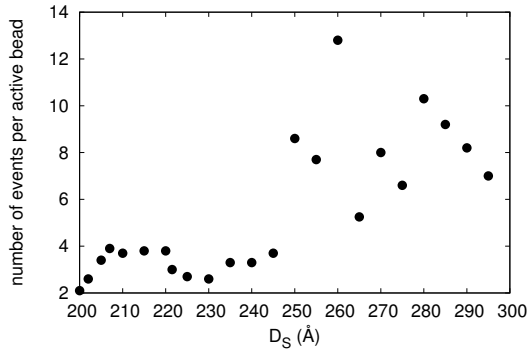

(b) Number of events per active bead.

Figure 6.12 – Number of PDMA active beads and number of events they undergo.

Examining the residence time of beads also gives insight into the polymer behavior as

D_S is increased. It is however difficult, in this situation, to quantify it. For instance, computing the residence time of active beads in region I, as shown in figure 6.13(a), does not give any convincing information on the evolution of the residence time of the active beads close to the surfaces. However, we saw in figures 6.10 and 6.12(a) that when D_S increases, the number of active beads decreases, but that a few "stuck" beads remain close to the surfaces and that those beads are an important component that prevent PDMA from desorbing. It is therefore necessary to take into account the residence time of those "stuck" beads if we want to quantify the time spent by beads close to surfaces. Figure 6.13(b) is an average of the residence time of the active beads, but also of the beads that remain in region I during the whole simulation time. This plot indicates that, even if there are less PDMA beads in region I as D_S increases, the resulting residence time of the beads increases. This underlines the fact that when D_S increases, labile beads are replaced by strongly adsorbed beads that remain attached to the silica surfaces.

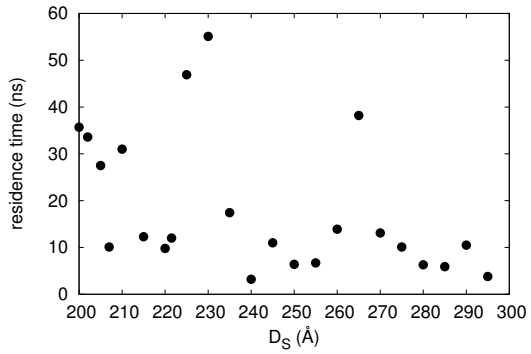

(a) Residence time in region I of active beads.

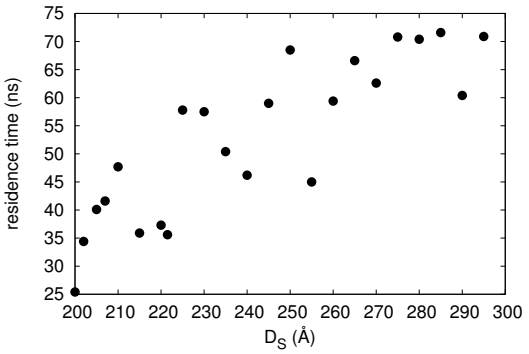

(b) Averaged residence time in region I of active beads and of beads that remain in region I for 250 ns.

Figure 6.13 – Number of PDMA active beads and number of events they undergo.

It is finally interesting to make connections between the PDMA behavior as D_S increases and the mechanical properties. In order to achieve this goal, we computed the force strength occurring between the polymer chain and the silica surfaces. The resulting evolution is presented in figure 6.14. When D_S is below 220 Å, the latter shows a strengthen of the force applied by the polymer chain on the surfaces. The force is then

weakened when D_S increases.

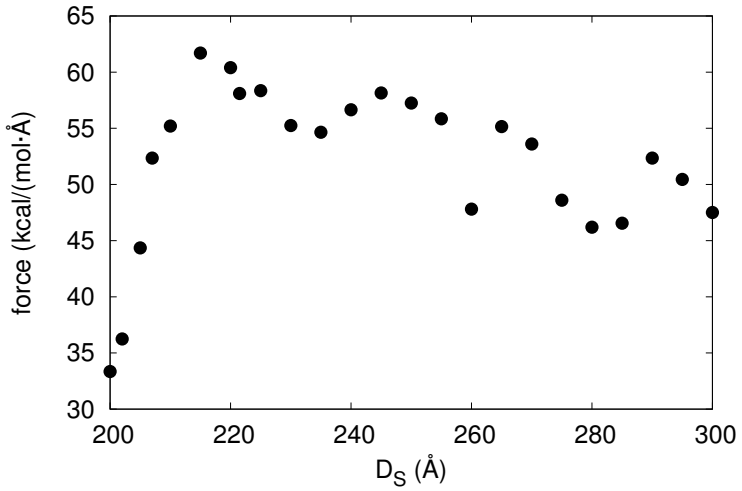

Figure 6.14 – Force strength between PDMA and surfaces.

6.4 Conclusion

In this chapter, different behaviors of PDMA and PAAm were investigated. We underlined the fact that PDMA interacts strongly with the silica surface by forming long trains that remain on the surface for tens of nanoseconds, which is not the case of PAAm. We then focused on the detachment of one PDMA chain when two silica surfaces are pulled apart. We highlighted how difficult it is to study such system, and that one has to be careful when choosing which quantities to compute. Gathering the results of this section shows that two phenomena are occurring when taking away the two surfaces. On the one hand, the number of active beads, that are adsorbing and desorbing from the surface, decreases rapidly. On the other hand, a few monomers remain strongly adsorbed on the silica surfaces. This shows that strongly adsorbed beads are necessary for PDMA to remain attached to the surfaces, and this adsorption process is assisted by the presence of active beads, that will relax the stress that adsorbed beads are enduring.

Outcome of the chapter

The fact that PDMA remains strongly adsorbed on both silica surfaces, even when the distance between surfaces is enlarged, is due to the presence of two types of beads: the ones that remain adsorbed on the surfaces, are the one that are moving faster, relaxing the stress.

Chapter 7

Adsorption isotherms of polymers on silica nanoparticles

This last chapter aims at presenting the experiments that I had the chance to carry out at the SIMM laboratory of ESPCI, with Anne-Charlotte Le Gulluche, PhD student under the supervision of Alba Marcellan. The aim of those experiments is to have an experimental insight into the quantity of polymer chains that adsorbs onto silica nanoparticles. It was also a chance for me to handle polymers and silica nanoparticles and to get a better understanding of those systems.

7.1 The question we address

As mentioned in chapter 1, the strength of the interaction between polymer chains and silica nanoparticles strongly depends on the pH, on the polymer length and on the temperature [40, 41]. The quantity of adsorbed polymer chains on the surface of silica nanoparticles evolves with the polymer concentration [38]. Below a critical polymer concentration, chains start to form an adsorbed monolayer on the silica surface and remain flat on the nanoparticles surface. Above this critical concentration, chains start to form various configurations such as trains, tails, loops, and undergo numerous rearrangements. In order to investigate the adsorbed polymer quantity as a function of the polymer concentration, we carry out adsorption isotherm (see figure 7.1). It represents the quantity of adsorbed polymer chains per silica surface area, Γ (mg/m^2), as a function of the initial polymer concentration, C_0 (g/L). Figure 7.1 corresponds to a situation were polymer adsorbs readily onto the silica surface. The polymer adsorbed quantity first increases with the polymer

concentration and then remains stable as the polymer concentration keeps increasing. The first part corresponds to a situation where the available surface is not completely covered with polymer chains. The second part, stable, accounts for the fact that silica surface is saturated with polymer chains.

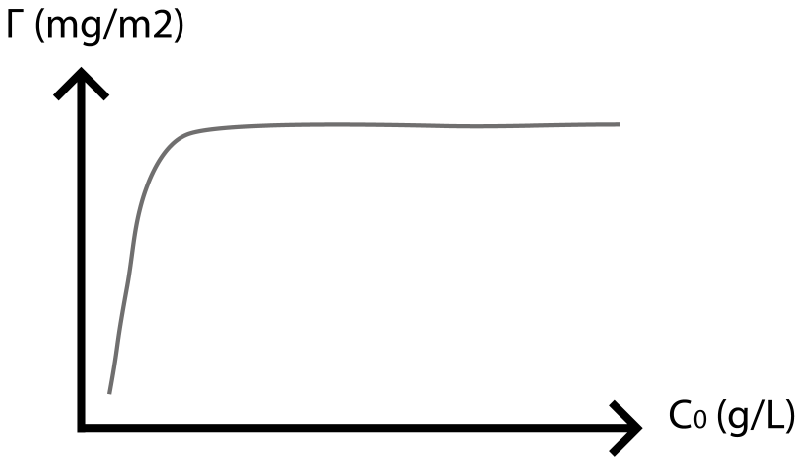

Figure 7.1 – Representation of an adsorption isotherm: quantity of adsorbed polymer chains per silica surface area, Γ, as a function of the initial polymer concentration, C_0.

7.2 Experimental setup

We performed adsorption isotherms for both linear PAAm and PDMA on silica NP. We first dissolve the desired polymer quantity in water and put the solution under stirring for 24 hours. We used six different initial polymer concentration with C_0 from 0.1 to 2.5 g/L. The pH of polymer solutions is adjusted between 8.5 and 9.5 using NaOH or HCl, which corresponds to the stability region of silica (see figure 1.10 of chapter 1). Then, 0.143 mL of a silica solution of 52 % in weight is added to polymer solutions. Solutions are let under stirring for 48 hours in order to reach adsorption equilibrium. After this time lapse, polymer chains are supposed to be adsorbed on the silica surface. The goal is now to separate polymer chains that are not adsorbed on silica NP and are in the supernatant from polymer chains that are adsorbed on silica NP. In order to do so, solutions are loaded into an ultra-fast centrifuge (70 000 rpm at room temperature) for 30 minutes to 1 hour and the liquid supernatant, containing non-adsorbed polymer chains, is separated from

the solid part containing silica NP and adsorbed chains. Centrifugation at 10 000 rpm for 72 hours under 5°C was not able to separate the supernatant from silica NP. The supernatant is then filtered using cellulose acetate filter-syringes with cut off of 45 μm to remove residual dusts and probed under Dynamic Light Scattering (DLS) technique in order to check whether silica NP remain in the supernatant. If the supernatant is clean from any NP, it is then study under Total Organic Carbon (TOC) analysis to quantify the carbon quantity of the supernatant. As we work with low polydispersity polymer chains, TOC analysis give us an insight into the polymer concentration remaining in the supernatant, that is to say, the polymer concentration that did not adsorb onto silica NP. As the initial polymer concentration is known, we therefore deduce the polymer concentration that adsorbed on silica NP.

7.2.1 PAAm, PDMA and silica

Silica Ludox® TM-50 water solution with concentration of 52 wt% at pH 9 and radius of 13 nm was purchased from Sigma Aldrich and used as received. The specific surface of silica is 100.3 m^2/g. Specific surface was estimated using the measured nanoparticles radius and according to:

$$S_{spe} = \frac{4\pi r^2}{\rho \frac{4}{3}\pi r^3}, \tag{7.1}$$

where ρ equals 5 g/L.

On the one hand, one chain type of PAAm is considered. On the other hand, two PDMA chain sizes are used. As for the latter, I performed experiments with PDMA having a molecular weight of 45 000 g/mol (called PDMA-45k) and 155 000 g/mol (called PDMA-155k). PDMA-155k was synthetized at the SIMM laboratory at ESPCI by Anne-Charlotte Le Gulluche using ATRP synthesis. Gel permeation chromatography (GPC) analysis shows that resulting PDMA-155k chains are linear with a polydispersity of 1.7 and an hydrodynamic radius of 17 nm. PDMA-45k was purchased from Polymer Source and used as received. However, further analysis showed that its polydispersity is relatively high: 2.4, its molecular weight is around 50 000 g/mol and, surprisingly, that it presents

a broad range of chains lengths. PAAm with a molecular weight of 40 000 g/mol was purchased from Sigma Aldrich. However, further analysis showed that its molecular weight is around 100 000 g/mol instead of 40 000 g/mol with a polydispersity of 2.0. For this reason, adsorption isotherms of PAAm are not displayed in this manuscript. All products were used as such without further purification. Distilled water (MilliQ) was used.

7.2.2 Analysing methods

We used centrifugation to separate silica NP and adsorbed polymer chains from non-adsorbed polymer chains. Then DLS analysis enables us to verify whether silica NP remain in the supernatant or not. If yes, other centrifugations have to be done. If no, supernatant is clean from any NP and it can be analysed with TOC method. It is actually important that no silica NP remain in the supernatant during the TOC analysis for two reasons: (i) TOC device can be damage by silica NP, which might block its system and (ii) before TOC analysis, pH is lowered to around 5, which corresponds to a non-stable region for silica, and can lead to aggregation of silica (see figure 1.10 of chapter 1).

Centrifugation

We started using a centrifugation that can reach 10 000 rpm and we thermostated the solution at 5°C. However, after 72 centrifugation hours, we still could detect silica NP under DLS analysis. We therefore use an ultra-fast centrifugation that can reach 100 000 rpm but which uses very small solution quantity. This can be an issue because TOC analysis requires around 5 mL of solution. Nevertheless, centrifugation for 30 min to 1 hour at room temperature and 70 000 rpm was able to separate silica NP and adsorbed polymer chains from the supernatant (see figure 7.2).

Dynamic Light Scattering

DLS analysis is a method that uses light scattering to compute the hydrodynamic radius of particles [191]. DLS provides information on dynamic of an isotropic solution. It measures the instantaneous scattering intensity $I(q,t)$ at wavevector of magnitude q and at

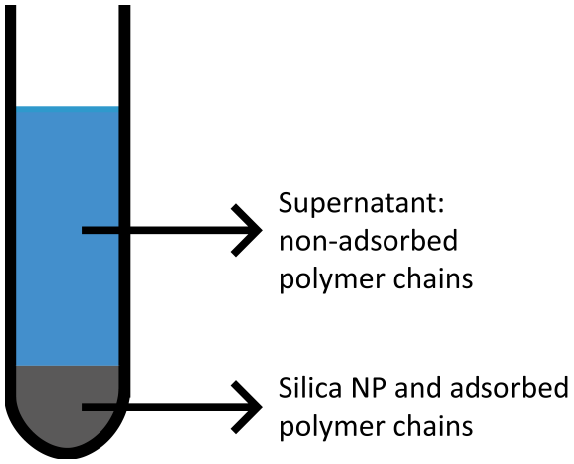

Figure 7.2 – Representation of a centrifugation tube.

time t. $I(q,t)$ changes when positions and conformations of scattering particles change. Therefore, as particles move, $I(q,t)$ fluctuates in time (see figure 7.3).

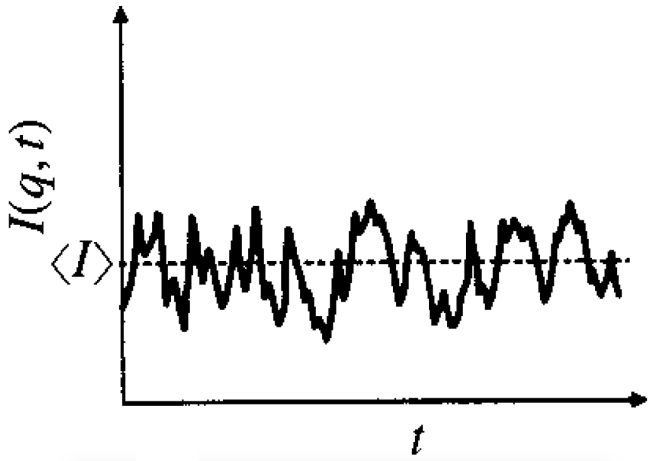

Figure 7.3 – Scattered intensity as a function of time. Picture from reference [191].

The time autocorrelation function of $I(q,t)$ is then computed using:

$$< I(q,0)I(q,t) >= \lim_{t' \to \infty} \int_0^{t'} I(q,t'')I(q,t''+t)dt''. \tag{7.2}$$

$< I(q,0)I(q,t) >$ corresponds to the "memory" of $I(q,t)$ and represents how fast $I(q,t)$ "forgets" about its initial state $I(q,0)$. Figure 7.4 is a representation of $< I(q,0)I(q,t) >$. Large par as a faster decay. The time autocorrelation of the scattered intensity decays with a correlation time τ.

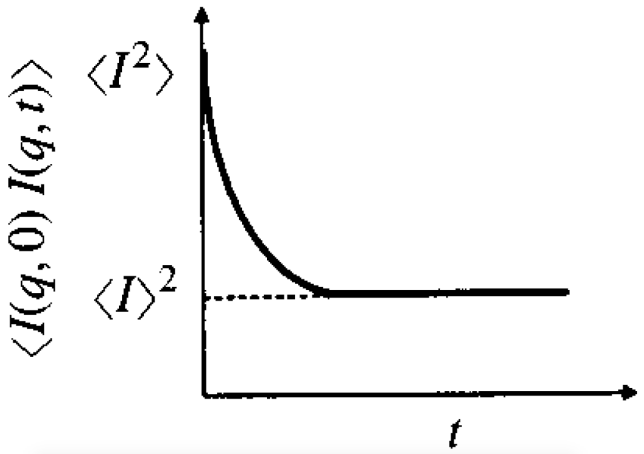

Figure 7.4 – Time autocorrelation function of $I(q,t)$ as a function of time. Picture from reference [191].

The correlation time τ depends on the diffusion coefficient D_{diff}:

$$\tau = \frac{1}{2q^2 D_{diff}}. \tag{7.3}$$

The hydrodynamic radius R_h is then computed using the Stokes-Einstein equation:

$$R_h = \frac{k_B T}{6\pi\eta_s D_{diff}} = \frac{k_B T q^2 \tau}{3\pi\eta_s}, \tag{7.4}$$

where k_B is the Boltzmann constant, T is the temperature and η_s is the solvent viscosity. Therefore, DLS measures the scattered intensity $I(q,t)$, computes the time autocorrelation function $< I(q,0)I(q,t) >$, deduces the correlation time τ and outputs the hydrodynamic radius R_h. Because the hydrodynamic radius of silica NP is better defined than the one of PAAm and of PDMA and leads to a clear decay of the time autocorrelation function of $I(q,t)$, DLS clearly indicates us whether there are silica NP in the supernatant. If there are remaining NP in the supernatant, it is necessary to do an additional centrifugation. Size measurements and control of the presence of remaining particles were conducted on a Malvern Zetasizer Nanoseries SZ90 device with PMMA cells.

Total Organic Carbon

Once supernatant is clean from silica NP, we perform a TOC analysis in order to know the carbon quantity that remains in the supernatant. The total concentration of free polymer chains in the supernatant (C_f) is therefore determined by titration of the total organic carbon. Because the polymer chains length or molecular weight is known, we can deduce the polymer chain quantity that remains in the supernatant, and therefore the polymer quantity adsorbed on silica NP. TOC experiments were performed on Shimadzu VCSH COT.

TOC analysis is widely used in water purification process as a method to measure water quality. It measures the carbon content which arises from humic acid[1], amines and urea for instance and from some detergents, fertilizers and herbicides. TOC analysis is also widely used in research laboratory as a precise and efficient method to quantify the carbon content of a diluted solution.

We first perform a TOC analysis on reference samples that contain a solution with a known polymer concentration and no silica NP. This allows us to then draw a calibration curve (see figure 7.5). We then perform the TOC analysis of the samples that were in contact with silica NP. TOC analysis relies on the following main steps. (i) The remaining carbon content of the sample is oxidized to form carbon dioxide. The sample is combusted in an oxygen-rich atmosphere at 680 °C. (ii) The carbon content is finally quantified by integrating the area under the peak that is measured with non-dispersive infrared method.

The adsorbed quantity of polymer on silica NP, Γ (in mg/m^2), is then calculated using:

$$\Gamma = \frac{C_0 - C_f}{1000 \times C_{SiO_2} \times S_{Spe}}, \tag{7.5}$$

where C_0 is the initial polymer concentration in g/L, C_f the final polymer concentration measured in the supernatant (g/L), C_{SiO_2} the initial silica NP concentration in g/L and

1. Humic acid is a mixture of many different acids produced by biodegradation of dead organic matter.

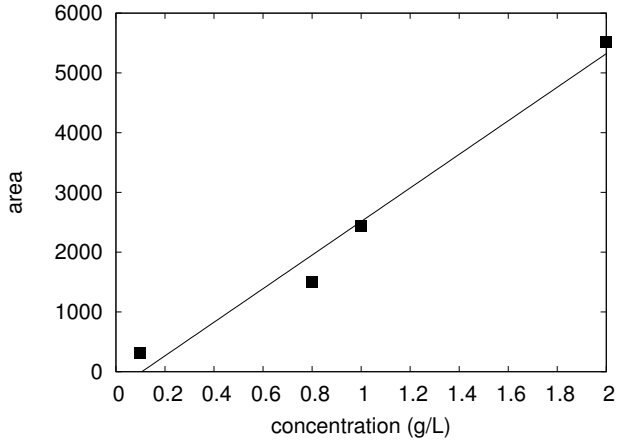

Figure 7.5 – TOC calibration curve of PDMA-155k.

S_{Spe} the silica specific surface in m^2/g.

7.3 Results: Adsorption isotherms

We prepared 10 solutions containing PDMA and 10 solutions containing PAAm whose respectively 4 TOC calibration solutions for PDMA containing no silica NP and 4 TOC calibration solutions for PAAm containing no silica NP. Total solution volume is 20 mL. Polymer and silica NP solution quantity we add are summarized in table 7.1. First column of table 7.1 presents the polymer quantity of the solution that is considered and the second row shows the silica NP solution quantity. The third row indicates if a second solution, containing the same amount of polymer chains but no silica NP, that is used for further TOC calibration, has been done. We choose polymer concentrations in such a way that the whole adsorption isotherm curve is covered.

PDMA/PAAm concentration (g/L)	Ludox® TM-50 solution (g)	calibration solution ?
0.1	0.2	yes
0.5	0.2	no
0.8	0.2	yes
1.0	0.2	yes
2.0	0.2	yes
2.5	0.2	no

Table 7.1 – The solutions we prepared.

Figure 7.6(a) is the adsorption isotherm for PDMA having a molecular weight of

45 000 g/mol (black squares) and of 155 000 g/mol (gray squares). We translated this datas in terms of number of adsorbed chains per nm^2 in order to have an idea of the surface coverage (see Figure 7.6(b)). The latter would be interesting to use for further modelling.

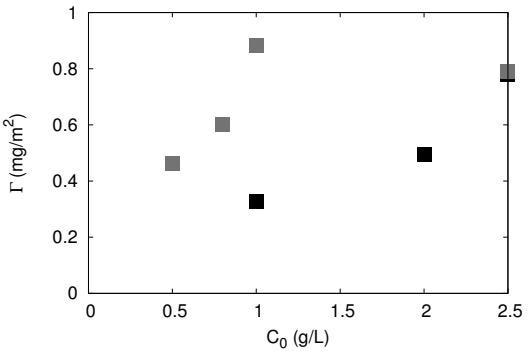

(a) Adsorption isotherm of PDMA with molecular weight of 45 000 g/mol (black squares) and 155 000 g/mol (gray squares). Corresponds to the adsorbed quantity of PDMA per surface unit as a function of the initial PDMA concentration.

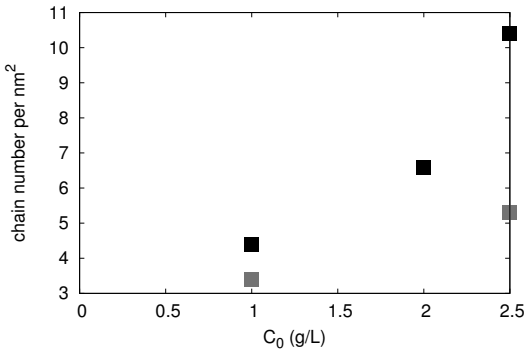

(b) Number of adsorbed PDMA chains per nm^2 as a function of the initial PDMA concentration. PDMA with molecular weight of 45 000 g/mol is in black and 155 000 g/mol in gray.

Figure 7.6 – Adsorption isotherm and adsorbed chains number.

Figure 7.6(a) indicates that for PDMA chains with a molecular weight of 155 000 g/mol, the stable regime of the adsorption isotherm is reached for an initial concentration about 1 g/L. PDMA with a 45 000 g/mol molecular weight reaches the stable regime at further initial concentrations, around 2.5 g/L. This is in good agreement with what has already been experimentally observed [38]. The authors of reference [38] observed a maximum PDMA adsorbed quantity around 1 mg/m^2, which is what we observe for PDMA-155k. It is noteworthy that PDMA-45k, purchased from Polymer source, has an high degree of polydispersity and is composed of several chain lengths, therefore invalidating our result.

Figure 7.6(b) is the number of adsorbed PDMA chains per nm^2, N_{ads}, computed from Γ and the molecular weight M_w using:

$$N_{ads} = \frac{\Gamma \mathcal{N}_A}{M_w 10^{18}}. \tag{7.6}$$

It shows that, for the same initial polymer concentration, there are more PDMA chains having a molecular weight of 45 000 g/mol that are adsorbed per nm^2 on silica surface. Even though the adsorbed chains quantity per surface unit is higher when molecular weight is larger, the adsorbed chain number per surface unit is lower when molecular weight is larger. This gives us interesting insight into the polymer chains conformation on silica NP surface. When molecular weight is lower, chains clearly form tails on silica NP, therefore allowing for a large adsorbed chain number per nm^2. When molecular weight is higher, chains form more trains, leading to a smaller adsorbed chain number per nm^2.

Outcome of the chapter

Those experimental results need to be deepen to be properly linked to computer simulations. Nevertheless, they already give us good insight into the change of polymer conformation when molecular weight increases.

Conclusion

Conclusion

The aim of this project was to get a better understanding of the polymer behavior when located on a silica surface and to connect it to mechanical properties. More precisely, our idea was to rationalize the reason why PAAm does not glue on silica nanoparticles whereas PDMA does. In order to understand the drastically different behaviors between two not-so-different polymers and more generally to rationalize the adsorption / desorption mechanism of polymer chains on a solid surface, we built a model and developed analyzing tools. Combining different simulation methods, quantum as well as classical, designing a made to measure yet transferable model and developing various modelling devices enabled us to uncouple important features during adsorption and desorption of polymer chains on silica surfaces.

The first aim of this work was to build a simple yet reasonable and robust polymer / silica surface model. We pointed out that using DFT calculations on a small model system was not able to give us a complete insight into processes occurring at the interface between polymer, solvent, and silica. Using coarse-grained molecular dynamics and the Martini force field finally provided us a mean to probe this complex interface. An extensive comparison of the explicit solvent and of the implicit solvent provided within the Martini force field framework have oriented our choice towards the use of an explicit solvent. This decision is motivated by the important role played by the solvent regarding several issues: (i) its competition with regard to polymers for adsorption on the silica surface, (ii) the manner it solvates PAAm and PDMA, and (iii) the different solvation of bulk polymers and of polymers at the interface.

One of the main interest of this work was to probe PAAm and PDMA behavior when

chains are under pressure. We therefore built a model system containing PAAm or PDMA, a large amount of solvent beads and a silica surface. Umbrella sampling free energy method was employed to compute the free energy profile along the distance between the center of mass of the polymer and the silica surface. This study has highlighted two drastically different behaviors between PAAm and PDMA which correspond to experiments: PAAm is not stabilized close to the surface whereas PDMA is. Further studies on this system emphasized the role played by each interaction occurring within this complex system.

It is helpful to remind a few points that were tackled in chapter 1. In this chapter, we introduced several models that have attempted to explain why PDMA glues on silica nanoparticles whereas PAAm does not. On the one hand, it has been proposed that water molecules readily adsorb on silica surface silanols, therefore preventing PAAm from adsorbing on silica [36, 37]. On the other hand, the authors of reference [43] have suggested that hydrophobic interactions allow PDMA to adsorb on silica.

Our investigation shows that only two interaction types are responsible for the drastically different behavior between PDMA and PAAm: A bead / S bead as well as A bead / C bead interaction parameter. To move from PAAm to PDMA, C / A interaction is increased: this favors intra molecular interactions within the polymer with regard to polymer / solvent interactions. A / S is also increased and reaches the value of A / solvent interaction parameter. There is nothing surprising about the fact that polymer prefers to adsorb on the surface when A / S interaction increases. Nevertheless, it is surprising that a polymer prefers to remain adsorbed on a silica surface when A / S interaction equals the one between A and solvent beads. This is explained by the fact that PDMA does not move a lot when adsorbed on silica or when solvated by solvent beads. It is therefore entropically favorable that PDMA, which is moving more slowly than solvent beads, remains adsorbed on silica surface and releases solvent beads that are moving faster. This behavior favors the solvent entropy.

When nanocomposites are experimentally synthesized, nanoparticles are usually introduced after the polymerization process. One therefore has to wait for silica nanoparticles to diffuse within the polymer network. Silica nanoparticles aggregate when introduced into a PAAm hydrogel. This is explained by the higher affinity of PAAm for water than for silica nanoparticles and by the fact that silica nanoparticles are covered with solvent molecules, preventing PAAm from adsorbing onto silica, which is supported by our theoretical model. However, when silica nanoparticles are introduced into a PDMA hydrogel, the former do not aggregate and the resulting nanocomposite material is nicely homogeneous. Considering our theoretical model, this observation is rationalized by the following assumption: PDMA is not as swollen as PAAm in water. When silica nanoparticles are introduced into the PDMA network, increasing PDMA / silica interactions allows to decrease PDMA / water interactions and to release water, which is entropically favored.

This theoretical model therefore gives us a better understanding of the silica / polymer system and allows us to draw some assumptions about the different experimental behavior of PAAm and of PDMA. It is of course incomplete and further investigations or a more complete model would be needed for a deeper understanding of the nanocomposite material. In particular, it is necessary to complete our main hypothesis, namely the lack of cross-links between polymer chains and the surface curvature, to have a better insight into the material. It is also of first importance to probe mechanical properties such as the Young modulus, or shear properties with a more realistic model, containing more polymer chains, cross-links, and several nanoparticles. I have attempted to compute the Young modulus of a system containing several PAAm or PDMA chains, with and without a silica surface. However, this system being too far from reality, those results were not conclusive on a reinforcement of the polymer network with the introduction of a surface. This attempt suffers from the general difficulty to theoretically compute mechanical properties that are consistent and in good agreement with experiments. Once our model is more complete, it will be interesting to transfer it to other polymers such as PNiPAM which has the advantage to have an A bead which is more hydrophobic than the one of PDMA.

It will give us insight into the significance of this hydrophobic group. This model could also be used to probe the impact of curvature and of nanoparticle size on the dynamics and on the resulting mechanical properties of a nanocomposite material.

Publications

- W. Louisfrema, J.-L. Paillaud, F. Porcher, **E. Perrin**, T. Onfroy, P. Massiani, A. Boutin, B. Rotenberg, "Cation migration and structural deformations upon dehydration of Nickel-exchanged NaY zeolite: A combined neutron diffraction and Monte Carlo study", *The Journal of Physical Chemistry C*, 120, 18115-18125, 2016

- L. Daukiya, C. Mattioli, D. Aubel, S. Hajjar-Garreau, F. Vonau, E. Denys, G. Reiter, J. Fransson, **E. Perrin**, M.-L. Bocquet, C. Bena, A. Gourdon, L. Simon, "Covalent functionalization by cycloaddition reactions of pristine defect-free graphene", *ACS nano*, 11, 627-634, 2017

- **E. Perrin**, M. Schoen, F.-X. Coudert, A. Boutin, "Structure and Dynamics of Solvated Polymers Near a Silica Surface: on the Different Roles Played by Solvent", *The Journal of Physical Chemistry B*, *submitted*

Bibliography

(1) Rose, S.; Prevoteau, A.; Elzière, P.; Hourdet, D.; Marcellan, A.; Leibler, L. *Nature* **2013**, *505*, 382–385.

(2) Tamagawa, H.; Takahashi, Y. *Materials Chemistry and Physics* **2008**, *107*, 164–170.

(3) Saito, J.; Furukawa, H.; Kurokawa, T.; Kuwabara, R.; Kuroda, S.; Hu, J.; Tanaka, Y.; Gong, J. P.; Kitamura, N.; Yasuda, K. *Polymer Chemistry* **2011**, *2*, 575–580.

(4) Perrin, B.; Brichon, P.-y.; Bracini, M.; Derail, C.; Leterrier, Y.; Papon, É.; Barrandon, Y.; Sessa, C.; Chavanon, O. *Chirurgie Thoracique et cardio-vasculaire* **2012**, *16*, 33–42.

(5) Duarte, A. P.; Coelho, J. F.; Bordado, J. C.; Cidade, M. T.; Gil, M. H. *Progress in Polymer Science* **2012**, *37*, 1031–1050.

(6) Lake, G. J.; Thomas, A. G. *Proc. R. Soc* **1967**, *300*, 108–119.

(7) Gennes, P. G. D. *Langmuir* **1996**, *12*, 4497–4500.

(8) Annabi, N.; Tamayol, A.; Ryon, S.; Ghaemmaghami, A. M.; Peppas, N. A.; Khademhosseini, A. *Nano Today* **2014**, *9*, 574–589.

(9) Meddahi-pellé, A.; Legrand, A.; Marcellan, A.; Louedec, L.; Letourneur, D. *Angewandte Chemie International Edition* **2014**, *53*, 6369–6373.

(10) Discher, D. E.; Mooney, D. J.; Zandstra, P. W. *Science* **2009**, *324*, 1673–1678.

(11) Ahmed, E. M. *Journal of Advanced Research* **2015**, *6*, 105–121.

(12) Qiu, Y.; Park, K. *Advanced Drug Delivery Review* **2001**, *53*, 321–339.

(13) Dong, L.; Agarwal, A. K.; Beebe, D. J.; Jiang, H. *Nature* **2006**, *442*, 551–554.

(14) Lee, K. Y. K.; Mooney, D. J. *Progress in Polymer Science* **2012**, *37*, 106–126.

(15) Calvert, P. *Advanced Materials* **2009**, *21*, 743–756.

(16) Bonn, D.; Kellay, H.; Ben-djemiaa, K.; Meunier, J. *Science* **1998**, *280*, 265–268.

(17) Tanaka, Y; Fukao, K; Miyamoto, Y *The European Physical Journal E* **2000**, *3*, 395–401.

(18) Sun, J.-y.; Zhao, X.; Illeperuma, W. R. K.; Chaudhuri, O.; Oh, K. H.; Mooney, D. J.; Vlassak, J. J.; Suo, Z. *Nature* **2012**, *489*, 133–136.

(19) Zhao, X. *Soft Matter* **2014**, *10*, 672–687.

(20) Long, R.; Hui, C.-y. *Soft Matter* **2016**, *12*, 8069–8086.

(21) Bastide, J.; Leibler, L. *Macromolecules* **1988**, *21*, 2649–2651.

(22) Furukawa, H.; Horie, K.; Nozaki, R.; Okada, M. *Physical Review E* **2003**, *68*, 1–14.

(23) Simha, N. K.; Carlson, C. S.; Lewis, J. L. *Journal of Materials Science: Materials in medicine* **2003**, *4*, 631–639.

(24) Tanaka, Y.; Kuwabara, R.; Na, Y.-h.; Kurokawa, T.; Gong, J. P.; Osada, Y. *Journal of Physical Chemistry B* **2005**, *109*, 11559–11562.

(25) Gong, J. P. *Soft Matter* **2010**, *6*, 2583–2590.

(26) Li, J; Celiz, A. D.; Yang, J; Yang, Q; Wamala, I; Whyte, W; Seo, B. R.; Vasilyev, N. V.; Vlassak, J. J.; Suo, Z; Mooney, D. J. *Science* **2017**, *381*, 378–381.

(27) Kong, H. J.; Wong, E.; Mooney, D. J. *Macromolecules* **2003**, *36*, 4582–4588.

(28) Henderson, K. J.; Zhou, T. C.; Otim, K. J.; Shull, K. R. *Macromolacules* **2010**, *43*, 6193–6201.

(29) Shull, K. R. *Nature* **2012**, *489*, 8–9.

(30) Sun, T. L.; Kurokawa, T.; Kuroda, S.; Ihsan, A. B.; Akasaki, T.; Sato, K.; Haque, A.; Nakajima, T.; Gong, J. P. *Nature Materials* **2013**, *12*, 932–937.

(31) Haraguchi, K.; Takehisa, T.; Fan, S. *Macromolecules* **2002**, *35*, 10162–10171.

(32) Haraguchi, K.; Takada, T. *Macromolecular Chemistry and Physics* **2005**, *206*, 1530–1540.

(33) Haraguchi, K. *Macromolecular Symposia* **2007**, *256*, 120–130.

(34) Schmidt, G.; Malwitz, M. M. *Current Opinion in Colloid and Interface Science* **2003**, *8*, 103–108.

(35) Kabiri, K; Omidian, H; Zohuriaan-Mehr, M. J.; Doroudiani, S *Polymer Composites* **2011**, 277–289.

(36) Griot, O.; Kitchener, J. A. *Transactions of the Faraday Society* **1964**, *61*, 1026–1032.

(37) Griot, O.; Kitchener, J. A. *Transactions of the Faraday Society* **1964**, *61*, 1032–1038.

(38) Hourdet, D.; Petit, L. *Macromolecular Symposia* **2010**, *291-292*, 144–158.

(39) Santore, M. M. *Current Opinion in Colloid and Interface Science* **2005**, *10*, 176–183.

(40) Pefferkorn, E.; Haouam, A.; Varoqui, R. *Macromolecules* **1988**, *21*, 2111–2116.

(41) Haouam, A; Pefferkorn, E *Colloids and Surfaces* **1988**, *34*, 371–379.

(42) Doherty, E. A. S.; Berglund, K. D.; Buchholz, B. A.; Kourkine, I. V.; Przybycien, T. M.; Tilton, R. D.; Barron, A. E. *Electrophoresis* **2002**, *23*, 2766–2776.

(43) Zhang, P.; Ren, J. *Analytica Chimica Acta* **2004**, *507*, 179–184.

(44) Pefferkorn, E.; Carroy, A.; Varoqui, R. *Macromolecules* **1985**, *18*, 2252–2258.

(45) Pefferkorn, E.; Carroy, A.; Varoqui, R. *Journal of Polymer Science Part B: Polymer physics* **1985**, *23*, 1997–2008.

(46) Pefferkorn, E; Nabzar, L; Carroy, A. *Journal of Colloid and Interface Science* **1985**, *106*, 94–103.

(47) Inomata, H.; Goto, S.; Saito, S. *Macromolecules* **1990**, *23*, 4887–4888.

(48) Macron, J. Hydrogels en milieux immergés : de l'adhésion macroscopique aux mécanismes moléculaires., Ph.D. Thesis, 2014.

(49) Gracia, M. Collage d'hydrogels par des nanoparticules de silice., Ph.D. Thesis, 2017.

(50) Carman, P. C. *Transactions of the Faraday Society* **1940**, *36*, 964–973.

(51) Depasse, J.; Watillon, A. *The Journal of Colloid and Interface Science* **1970**, *33*, 430–438.

(52) Iler, R. K. *Colloid and Surface Properties, and Biochemistry* **1979**, *866*.

(53) Abe, H.; Hara, Y.; Maeda, S.; Hashimoto, S. *The Journal of Physical Chemistry B* **2014**, *118*, 2518–2522.

(54) Beecroft, L. L.; Ober, C. K. *Chemistry of Materials* **1997**, *9*, 1302–1317.

(55) Gangopadhyay, R.; De, A. *Chemistry of Materials* **2000**, *12*, 608–622.

(56) Xu, C.; Ohno, K.; Ladmiral, V.; Milkie, D. E.; Kikkawa, J. M.; Composto, R. J. *Macromolecules* **2009**, *42*, 1219–1228.

(57) Tu, Y.; Zhou, L.; Jin, Y. Z.; Gao, C.; Ye, Z. Z.; Yang, F. Y.; Wang, Q. L. *Journal of Materials Chemistry* **2010**, *20*, 1594–1599.

(58) Kumar, S. K.; Ganesan, V.; Riggleman, R. A. *The Journal of Chemical Physics* **2017**, *147*.

(59) Zeng, Q.; Yu, A.; Lu, G. *Progress in Polymer Science* **2008**, *33*, 191–269.

(60) Smith, G. D.; Bedrov, D; Borodin, O *Physical Review Letters* **2003**, *90*, 226103–226104.

(61) Smith, K. A.; Vladkov, M.; Barrat, J. L. *Macromolecules* **2005**, *38*, 571–580.

(62) Johnston, K.; Nieminen, R. M.; Kremer, K. *Soft Matter* **2011**, *7*, 6457.

(63) Mangal, R.; Srivastava, S.; Archer, L. A. *Nature Communications* **2015**, *6*, 1–9.

(64) Kalathi, J. T.; Kumar, S. K.; Grest, G. S. *Soft Matter* **2015**, *11*, 4123–4132.

(65) Knauert, S. T.; Douglas, J. F.; Starr, F. W. *Journal of Polymer Science Part B: Polymer physics* **2007**, *45*, 1882–1897.

(66) Karatrantos, A.; Clarke, N.; Composto, R. J.; Winey, K. I. *Soft Matter* **2014**, *11*, 382–388.

(67) Senses, E.; Ansar, S. M.; Kitchens, C. L.; Mao, Y.; Narayanan, S. *Physical Review Letters* **2017**, *118*, 1–5.

(68) Cheng, S.; Xie, S.-j.; Carrillo, J.-m. Y.; Carroll, B.; Martin, H.; Cao, P.-f.; Dadmun, M. D.; Sumpter, B. G.; Novikov, V. N.; Schweizer, K. S.; Sokolov, A. P. *ACS Nano* **2017**, *11*, 752–759.

(69) Carrillo, J.-m. Y.; Potter, M. E.; Sakwa-novak, M. A.; Pang, S. H.; Jones, C. W.; Sumpter, B. G. *Langmuir* **2017**, *33*, 5412–5422.

(70) Hoeve, C. A. J.; Dimarzio, E. A.; Peyser, P *The Journal of Chemical Physics* **1965**, *42*, 2558–2563.

(71) Hoeve, C. A. J. *The Journal of Chemical Physics* **1966**, *44*, 1505–1509.

(72) Hoeve, A. J. *Journal of Polymer Science: Part C* **1971**, *34*, 1–10.

(73) Matsuda, T.; Smith, G. D.; Winkler, R. G.; Yoon, D. Y. *Macromolecules* **1995**, *28*, 165–173.

(74) Mendez-Alcaraz, J. M.; Johner, A.; Joanny, J. F. *Macromolecules* **1998**, *31*, 8297–8304.

(75) Brown, D; Mele, P; Marceau, S.; Alberola, N. D. *Macromolecules* **2003**, *36*, 1395–1406.

(76) Borodin, O.; Smith, G. D.; Bandyopadhyaya, R.; Byutner, O. *Macromolecules* **2003**, *36*, 7873–7883.

(77) Andrienko, D.; Leon, S.; Site, L. D.; Kremer, K. *Macromolecules* **2005**, *38*, 5810–5816.

(78) Harmandaris, V. a.; Daoulas, K. C.; Mavrantzas, V. G. *Macromolecules* **2005**, 5780–5795.

(79) Harmandaris, V. a.; Daoulas, K. C.; Mavrantzas, V. G. *Macromolecules* **2005**, 5796–5809.

(80) Metzger, S.; Müller, M.; Binder, K.; Baschnagel, J. *Macromolecular Theory and Simulations* **2002**, *11*, 985–995.

(81) Nath, S. K.; Frischknecht, A. L.; Curro, J. G.; McCoy, J. D. *Macromolecules* **2005**, *38*, 8562–8573.

(82) Surve, M.; Pryamitsyn, V.; Ganesan, V. *Langmuir* **2006**, *22*, 969–981.

(83) Puddu, V.; Perry, C. C. *ACS Nano* **2012**, *6*, 6356–6363.

(84) Virgiliis, A. D.; Milchev, A; Rostiashvili, V. G.; Vilgis, T. A. *The European Physical Journal E* **2012**, *35*, DOI: 10.1140/epje/i2012-12097-6.

(85) Cimino, R; Rasmussen, C. J.; Neimark, A. V. *The Journal of Chemical Physics* **2013**, *139*, 1–4.

(86) Ganesan, V.; Jayaraman, A. *Soft Matter* **2014**, *10*, 13–38.

(87) Smith, G. D.; Bedrov, D.; Li, L.; Byutner, O. *Journal of Chemical Physics* **2002**, *117*, 9478–9489.

(88) Odegard, G. M.; Clancy, T. C.; Gates, T. S. *Polymer* **2005**, *46*, 553–562.

(89) Surve, M.; Pryamitsyn, V.; Ganesan, V. *Physical Review Letters* **2006**, *96*, 1–4.

(90) Pryamitsyn, V.; Ganesan, V. *Macromolecules* **2006**, *39*, 844–856.

(91) Hantal, G.; Brochard, L.; Pellenq, R. J.-M.; Ulm, F.-j.; Coasne, B. *Langmuir* **2017**, *33*, 11457–11466.

(92) Surve, M.; Pryamitsyn, V.; Ganesan, V. *The Journal of Chemical Physics* **2017**, *125*, 1–13.

(93) An, R.; Huang, L.; Mineart, K. P.; Dong, Y.; Spontak, R. J.; Gubbins, K. E. *Soft Matter* **2017**, *13*, 3492–3505.

(94) Liang, L.; Liu, J.; Gong, X. *Langmuir* **2000**, *16*, 9895–9899.

(95) Sheeney-Haj-Ichia, B. L.; Sharabi, G.; Willner, I. *Advanced Functional Materials* **2002**, *91904*, 27–32.

(96) Berriot, J.; Montes, H.; Lequeux, F.; Long, D.; Sotta, P. *Macromolecules* **2002**, *35*, 9756–9762.

(97) Berriot, J; Montes, H; Lequeux, F; Long, D; Sotta, P *Europhysics Letters (EPL)* **2003**, *64*, 50–56.

(98) Reinhardt, M.; Dzubiella, J.; Trapp, M.; Gutfreund, P.; Kreuzer, M.; Gro, A. H.; Mu, A. H. E.; Ballau, M.; Steitz, R. *Macromolecules* **2013**, *46*, 6541–6547.

(99) Angioletti-uberti, S.; Lu, Y.; Dzubiella, J. *The Journal of Physical Chemistry C* **2015**, *119*, 15723–15730.

(100) Jia, H.; Roa, R.; Angioletti-uberti, S.; Henzler, K.; Ott, A.; Dzubiella, J.; Ballau, M.; Lu, Y. *Journal of Materials Chemistry A* **2016**, *4*, 9677–9684.

(101) Rose, S. Interactions polymère/silice : de la structure locale au renforcement mécanique d' hydrogels hybrides., Ph.D. Thesis, 2013.

(102) Netz, R. R.; Andelman, D. *Physics Reports* **2003**, *380*, 1–95.

(103) Alder, B. J.; Wainwright, T. E. *The Journal of Chemical Physics* **1957**, *27*, 1208–1209.

(104) Gibbs, J. W., *Elementary principles in statistical mechanics*, 1902.

(105) Born, M; Oppenheimer, R. *Annalen der Physik* **1927**, *20*, 457–484.

(106) Hohenberg, P.; Kohn, W. *Physical Review* **1964**, *136*, B864–B871.

(107) Kohn, W; Sham, L. J. *Physical Review* **1965**, *140*, 1133–1138.

(108) Perdew, J. P.; Zunger, A. *Physical Review B* **1981**, *23*, 5048–5079.

(109) Kresse, G; Hafner, J *Physical Review B* **1993**, *47*, 558–561.

(110) Kresse, G; Hafner, J *Physical Review B* **1994**, *49*, 14251–14269.

(111) Kresse, G; Furthmu, J *Physical Review B* **1996**, *54*, 11169–11186.

(112) Perdew, J. P.; Burke, K.; Ernzerhof, M. *Physical Review Letters* **1996**, *77*, 3865–3868.

(113) Swope, W. C.; Andersen, H. C.; Berens, P. H.; Wilson, K. R. *The Journal of Chemical Physics* **1982**, *76*.

(114) Andersen, H. C. *The Journal of Chemical Physics* **1980**, *72*.

(115) Nosé, S. *The Journal of Chemical Physics* **1984**, *81*, 511–519.

(116) Hoover, W. G. *Physical Review A* **1985**, *31*, 1695–1697.

(117) Tuckermann, M. E., *Statistical Mechanics: Theory and Molecular Simulation*; Oxford University Press: 2010.

(118) Binder, K. In *Monte Carlo and Molecular Dynamics Simulations in Polymer Science*, 1996.

(119) Glotzer, S. C.; Paul, W. *Annual Review Materials Research* **2002**, *32*, 401–436.

(120) Madras, N.; Sokal, A. D. *Journal of Statistical Physics* **1988**, *50*, 109–186.

(121) Geyler, S.; Pakula, T.; Reiter, J.; Geyler, S.; Pakula, T.; Reiter, J. *The Journal of Chemical Physics* **1990**, *92*, 2676–2680.

(122) Carmesin, I; Kremer, K *Macromolecules* **1988**, *21*, 2819–2823.

(123) Carmesin, I; Kremer, K. *Journal de Physique* **1990**, *51*, 915–932.

(124) Paul, W.; Binder, K.; Heermann, D. W.; Kremer, K. *The Journal of Chemical Physics* **1991**, *95*, 7726–7740.

(125) Paul, W.; Binder, K.; Heermann, D. W.; Kremer, K. *Journal de Physique II* **1991**, *1*, 37–60.

(126) Smith, S. W.; Hall, C. K.; Freeman, B. D. *Physical Review Letters* **1995**, *75*, 1316–1319.

(127) Smith, S. W.; Hall, C. K.; Freeman, B. D. *The Journal of Chemical Physics* **1996**, *104*, 5616–5637.

(128) Grest, G.; Kremer, K. *Physical Review A* **1986**, *33*, 3628–3631.

(129) Kremer, K.; Grest, G. S. *The Journal of Chemical Physics* **1990**, *92*, 5057–5086.

(130) Dünweg, B.; Kremer, K. *Physical Review Letters* **1991**, *66*, 2996–2999.

(131) Dünweg, B.; Kremer, K. *The Journal of Chemical Physics* **1993**, *99*, 6983–6997.

(132) Dünweg, B. *The Journal of Chemical Physics* **1993**, *99*, 6977–6982.

(133) Kröger, M.; Hess, S. *Physical Review Letters* **2000**, *85*, 1128–1131.

(134) Vladkov, M.; Barrat, J. L. *Macromolecular Theory and Simulations* **2006**, *15*, 252–262.

(135) Ethier, J. G.; Hall, L. M. *Soft Matter* **2018**, *14*, 643–652.

(136) Marrink, S. J.; de Vries, A. H.; Mark, A. E. *The Journal of Physical Chemistry B* **2004**, *108*, 750–760.

(137) Marrink, S. J.; Risselada, H. J.; Yefimov, S.; Tieleman, D. P.; Vries, A. H. D. *Journal of Physical Chemistry B* **2007**, *111*, 7812–7824.

(138) Monticelli, L; Kandasamy, S. K.; Periole, X; Larson, R. G.; Tieleman, D. P.; Marrink, S. J. *J. Chem. Theory Comput.* **2008**, *4*, 819–834.

(139) Marrink, S. J.; Tieleman, D. P. *Chem. Soc. Rev.* **2013**, *42*, 6801–6822.

(140) De Jong, D. H.; Singh, G.; Bennett, W. F. D.; Arnarez, C.; Wassenaar, T. A.; Schäfer, L. V.; Periole, X.; Tieleman, D. P.; Marrink, S. J. *Journal of Chemical Theory and Computation* **2013**, *9*, 687–697.

(141) Wohlert, J.; Berglund, L. A. *Journal of Chemical Theory and Computation* **2011**, *7*, 753–760.

(142) Rossi, G.; Monticelli, L.; Puisto, S. R.; Ala-nissila, T. *Soft Matter* **2011**, *7*, 698–708.

(143) Lee, H.; Vries, A. H. D.; Marrink, S.-j.; Pastor, R. W. *Journal of Physical Chemistry B* **2009**, *113*, 13186–13194.

(144) Milani, A.; Casalegno, M.; Castiglioni, C.; Raos, G. *Macromolecular Theory and Simulations* **2011**, *20*, 305–319.

(145) Uttarwar, R. G.; Huang, Y.; Potoff, J. *Industrial & Engineering Chemistry Research* **2012**, *52*, 73–82.

(146) Plimpton, S. *Journal of Computational Physics* **1995**, *117*, 1–19.

(147) http://lammps.sandia.gov.

(148) Rimola, A.; Costa, D.; Sodupe, M.; Ugliengo, P. *Chemical Reviews* **2013**, *113*, 4216–4313.

(149) Sahai, N.; Rosso, K. M. In *Surface Complexation Modelling*, 2006, pp 359–395.

(150) Zhuravlev, L. T. *Langmuir* **1987**, *3*, 316–318.

(151) Zhuravlev, L. T. *Colloids and Surfaces A: Physicochemical and Engineering Aspects* **1993**, *74*, 71–90.

(152) Zhuravlev, L. T. *Colloids and Surfaces A: Physicochemical and Engineering Aspects* **2000**, *173*, 1–38.

(153) Pfeiffer-Laplaud, M.; Costa, D.; Tielens, F.; Gaigeot, M. P.; Sulpizi, M. *Journal of Physical Chemistry C* **2015**, *119*, 27354–27362.

(154) Sindorf, D. W.; Maciel, G. E. *Journal of the American Chemical Society* **1983**, *105*, 1487–1493.

(155) Vigné-Maeder, F.; Sautet, P *Journal of Physical Chemistry B* **1997**, *101*, 8197–8203.

(156) Demuth, T.; Jeanvoine, Y.; Hafner, J.; Angyan, J. G. *Journal of Physics: Condensed Matter* **1999**, *11*, 3833–3874.

(157) Wright, A. F.; Leadbetter, A. J. *The Philosophical Magazine: A Journal of Theoretical Experimental and Applied Physics* **1975**, *31*, 1391–1401.

(158) Ceresoli, D; Bernasconi, M; Iarlori, S; Parrinello, M; Tosatti, E *Physical Review Letters* **2000**, *84*, 3887–3890.

(159) Mathew, K.; Sundararaman, R.; Letchworth-weaver, K.; Arias, T. A.; Hennig, R. G. *The Journal of Chemical Physics* **2014**, *140*, DOI: 10.1063/1.4865107.

(160) Mathew, K.; Hennig, R. G. *arXiv* **2016**, 1–6.

(161) MacKerell, A. D. et al. *The Journal of Physical Chemistry B* **1998**, *102*, 3586–3616.

(162) Simonson, T.; Roux, B. *Biophysical Chemistry* **1999**, *78*, 1–20.

(163) P.J., H.; J.M.V.A., K. *Europhysics Letters (EPL)* **1992**, *19*, 155–160.

(164) Ahlrichs, P.; Dünweg, B. **1999**, *111*, 8225–8239.

(165) Soddemann, T.; Dünweg, B.; Kremer, K. *Physical Review E* **2003**, *68*, 1–8.

(166) Junghans, C.; Praprotnik, M.; Kremer, K. *Soft Matter* **2008**, *4*, 156–161.

(167) Chudoba, R.; Heyda, J.; Dzubiella, J. *Journal of Chemical Theory and Computation* **2017**, *13*, 6317–6327.

(168) Abbott, L. J.; Stevens, M. J. *The Journal of Chemical Physics* **2015**, *143*, 1–10.

(169) Wang, Q.; Suraweera, N. S.; Keffer, D. J.; Deng, S.; Mays, J. *Macromolecules* **2012**, *45*, 6669–6685.

(170) Chen, T.; Hynninen, A. P.; Prud'Homme, R. K.; Kevrekidis, I. G.; Panagiotopoulos, A. Z. *Journal of Physical Chemistry B* **2008**, *112*, 16357–16366.

(171) Shen, J. W.; Li, C.; Van Der Vegt, N. F. A.; Peter, C. *Journal of Chemical Theory and Computation* **2011**, *7*, 1916–1927.

(172) Fischer, J.; Paschek, D.; Geiger, A.; Sadowski, G. *The Journal of Physical Chemistry B* **2008**, *112*, 13561–13571.

(173) Bedrov, D.; Ayyagari, C.; Smith, G. D. *Journal of Chemical Theory and Computation* **2006**, *2*, 598–606.

(174) Arnarez, C.; Uusitalo, J. J.; Masman, M. F.; Ingólfsson, H. I.; de Jong, D. H.; Melo, M. N.; Periole, X.; de Vries, A. H.; Marrink, S. J. *Journal of Chemical Theory and Computation* **2014**, *11*, 260–275.

(175) Wang, S.; Larson, R. G. *Macromolecules* **2015**, *48*, 7709–7718.

(176) Wang, S.; Larson, R. G. *Langmuir* **2015**, *31*, 1262–1271.

(177) Chong, L.; Aydin, F.; Dutt, M. *Journal of Computational Chemistry* **2015**, *37*, 920–926.

(178) Ginzburg, V. V.; Dyk, A. K. V.; Chatterjee, T.; Nakatani, A. I.; Wang, S.; Larson, R. G. *Macromolecules* **2015**, *48*, 8045–8054.

(179) Bochicchio, D.; Pavan, G. M. *The journal of Physical Chemistry Letters* **2017**, *8*, 3813–3819.

(180) Li, Y.; Abberton, B. C.; Kroger, M.; Liu, W. K. *Polymers* **2013**, *5*, 751–832.

(181) Montarnal, D.; Capelot, M.; Tournilhac, F.; Leibler, L. *Science* **2011**, *334*, 965–969.

(182) Carlsson, L.; Rose, S.; Hourdet, D.; Marcellan, A. *Soft Matter* **2010**, *6*, 3619.

(183) Zwanzig, R. W. *The Journal of chemical physics* **1954**, *22*, 1420–1426.

(184) Torrie, G. M.; Valleau, J. P. *Chemical Physics Letters* **1974**, *28*, 578–581.

(185) Torrie, G. M.; Valleau, J. P. *Journal of Computational Physics* **1977**, *23*, 187–199.

(186) Mezei, M; Mehrotra, P. K.; Beveridge, D. L. *Journal of the American Chemical Society* **1985**, *107*, 2239–2245.

(187) Haydock, C.; Sharp, J. C.; Prendergast, F. G. *Biophysical Journal* **1990**, *57*, 1269–1279.

(188) Woolf, T. B.; Roux, B. *Journal of the American Chemical Society* **1994**, *116*, 5916–5926.

(189) Kumar, S.; Bouzida, D.; Swendsen, R. H.; Kollman, P. A.; Rosenberg, J. M. *Journal of Computational Chemistry* **1992**, *13*, 1011–1021.

(190) Alan, G. "WHAM: the weighted histogram analysis method" version 2.0.9.

(191) Rubinstein, M.; Colby, R. H. In, 2011.

Résumé

Les points de suture et les agrafes sont de plus en plus remplacés par ou accompagnés de colle chirurgicale. Cette dernière est un adhésif généralement déposé comme un pansement sur la plaie afin de maintenir fermés les bords de cette dernière. Les points de sutures ou les agrafes peuvent être douloureux pour le patient, laissent des traces sur la peau, sont difficiles à utiliser pour le médecin et requièrent en général une phase de retrait des points ou des agrafes. Enfin, ces derniers sont largement utilisés pour la cicatrisation de plaies externes, mais sont difficilement utilisables pour la réparation d'organes mous comme le foie, qui se déchire au passage de l'aiguille. Les colles chirurgicales possèdent de nombreux avantages par rapport aux points de suture et aux agrafes : leur application est plus simple (des vétérinaires les utilisent lors de la cicatrisation de plaies dans la gueule des animaux) et moins douloureuse pour un meilleur résultat esthétique.

Une colle chirurgicale doit en particulier remplir deux objectifs essentiels. D'une part, elle doit être capable de maintenir au contact les bords de la plaie par adhésion mécanique *in vivo* efficace sur le tissus biologique. D'autre part, elle doit assister l'hémostase[2] locale en améliorant les processus de coagulation et de cicatrisation [4]. De manière plus générale, les colles chirurgicales doivent permettre l'adhérence entre deux tissus biologiques ou entre un tissus biologique et une surface, comme dans le cas de prothèses, afin de contrôler les saignements et de servir de barrière aux liquides [5].

Il existe déjà de nombreuses colles chirurgicales sur le marché utilisées par médecins et vétérinaires. Elles sont généralement composées de polymères. Ces derniers assurent un bon contact avec les surfaces à coller grâce à leur capacité à couvrir les aspérités de la sur-

2. L'hémostase est le premier stade de la cicatrisation d'une plaie. Elle correspond à l'ensemble des processus contribuant à l'arrêt des saignements.

face concernée et dissipent bien l'énergie quand ils sont soumis à une contrainte, retardant ainsi la fracture [6, 7]. Ces propriétés font des polymères un matériau de choix pour la cicatrisation de tissus biologiques. L'essentiel des colles existant sur le marché sont composées de polymères naturels, c'est-à-dire contenant des composés présents dans le corps humain, de polymères synthétiques, ou d'un mélange des deux. Cependant, elles présentent un certain nombre de limites. Les plus importantes sont leur cytotoxicité[3] liée à une faible biocompatibilité[4], une dégradation lente, un temps de séchage long, une polymérisation *in vivo* difficile à maîtriser[5] et une faible adhésion sur des surfaces humides[6].

Des chercheurs de l'École Supérieure de Physique et de Chimie Industrielles de la ville de Paris (ESPCI), dont Alba Marcellan et Ludvik Leibler, ont développé en 2014 une colle chirurgicale innovante, sans polymère, composée de nanoparticules de silice et d'eau [1]. Ils ont observé une très bonne adhésion entre deux morceaux de foie de veau collés grâce à la solution de nanoparticules de silices (figure 7.7). La solution de nanoparticules a été déposée sur les deux morceaux de foie. Après les avoir pressés à la main pendant 30 secondes, une énergie d'adhésion de 25 ± 5 J/m^2 a été mesurée. C'est la première fois que des nanoparticules de silice sont utilisées en tant que colles chirurgicales.

Cette méthode a ensuite été appliquée avec succès à la cicatrisation d'un foie de rat vivant, et même d'un coeur vivant de rat [9]. La très bonne adhésion des nanoparticules de silice sur ces surfaces humides ainsi que les propriétés mécaniques remarquables des nanoparticules adsorbées sur les tissus biologiques ont permis aux plaies de ne pas se réouvrir malgré des contraintes mécaniques constantes : le coeur du rat réparé avec cette méthode a continué de fonctionner normalement. La méthode utilisée, simple à mettre

3. La cytotoxicité correspond à la capacité d'un agent chimique ou biologique à être toxique pour les cellules.

4. La biocompatibilité correspond à la capacité d'un matériau à ne pas interagir avec et à ne pas dégrader le milieu biologique dans lequel il se trouve.

5. La polymérisation de la colle se fait en général directement sur la cicatrice du patient. Les composants nécessaires à la polymérisation sont mis en contact sur la peau, en utilisant une seringue à double réservoir ou un spray. Une fois que la polymérisation a eu lieu, la colle est généralement difficile à déplacer.

6. Ce dernier point limite drastiquement la gamme d'application des colles chirurgicales à des applications externes sur tissus sec. Il est dont nécessaire de bien sécher la peau avant d'appliquer la colle.

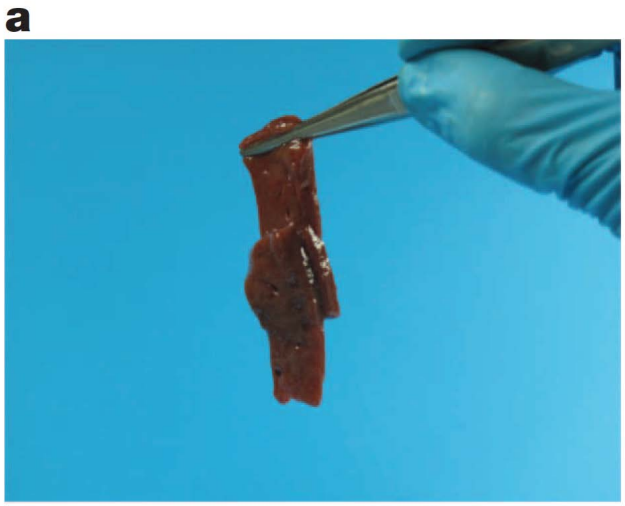

Figure 7.7 – Deux morceaux de foie de veau sont collés ensemble grâce à une solution de nanoparticules de silice déposée entre eux. Image de la référence [1].

en oeuvre, est illustrée en figure 7.8. Une solution aqueuse de nanoparticules de silice est déposée avec une micropipette ou un pinceau sur la surface de la plaie (image de gauche sur la figure 7.8). Les bords de cette dernière sont pressées l'un contre l'autre avec les doigts (flèches bleues sur la partie droite de la figure 7.8). Les nanoparticules forment ainsi des connexions multiples entre les deux bords de la plaie, maintenant cette dernière fermée.

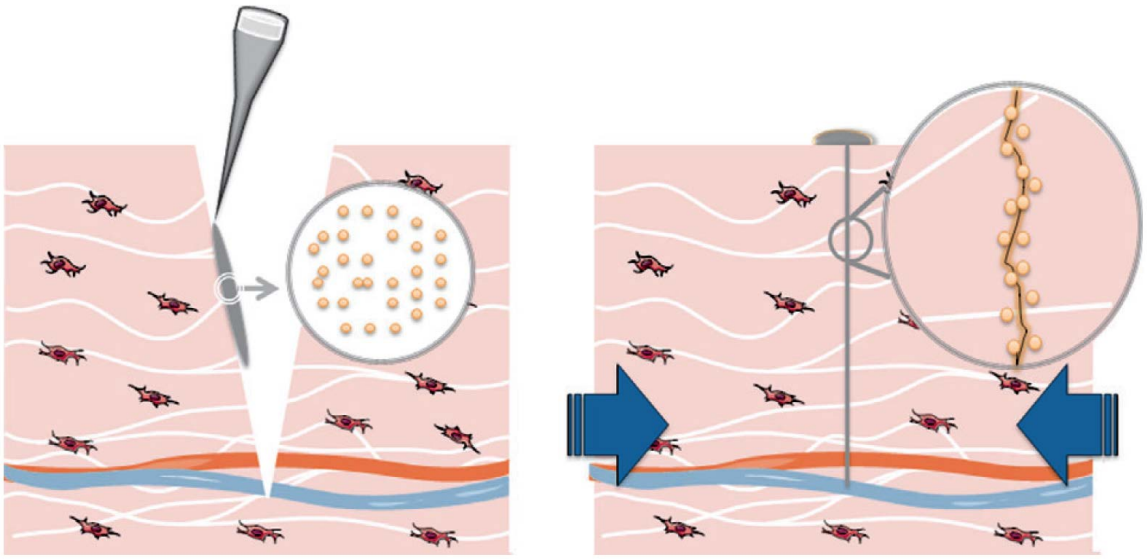

Figure 7.8 – Utiliser des nanoparticules pour la fermeture de cicatrices : principe de la méthode. Image de la référence [9].

Cette méthode a ensuite été comparée aux points de suture classiques et à une colle chirurgicale à base de polymères synthétiques, Dermabond® [9]. Une plaie dorsale de 1,5 cm de long et 3 mm de profondeur a été réparée à l'aide des trois méthodes présentées en figure 7.9. Dans les trois cas, la plaie de s'est pas réouverte. Après trois jours, il est visible que le processus de cicatrisation est plus efficace lorsque qu'une solution de nanoparticules de silice est utilisée. Cette dernière, par la grande quantité d'eau qu'elle apporte à la plaie, facilite l'hémostase locale. La plaie traitée avec Dermabond® montre une inflammation locale qui forme une couche dure, empêchant un bon contact entre les bords de la plaie et ralentissant la cicatrisation. L'utilisation d'une solution de nanoparticules de silice s'avère être une solution satisfaisante en termes de biocompatibilité (pas d'inflammation locale de la plaie), de propriétés mécaniques (la plaie ne s'est pas réouverte) et d'hémostase (la cicatrisation a été rapide).

Figure 7.9 – Comparaison *in vivo* de la cicatrisation de plaies sur le dos d'un rat avec une solution de nanoparticules de silice (à gauche), des points de suture (au milieu) et une colle chirurgicale à base de polymères synthétiques, Dermabond®. Image de la référence [9].

Les auteurs de la référence [1] ont utilisé un système modèle pour étudier le mécan-

isme d'adhérence entre la solution de nanoparticules de silice et les tissus biologiques. Ce modèle est un hydrogel, c'est-à-dire un réseau à trois dimensions de chaînes polymériques réticulées gonflé d'eau. Les hydrogels peuvent contenir jusqu'à 90% d'eau. Leur capacité à absorber une grande quantité de liquide explique leur utilisation dans les couches ou les serviettes hygiéniques. Leur aptitude à relâcher cette eau les rend très utiles dans les pansements. Enfin, leur grande contenance d'eau fait qu'ils sont utilisés dans les lentilles de contact. On trouve aussi des hydrogels dans de nombreuses applications médicales en tant que véhicules à délivrance ciblée de médicaments ou en tant qu'échafaudage pour la création d'organes synthétiques. De plus, ils ont de grandes similarités avec des organes mous comme la peau, le foie ou les poumons. Les propriétés biochimiques, osmotiques et structurelles de ces organes ne sont évidemment pas représentées par les hydrogels. Néanmoins, ils restent un modèle convenable de la matrice extérieure de ces organes. C'est pour cette dernière raison que les auteurs de la référence [1] ont étudié l'adhésion de nanoparticules de silice sur des hydrogels. Cependant, leur utilisation reste limitée par leur fragilité.

De nombreuses solutions existent pour renforcer les réseaux d'hydrogels. Certaines méthodes utilisent une seconde matrice pénétrant la première, des nanofibres ou des nanoparticules pour renforcer le réseau de polymères. L'introduction de nanoparticules dans un hydrogel correspond à un nanocomposite. Un matériau est dit nanocomposite si au moins l'une de ses phases a une dimension inférieure à 100 nm. Cette définition rassemble une grande variété de matériaux et rend le champ des matériaux nanocomposites varié et riche. L'introduction de nanoparticules dans un réseau polymérique améliore les propriétés du réseau bien au-delà de ce qui pouvait être prévu, et les propriétés résultantes sont souvent très différentes des propriétés du réseau polymérique seul. Le système nanocomposite qui nous intéresse est composé de nanoparticules de silice et de polyacrylamide (PAAm) d'une part ou de poly(N,N-diméthylacrilamide) (PDMA) d'autre part (figure 7.10(a)). La surface de silice amorphe présente différentes sortes de terminaisons silanol Si-OH représentées en figure 7.10(b) [148, 149]. Les silanols isolés n'interagissent pas avec d'autres silanols

de la surface. Certains sont liés par liaison hydrogène avec leurs voisins. Les silanols vicinaux forment des ponts Si–O–Si. Enfin, un atom de silicium porte deux groupements OH dans le cas des silanols géminaux. Dans un premier temps, nous modélisons un système nanocomposite simplifié. Les principales hypothèses sont les suivantes : (i) nous considérons des surfaces infinies et plates de silice et (ii) nos chaînes polymériques ne sont pas réticulées.

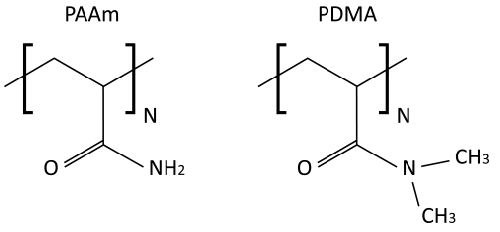

(a) Polyacrylamide (PAAm) et poly(N,N-dimethylacrylamide) (PDMA).

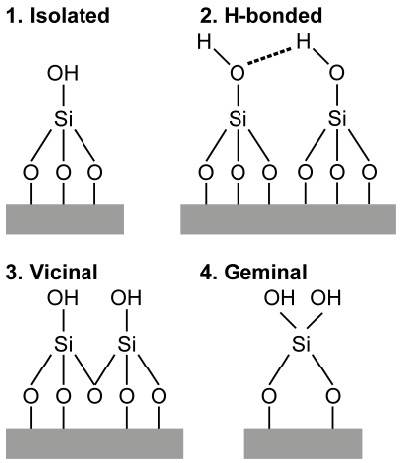

(b) Représentation des terminaisons silanol Si-OH présentes sur la surface de silice amorphe.

Figure 7.10 – Représentation des polymères et de la surface de silice.

La figure 7.10(a) indique que le PAAm est moins encombré stériquement que le PDMA. Il est ainsi davantage disponible pour former des liaisons hydrogènes avec les silanols Si-OH de la surface de silice. PAAm devrait donc mieux coller sur les nanoparticules de silice. Cependant, il a été montré expérimentalement que le PAAm ne colle pas sur les nanoparticules de silice [36, 37] tandis que le PDMA colle très bien [38]. Coller deux bandes de PDMA à l'aide d'une solution de nanoparticules de silice donne un système très résistant ayant une énergie d'adhésion de 6.6 ± 1.6 J/m^2 entre les deux bandes de PDMA [1]. Il est en revanche difficile de mesurer une énergie d'adhésion entre deux bandes de PAAm collées par des nanoparticules de silice, puisque les bandes de PAAm se décollent dès que l'expérimentateur essaie de les manipuler, empêchant toute mesure. Le but de ce travail est de comprendre l'origine de ces comportements radicalement différents alors même que

la structure du PAAm et celle du PDMA sont proches.

Dans un premier temps, nous avons utilisé une méthode de calcul quantique, la théorie de la fonctionnelle de la densité (*density functional theory* ou DFT) afin d'étudier l'adsorption de petits fragments de PAAm et de PDMA, contenant une à dix unités de répétition, sur des surfaces idéales de silice. Ces surfaces correspondent aux faces 100 et 111 (selon les indices de Miller) de la cristobalite β, considérée comme modélisant raisonnablement la surface de la silice amorphe [154] . Modéliser avec des méthodes quantiques une surface de silice amorphe serait en effet particulièrement coûteux en temps de calcul, même si cela a déjà été réalisé en dynamique moléculaire *ab initio* [153]. L'étude quantique de l'adsorption du PAAm et du PDMA sur des surfaces modèles de silice nous a permis de conclure que les polymères s'adsorbent sur la silice en créant des liaisons hydrogènes avec la surface de silice. L'utilisation de cette méthode présente cependant des lacunes : l'eau par exemple n'y est pas représentée car trop coûteuse en temps de calcul.

Dans un second temps, nous avons utilisé une méthode de dynamique moléculaire gros-grain permettant de modéliser des systèmes plus important pendant des temps plus longs. Le principe de la méthode gros-grain est le suivant : il s'agit de grouper des atomes en "billes" et de faire évoluer ces billes en dynamique moléculaire. La représentation gros-grain de notre système est en figure 7.11. Nous avons choisi une représentation avant tout transférable avec le moins de différences possible entre le PAAm et le PDMA. Cela permet de limiter les divergences entre les deux types de polymères et de découpler ensuite plus facilement les caractéristiques responsables des comportements radicalement différents du PAAm et du PDMA. Nous avons utilisé des simulations tout-atomes et certains paramètres du champ de force Martini [136, 137, 174] afin de trouver les paramètres des potentiels d'interaction permettant de correctement décrire les interactions intra et inter moléculaires.

Une fois le modèle gros-grain construit et validé, nous avons commencé par étudier un

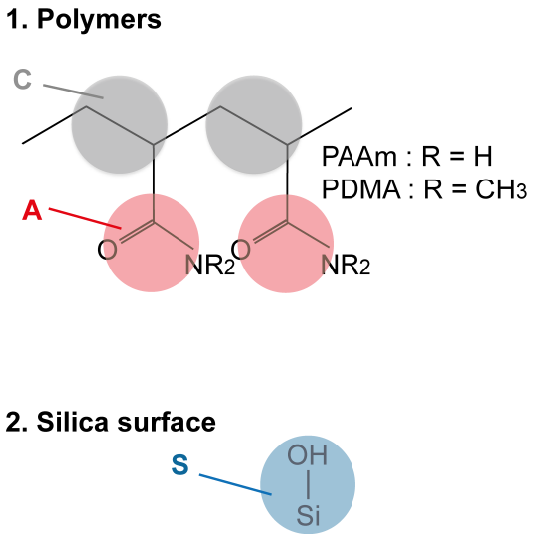

Figure 7.11 – Représentation gros-grain des polymères et de la surface de silice.

système relativement dense contenant des chaînes polymèriques, un solvant et une surface de silice. Les chaînes contiennent 90 monomères. Nous avons testé deux modèles de solvant : implicite et explicite. Le solvant implicite représente le plus fidèlement possible certaines caractéristiques importantes du solvant, comme l'éventuel écrantage des interactions inter moléculaires dû à la présence du solvant ou les interactions hydrodynamiques du solvant sans explicitement modéliser les molécules de solvant. Il existe de nombreuses méthodes de solvant implicite utilisables en dynamique moléculaire et largement utilisées dans le domaines des polymères. Pour en nommer quelques unes et sûrement les plus importantes, la dynamique brownienne (*Borwnian dynamic*, BD [122]) ainsi que la dynamique dissipative de particules (*Dissipative Particles Dynamic*, DPD [163]) prennent en compte l'effet du solvant dans un terme de force aléatoire et dans un terme de forces dissipatives. D'autres méthodes se basent sur les résultats de dynamique moléculaire à différentes densités en solvant et ajustent les paramètres gros-grain [169–173]. La méthode utilisée dans ce travail est basée sur les travaux de l'équipe de Marrink *et al.* qui, dans la continuité du champ de force Martini, ont adapté ce dernier à l'utilisation d'un solvent implicite. Il s'agit du champ de force dry Martini [174]. Son principe est simple : modifier les paramètres d'interaction afin de prendre en compte l'effet du solvant. L'interaction entre deux billes "solvophiliques" sera ainsi diminuée en raison de l'écrantage lié au solvant. En revanche, l'interaction entre deux billes "solvophobiques" sera augmentée.

Nous avons donc comparé l'utilisation de solvants explicite et implicite sur un système polymérique dense, en contact avec une surface de silice. La force de l'interaction entre les chaînes polymèriques et la surface ainsi que la labilité des monomères à l'interface ont été étudiées en détail, tout comme l'importance de la solvatation des chaînes de polymère près de la surface. La figure 7.12 indique en effet que dans la boîte contenant le PAAm, les billes de solvant quittent la région bulk pour venir à l'interface, empêchant le PAAm de s'adsorber sur la surface de silice. Ce phénomène n'est pas présent dans le cas du PDMA, qui s'adsorbe bien sur la surface de silice. Ces résultats indiquent qu'il est nécessaire, dans le cadre de cette étude, de considérer un solvant explicite.

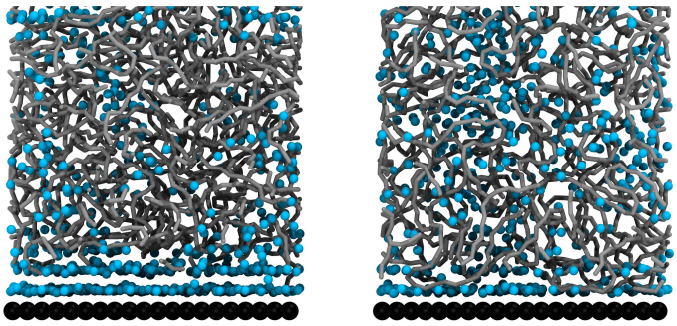

Figure 7.12 – Moitié d'une boîte de simulation. La boîte contenant du PAAm est à gauche et celle contenant du PDMA est à droite. La surface est en noire, le solvant en bleu et les chaînes polymèriques en gris.

Nous étudions ensuite le mécanisme de détachement des chaînes. Cependant, étudier ce mécanisme sur un système dense de chaînes polymèriques comme précédemment serait trop compliqué à mettre en oeuvre et ne nous donnerait pas directement accès à l'énergie nécessaire pour décoller une chaîne de la surface. Nous nous sommes donc tourné vers un système composé d'une seule chaîne sur une surface de silice, le tout entouré d'eau. Nous avons utilisé la méthode d'*umbrella sampling* qui est une méthode d'énergie libre permettant de sonder l'ensemble de la courbe d'énergie libre en fonction d'une coordonnée

réactionnelle. Dans notre cas, la coordonnée réactionnelle est la distance D entre le centre de masse de la chaîne de polymère et la surface de silice, comme indiqué en figure 7.13.

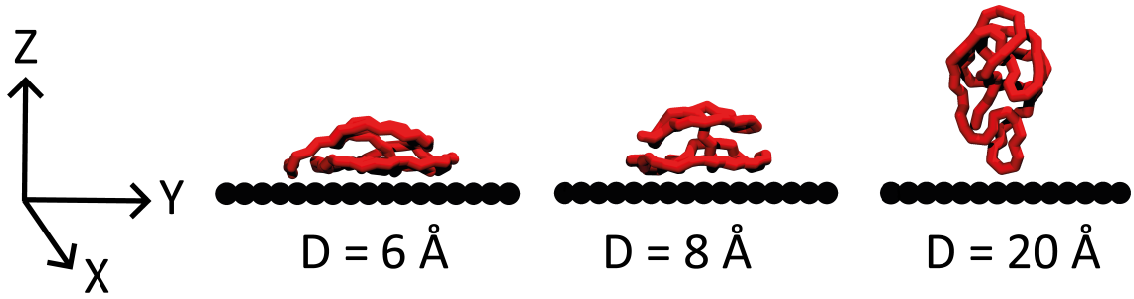

Figure 7.13 – Le centre de masse du polymère est contraint à différentes distances de la surface D.

La méthode d'umbrella sampling, couplée avec le *Weighted Histogram Analysis Method* (WHAM) nous permet de construire la courbe d'énergie libre en fonction de la distance entre le centre de masse du polymère et la surface D présentée en figure 7.14. Cette courbe indique deux comportements radicalement différents entre le PAAm et le PDMA vis-à-vis de leur éloignement de la surface. En particulier, le PAAm ne présente pas de puit d'énergie libre près de la surface alors que le PDMA en présente un. Cela signifie que le premier est plus stabilisé quand il se situe loin de la surface et solvaté que quand il est adsorbé sur la surface. En revanche, le second est stabilisé près de la surface et déstabilisé lorsqu'il se retrouve détaché de la surface et solvaté.

En effet, si nous partons de la même configuration pour le PAAm et pour le PDMA près de la surface et que nous les laissons évoluer pendant 100 ns, nous obtenons la configuration finale présentée en figure 7.15(a). Cette figure indique bien que le PDMA reste près de la surface tandis que le PAAm s'en détache. Les courbes de la figure 7.15(b) montrent l'évolution de la distance entre le centre de masse du PAAm et du PDMA et la surface. Il est clair que le PDMA reste près de la surface tandis que le PAAm se décolle de la silice au cours du temps.

Nous avons ensuite réalisé une étude extensive du rôle joué par les différents paramètres

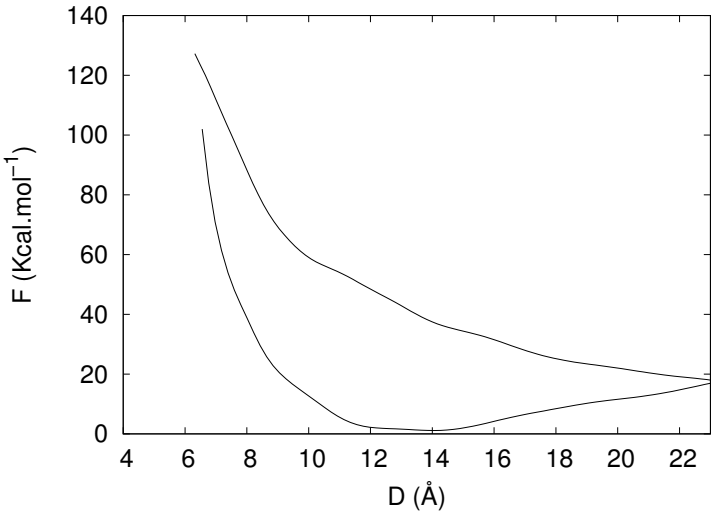

Figure 7.14 – Profil d'énergie libre pour le PAAm (ligne pleine) et le PDMA (ligne pointillée) dans un solvant explicite.

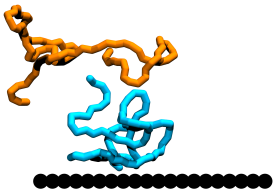

(a) Configuration finale du PAAm (orange) et du PDMA (bleu) lors d'une évolution sans contrainte sur le centre de masse des polymères. Le PAAm et le PDMA sont seulement superposés pour la figure.

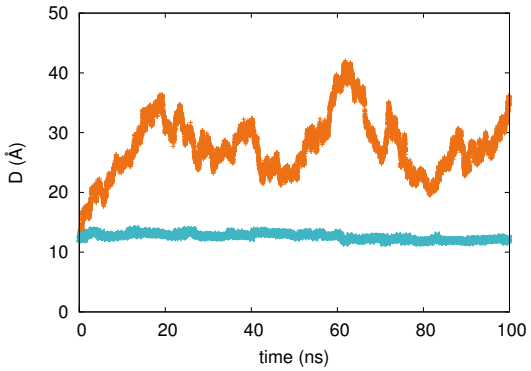

(b) Distance entre le centre de masse du polymère et la surface au cours de la simulation. La trajectoire du PAAm est en orange et celle du PDMA est en bleu.

Figure 7.15 – Évolution sans contrainte du PAAm et du PDMA.

d'interaction dans l'adsorption – ou non – des polymères sur la surface de silice. La conclusion de cette étude indique que les interactions intra moléculaire au sein du polymère, mais aussi des interactions inter moléculaires entre le polymère et la surface jouent un rôle primordial dans l'adsorption du PDMA sur la surface de silice. Les interactions intra moléculaires font que le PDMA est mal solvaté et lui permettent de ne pas trop gonfler dans l'eau. Les interactions polymère / surface favorisent l'adsorption du polymère sur la surface. C'est la combinaison de ces deux types d'interactions qui font que le PDMA s'adsorbe sur la surface de silice. Il est intéressant de noter que ce ne sont pas directement les interactions polymère / solvant ou surface / solvant qui jouent un rôle déterminant dans la différence de comportement entre le PAAm et le PDMA.

Enfin, nous avons étudié le comportement du PAAm et du PDMA piégés entre deux surfaces. Nous considérons maintenant une seule longue chaîne polymèrique, contenant 2000 monomères, entre deux surfaces de silice séparées de 200 Å. La configuration initiale est représentée en figure 7.16(a). Lorsque la distance entre les deux surfaces est de 200 Å et que le système évolue librement pendant 500 ns, le PAAm adopte la configuration finale présentée en figure 7.16(c) tandis que le PDMA évolue vers la figure 7.16(b). Vu la configuration adoptée par le PAAm, qui désorbe directement de la silice, il n'est pas pertinent d'étudier son mécanisme de décollement entre deux surfaces de silice. En revanche, le PDMA adopte une configuration très intéressante : il reste adsorbé sur les deux surfaces de silice, mais a tendance à se rassembler sur lui-même.

Nous avons ensuite progressivement augmenté la distance entre les deux surfaces de silice, de 5 Å en 5 Å, et étudié la labilité des billes du polymère sur la surface ainsi que la force appliquée par le polymère sur les surfaces quand la distance entre ces deux surfaces augmente. Nous observons ainsi un comportement intéressant du PDMA. Quand les deux surfaces sont séparées de 200 Å, certaines billes du polymère sont fermement attachées aux surfaces et leur temps de résidence près des surfaces est de l'ordre de plusieurs centaines de nanosecondes, tandis que d'autres billes sont plus labiles et font des aller-retours

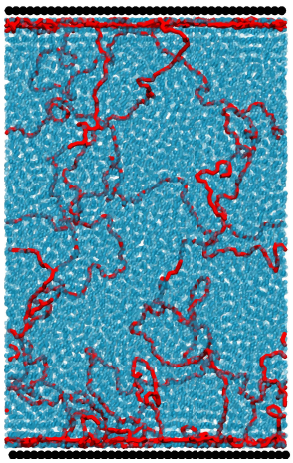

(a) Configuration initiale du PAAm et du PDMA.

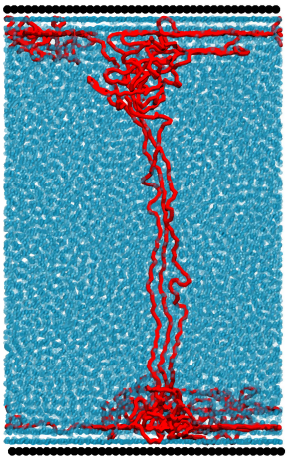

(b) Configuration finale du PDMA

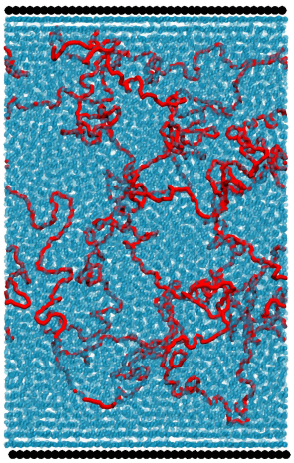

(c) Configuration finale du PAAm.

Figure 7.16 – Images des configurations initiales et finales du PDMA et du PAAm entre deux surfaces de silice. La surface de silice est en noir, les billes de solvant sont en bleu et les polymères sont en rouge.

rapides près et loin de la surface. Lorsque la distance entre les deux surfaces augmente jusqu'à 300 Å, les billes rapides disparaissent et il reste seulement des billes fermement adsorbées sur les surfaces. Enfin, lorsque les surfaces sont séparées de plus de 300 Å, les billes qui étaient fermement attachées deviennent labiles. Ces différents régimes permettent d'avoir des informations sur le mécanisme de détachement des chaînes de PDMA des nanoparticules de silice quand le système est soumis à une contrainte. Dans un premier temps, certaines parties de la chaîne bougent rapidement afin de dissiper l'énergie tandis que d'autres sont fortement adsorbées sur les nanoparticules de silice. Quand la contrainte augmente, des parties de la chaîne restent bien adsorbées sur les nanoparticules de silice pendant que le reste de la chaîne, non adsorbé, se réorganise. Enfin, près du point de rupture, les parties de la chaîne qui étaient fortement adsorbées sont de plus en plus labiles. Dans le cas d'un système nanocomposite "réel", contenant un réseau polymérique réticulé et plusieurs nanoparticules de silice, les deux premières phases sont plus importantes : lorsque qu'une partie d'une chaîne se décolle de la surface, elle est rapidement remplacée par une partie d'une chaîne voisine.

Nous avons construit un modèle robuste, simple et flexible, permettant d'expliquer les mécanismes d'adsorption et de désorption du PAAm et du PDMA sur une surface de

silice. Nous avons compris comment une si petite différence dans la structure du PAAm et du PDMA pouvait mener à des propriétés mécaniques si différentes. Ce travail était un premier pas dans l'étude des propriétés mécaniques de systèmes nanocomposites. Les étapes suivantes sont nombreuses et variées, en commençant par un système plus réaliste contenant de nombreuses chaînes polymériques réticulées et plusieurs nanoparticules sphériques. L'impact de la taille des nanoparticules de silice sur les propriétés du système pourrait être exploré. De plus, le calcul et la prédiction de propriétés mécaniques en fonction de variables comme la nature, la taille, le taux de réticulation et le pourcentage massique d'eau pourraient être comparés avec des résultats expérimentaux.

Mots-clé: nanocomposites, silice, dynamique moléculaire gros-grain, adsorption.

Abstract

Polymer / silica interface is investigated using coarse-grained molecular dynamics simulations. In particular, the different behavior of poly(acrylamide) (PAAm) and of poly(N,N-dimethylacrylamide) (PDMA) on the silica surface is compared. First, we show that the macroscopic behavior of PAAm and of PDMA are correctly represented by a model containing an explicit solvent. Then, the umbrella sampling free energy method is used to probe the detachment of PAAm and of PDMA from a silica surface and to investigate important features that allow – or not – the polymer chain to remain adsorbed on the silica surface. We prove that intra molecular interactions within the polymer and polymer / surface interactions are of first importance for the polymer chain to adsorb on silica. Surprisingly, solvent / polymer as well as solvent / surface interactions are not discriminating criteria. Polymer chains are finally constrained to a particular configuration where one chain is adsorbed on two silica surfaces that are 200 Å apart. This yields interesting insights into the evolution of the monomers lability and of the surface / polymer strength interaction when the two silica surfaces are moved apart.

Keywords: adsorption, silica, coarse-grained, molecular dynamics, polymers.

Zusammenfassung

Im Rahmen dieses Vorhabens wird der Polymer-Siliziumdioxid-Heteroübergang vermittels einer grobkörnig modellierten Molekulardynamik-Simulation untersucht, wobei insbesondere das unterschiedliche Verhalten von Polyacrylamiden (PAAm) und Poly(N,N-dimethylacrylamiden) (PDMA) auf der Siliziumoberfläche verglichen werden soll. Zunächst werden wir nachweisen, dass gleichermaßen das makroskopische Verhalten von PAAm und PDMA korrekt durch eine Modellierung repräsentiert werden kann, die einen expliziten Solventen enthält. Daran anschließend wird die Umbrella Sampling-Free-Energy-Methode angewandt werden, um die Ablösung von PAAm und PDMA von der Siliziumdioxidoberfläche zu untersuchen bzw. die maßgeblichen Merkmale zu analysieren, die es den Polymerketten ermöglichen, an der Siliziumdioxidoberfläche adsorbiert zu bleiben – oder ebendies verhindern. In diesem Zusammenhang werden wir belegen, dass die Adsorption in erster Linie durch die intramolekularen Wechselwirkungen innerhalb der Polymere sowie die Polymer-Oberflächen-Wechselverhältnisse gestattet werden und die Interaktionen zwischen den Solventen und den Polymeren bzw. die Polymer-Oberflächen-Wechselwirkung hierfür überraschenderweise keine ausschlaggebenden Kriterien sind. In einem letzten Schritt werden die Polymere schließlich auf eine spezifische Konfiguration hin beschränkt, in der eine Polymerkette auf zwei Siliziumoxidoberflächen adsorbiert wird, die sich in einem Abstand von 200 Å zueinander befinden. Dieses Projekt bietet einen hervorragenden Einblick in die Herausbildung von labilen Monomeren und die Intensität von Polymer-Oberflächen-Wechselwirkungen im Kontext zweier sich auseinander bewegenden Siliziumoxidoberflächen.

Schlüsselwörter: Adsorption, Siliziumdioxid, grobkörnig Molekulardynamik-Simulation, Polymer.

Résumé

La dynamique moléculaire gros-grain nous permet d'étudier l'interface polymère / silice. En particulier, nous comparons les comportements divergents du poly(acrylamide) (PAAm) et du poly(N,N-dimethylacrylamide) (PDMA) sur la surface de silice. Tout d'abord, nous montrons que les comportements macroscopiques du PAAm et du PDMA sont correctement représentés par un modèle contenant un solvant explicite. Nous utilisons ensuite la méthode d'énergie libre umbrella sampling afin d'examiner le détachement du PAAm et du PDMA de la surface de silice et d'étudier les caractéristiques importantes qui permettent ou non à la chaîne de polymère de rester adsorbée sur la surface de silice. Nous soulignons l'importance des interactions intra moléculaires au sein du polymère ainsi que les interactions polymère/surface qui déterminent l'adsorption du polymère sur la silice. De manière surprenante, les interactions solvant/polymère et solvant/surface ne sont pas des critères discriminants lors de l'adsorption des polymères sur la surface. Les polymères sont finalement contraints de s'adsorber sur deux surfaces de silice séparées de 200 Å. Ce système nous permet d'analyser l'évolution de la labilité des monomères ainsi que la force appliquée par les monomères sur la surface quand la distance entre les deux surfaces augmente.

Mots Clés

Adsorption, silice, gros-grains, dynamique moléculaire, polymères

Abstract

Polymer/silica interface is investigated using coarse-grained molecular dynamics simulations. In particular, the different behavior of poly(acrylamide) (PAAm) and of poly(N,N-dimethylacrylamide) (PDMA) on the silica surface is compared. First, we show that the macroscopic behavior of PAAm and of PDMA is correctly represented by a model containing an explicit solvent. Then, the umbrella sampling free energy method is used to probe the detachment of PAAm and of PDMA from a silica surface and to investigate important features that allow - or not - the polymer chain to remain adsorbed on the silica surface. We proved that intra-molecular interactions within the polymer and polymer/surface interactions are of first importance for the polymer chain to adsorb on silica. Surprisingly, solvent/polymer as well as solvent/surface interactions are not discriminating criteria. Polymer chains are finally constrained to a particular configuration where one chain is adsorbed on two silica surfaces that are 200 Å apart. This yields interesting insights into the evolution of the monomers lability and of the surface/polymer strength interaction when the two silica surfaces are moved apart.

Keywords

Adsorption, silica, coarse-grained, molecular dynamics, polymers